PhD Thesis

Experimental Analysis of Emergent Dynamics in Complex Networks of Nonlinear Oscillators

University of Napoli "Federico II"

Department of Electrical Engineering
and Information Technology

Doctor of Philosophy in
Electrical Engineering

Soudeh Yaghouti

Coordinator of PhD Course

Prof. Claudio Serpico

Supervisor

Prof. Massimiliano de Magistris

Co-supervisor

Prof. Carlo Petrarca

2013–2016 (28° cycle)

Contents

List of Figures

List of Tables

Acknowledgment

I would like to express my special thanks to my advisor Prof. Massimiliano de Magistris and my coadvisor Prof. Carlo Petrarca for the support of my Ph.D study, their knowledge, motivation and patience.
I thank also the group of control engineering, specifically Prof. Mario di Bernardo for the novel ideas in area of complex network, which has greatly motivated this study.
A special thanks to Dr. Marco Colandrea for designing and testing the electric boards as well as Dr. Massimo Attanasio for supervising the activities at the Circuit Laboratory of Electrical Engineering and Information Technology Department.
Last but not the least, I would like to thank my family: my parents and my sister for their unconditional love and support.

Abstract

The aim of this thesis is to explore and investigate the emergent dynamics of complex networks through a novel and insightful experimental setup realized as a configurable network of chaotic Chua's circuits. In particular part of our work has been devoted to the implementation and characterization of a "2.0 hardware version" of it, where the interconnection network has improved greatly in its main features. In this way the setup has been fully automatized in providing control on network structure and coupling strength.

A large set of experiments has been carried out in networks with proportional coupling and arbitrary topology, showing, emergent dynamics encompassing synchronization, patterns and traveling waves, clusters formation. Also, the case of dynamic coupling has been experimentally addressed. The experimental observations have been compared with theoretical results by carrying out a local stability analysis of networks with static and dynamic links. Here we use the Master Stability approach (MSF) and its extensions to the case where the links are of dynamic nature (Proportional Derivative-MSF).

Last part of the work has been devoted to the experimental study of cluster synchronization, stimulated by novel theoretical advances based on group theory and network symmetries. A novel network structure referred as "Multiplexed Network" has been experimentally examined, resulting in a great enhancement in synchronization, for which no theoretical models are yet available.

Introduction

Numerous systems are characterized as complex where they can be seen as a collection of interacting individuals. An important property of such complex systems is their behavior, which might differ significantly from those of each individual subsystem due to the interaction effect [7, 33, 51]. Examples range from natural to man-made systems comprising network of blood vessels, neural networks, food web networks, protein networks, electrical power distribution systems, world wide web, social and economical networks, transportation systems and many more [34].

In particular, for human being dealing with modern life style and a constantly growing globalization, it is of great importance to learn about such an intricate world of complex systems around him. Take for instance communication and transportation networks that are in constant expansion. Consequently, it is necessary to answer crucial questions like: how systems behave when they are communicating to each other through a network of interconnections? Which components (or subsystems) play a key role in the collective behavior of the whole complex system? How to monitor and control their behavior? and how to troubleshoot and avoid failures whose cascading might cause huge defragmentation of the whole complex systems?
Answering to these questions has stimulated different disciplines based on a common and novel academic field called network science, where the complexity of the systems is captured by a network of interacting units, which in a mathematical notation is equivalent to graphs where subsystems (units) are assigned to a set of nodes (N) and the interconnections among them are represented by edges (L). Looking at complex systems from this perspective allows to analyze their emergent behavior, specifically as a function of the network structure [5, 6, 24, 25, 41, 47, 53, 58, 60, 61]. In this regard complex networks and their emergent behavior has been the main focus of many research works within the literature in physics, engineering and biology. A particular emergent behavior that has been widely studied is the case where the trajectories of each subsystem asymptotically converge toward each other. This phenomena is called synchronization and it has been widely studied since it has been observed in nature when fireflies synchronize their flashes [51], in human coordination, and even in electrical and mechanical systems like coupled metronomes and power grids

respectively.
In engineering, networks of chaotic oscillators have been considered as paradigm for studying many complex nonlinear systems [13, 18, 32, 39, 40, 59], and most of the research studies have have been theoretical and numerical, due to practical difficulties with realizing networks with large number of nodes and arbitrarily connections. Consequently, few experimental studies have been presented [10–12, 14, 15, 23, 26, 36–38, 45, 55, 56]. , where either small size networks with 2 or 3 nodes are considered [10, 11, 45] or scalable networks like regular nearest neighbor structure in the context of cellular neural networks [55]. Correspondingly, majority of the studies have concentrated on detecting complete synchronization, that is, the condition when all network's nodes converge asymptotically to the same solution and most often the solution is identical to that of an individual and isolated node. Therefore the pressing open problem is to study emergent behaviors different from the classical synchronization which have been scarcely addressed in the literature.
Thereupon, the need of exploring different dynamics emerging from complex networks with scalable number of nodes and arbitrary network architecture (topology) has motivated the study presented here. The work has been carried on by implementing a reconfigurable setup composed of Chua's circuits which is available in the circuits laboratory of University of Napoli Federico II. The setup has been realized the first time in 2011 for the same purpose of network studies, where several small size networks have been examined, although mainly focusing on occurrence of complete synchronization .
The aim of this thesis is to expand the state of the art in complex networks of dynamical systems, by providing novel and insightful experimental results on networks of chaotic Chua's circuits. Contrary to previous works, we have focused on more general emergent dynamics encompassing synchronization, patterns and traveling waves. Particularly, we have experimentally studied cluster synchronization, stimulated by novel theoretical advances based on group theory and network symmetries. Also, the case where the coupling functions between the nodes is dynamic has been addressed. Next, we present a list of the most relevant contributions of the thesis.

(i) We have provided an accurate characterization and modeling of individual Chua's circuits. This will allow to have a detailed description of its dynamics and also it is necessary to obtain a better agreement with theoretical analysis.

(ii) We have automatized some manual configuration in the former setup. Moreover the physical resistors have been replaced by a set of digital potentiometers which has transformed the setup to a compact and elegant form in which the accuracy has been increased and the wiring volume has been reduced. The present setup allows to study fully controllable complex networks with adjustable coupling links and types by which a wide rage of dynamics emerging from such networks can be explored. A large set of data produced by the setup can be monitored and analyzed online with considerable less time consuming process respect to numerical simulation.

The new setup has been characterized completely and emerging of full synchronization, further emergent dynamics like traveling waves and cluster formation as well as role of non-adjacent links have been explored. The experimental observations have been compared with theoretical results by carrying out a local stability analysis of networks with static and dynamic links. Here we use the Master Stability approach (MSF) and its extensions to the case where the links are of dynamic nature (PD-MSF).

(iii) Unlike classical studies on synchronization, we have taken a step forward studying other emergent dynamics, namely cluster synchronization. In particular we have observed and confirmed that clusters are highly related with symmetries on the network topology. Specifically, we have characterized those clusters and also we have exploited symmetries for controlling the patterns.

(iv) We have studied the influence on synchronization when considering different types of links in one network, i.e. coupling via resistors and/or capacitors. We have observed that this multiplex links have a beneficial effect since synchronization can be enhanced when resistor configuration is different from capacitor configuration.

The rest of this work is organized as follows. In the first chapter the fundamentals of nonlinear dynamical systems and complex networks are reviewed. In the second chapter the full description of the setup is given, where a modification of the Chua's circuit model has been proposed according to the experimental realization of the setup. This modified theoretical model for Chua's circuit is necessary for revealing the patterns generated by the experimental setup after loosing synchronization. In the third Chapter the experimental results obtained by various network's coupling is presented and in the last chapter the studies on cluster formation in the network have been reported.

Chapter. 1

Background: nonlinear dynamical systems, complex networks

Interaction among several dynamical systems in a complex way can give rise to such behaviors which cannot be understood by considering only properties of each individual subsystems. It is quite evident how the network architecture and the way agents communicate to each other should play a key role. To better understand the scenario underlying complex network we first review some fundamental concepts. First some important definitions and properties of nonlinear dynamical systems are given to then the focus on network modeling.

1.1. Nonlinear dynamical systems

Modeling, analysis and control of dynamical systems, specifically nonlinear ones are the core of different engineering disciplines [29, 48]. In spite of the availability of strong tools for analyzing dynamical linear systems, based on superposition principle, linear systems are often unable to capture the dynamics of real systems. Sustained oscillations, amplitude dispersion of waves, natural hazards such as earthquakes and cyclonic storms are all examples of nonlinearities. Nonlinear systems have some particular phenomena that cannot be observed in linear models [29]

(i) Finite escape time: tendency of nonlinear systems state to evolve to infinity even in finite time,

(ii) Multiple isolated equilibria: in opposite to linear system which can have a single isolated equilibrium point, nonlinear systems might have more than one equilibrium point. Depending on initial conditions the solution might converge to any of those multiple steady state operating points.

(iii) Limit cycle: nonlinear autonomous systems can oscillate with a fixed amplitude and frequency regardless of the initial conditions.

(iv) Subharmonic, harmonic or almost periodic oscillation: nonlinear systems can oscillate with frequencies with one multiple or sub-multiple of forcing

term, and also in non-periodic mode.

(v) Multiple asymptotic solution: The same nonlinear system might exhibit different solutions for $t \to \infty$.

(vi) chaos and unpredictable behavior in the presence of small variation of the initial conditions.

A nonlinear system can be described by a set of ordinary differential equations (ODE's) of the form [52]

$$\begin{aligned} \frac{dx_1}{dt} =& f_1(x_1, x_2, \cdots, x_n) \\ \vdots \quad & \quad \vdots \\ \frac{dx_n}{dt} =& f_n(x_1, x_2, \cdots, x_n) \end{aligned} \tag{1.1}$$

where $x_i \in \mathbb{R}$ is the ith state variable of the system and $f_i : \mathbb{R} \to \mathbb{R}$ for $i = \{1, \cdots, n\}$ is a scalar smooth function. Equation (1.1) can be rewritten in compact for as

$$\frac{d\mathbf{x}}{dt} = \mathbf{F}(\mathbf{x}) \tag{1.2}$$

where $\mathbf{x} = [x_1, x_2, \cdots, x_n]^T \in \mathbb{R}^n$ is the stack vector of the state variables and $\mathbf{F} = [f_1, f_2, \cdots, f_n]^T : \mathbb{R}^n \to \mathbb{R}^n$ is the system's vector field. The system's fixed point $\mathbf{x}^*$, representing the equilibrium or steady solution, is the point in which the system's states remain forever if the system starts at point. The equilibrium point can be found by setting the left hand side of (1.2) to zero yielding

$$\frac{d\mathbf{x}^*}{dt} \equiv 0 = \mathbf{F}(\mathbf{x}^*) \tag{1.3}$$

Given a fixed point is natural to wonder if starting from an arbitrary initial condition the system will converge to the equilibrium or not. To that aim we next review the fundamental concept of stability in dynamical systems.

1.1.1 Stability of solutions and attractors

The rate of the error growth corresponding to dynamical system's solution when one of the system's parameters, equilibrium points, initial conditions or system's trajectory is perturbed is studied in the concept of stability. Roughly speaking there are two main types of stability

(i) Structural Stability: Characterizing the qualitative behavior of a system respect to varying its parameters. If the qualitative properties of a system like number and stability of fixed points or periodic orbits remain unchanged under small perturbation of the system's parameters the system is said to be structurally stable [29, 52]. By loosing structural stability the system undergoes bifurcation (for example period multiplications of the system' dynamic, exceeding which, result in chaos). The parameters which cause

such transition are called bifurcation parameter and the specific value of bifurcation parameters at which the stability changes is called bifurcation point.

(ii) Lyapunov Stability: Here we are interested is answering the question whether the systems will or not converge to the equilibrium point (or periodic orbit) when the initial conditions are perturbed. Particularly, we have two types o Lyapunov stability, global and local [29]. While local stability guarantees convergence for a set $\Omega \subset \mathbb{R}^n$, global stability ensures convergence for any initial condition.

Definition 1.1.1. An equilibrium point say $\mathbf{x}^*$ of a dynamical system (1.2) is Lyapunov stable if for any $\epsilon > 0$ there exists $\delta > 0$ such that $||\mathbf{x}(0) - \mathbf{x}^*|| < \delta$, then $||\mathbf{x}(t) - \mathbf{x}^*|| < \epsilon$ for all $t \geq 0$. Otherwise, the equilibrium point is unstable

Definition 1.1.2. An equilibrium is attracting if in addition there exist some $\delta > 0$ such that $||\mathbf{x}(0) - \mathbf{x}^*|| < \delta$ implies that $\lim_{t \longrightarrow \infty} \mathbf{x}(t) = \mathbf{x}^*$.

The main and important difference of Definition 1.1.1 and Definition 1.1.2 is that trajectories are allowed to drift away from an attracting equilibrium point in some short time while in long term they have to converge to the equilibrium point. However when an equilibrium is Lyapunov stable the nearby trajectories are restricted to remain close for all the time (t).

Definition 1.1.3. An attracting equilibrium which is Lyapunov stable is called asymptotically stable

All the above definitions determine the local stability. By expanding the condition from the close by trajectories to equilibrium point to all trajectories in the phase plane i.e. if an equilibrium point attract all the trajectories in the phase space and all the trajectories in the phase space remain close to equilibrium point then the equilibrium point is globally attracting and globally Lyapunov stable respectively. It is worth noting that in linear systems the local stability would satisfy the global stability as well. Through this work we have studied the local stability whose relative analysis tools will be reviewed briefly. As long as the perturbations are very small, the system can be approximated as a linear system and local stability can be analyzed by linearization about the equilibrium point as it is described in the following.

Consider system of equation 1.2, then applying small perturbations e about the fixed point $\mathbf{x}^* = [x_1^*, x_2^*, \cdots, x_n^*]^T$ yields

$$\begin{aligned} e_1 &= x_1 - x_1^* \\ e_2 &= x_2 - x_2^* \\ &\vdots \quad \vdots \\ e_n &= x_n - x_n^* \end{aligned} \tag{1.4}$$

The variational equation governing the rate of decay or growth of the perturbation for the i_{th} state is

$$\frac{de_i}{dt} = \frac{dx_i}{dt} = f_i(x_1, x_2, \cdots, x_n) \tag{1.5}$$

From the fact that $f_i(x_i^*) = 0$, and using Taylor series expansion about fixed points equation (1.5) can be rewritten as

$$f_i(e_1+x_1^*, e_2+x_2^*, \cdots, e_n+x_n^*) = f_i(x_1^*, x_2^*, \cdots, x_n^*) + \frac{\delta f_i}{\delta x_1}e_1 + \frac{\delta f_i}{\delta x_2}e_2 + \cdots + \frac{\delta f_i}{\delta x_n}e_n$$

For very small perturbations the quadratic terms can be ignored; therefore, we can rewrite the error dynamics (1.5) as

$$\begin{bmatrix} \frac{de_1}{dt} \\ \\ \frac{de_2}{dt} \\ \vdots \\ \frac{de_n}{dt} \end{bmatrix} = \underbrace{\begin{bmatrix} \frac{\partial f_1}{\partial x_1} & \frac{\partial f_1}{\partial x_n} & \cdots & \frac{\partial f_1}{\partial x_n} \\ \\ \frac{\partial f_2}{\partial x_1} & \frac{\partial f_2}{\partial x_n} & \cdots & \frac{\partial f_2}{\partial x_n} \\ \vdots & \vdots & \ddots & \vdots \\ \frac{\partial f_n}{\partial x_1} & \frac{\partial f_n}{\partial x_2} & \cdots & \frac{\partial f_n}{\partial x_n} \end{bmatrix}}_{\mathbf{A}} \begin{bmatrix} e_1 \\ \\ e_2 \\ \vdots \\ e_n \end{bmatrix} \tag{1.6}$$

where matrix $\mathbf{A} \in \mathbb{R}^{n\times n}$ is the Jacobian matrix whose eigen values determine the stability of the fixed point. Stable equilibrium requires decay of all disturbances which means the real part of all eigen values of the systems must be strictly negative. Positive real part of minimum at least one eigen value destabilize the equilibrium point. Consequently the fixed point to which all nearby solutions converge is called *sink* and the one from which all the solutions repel is known as *source* and if some solutions approach to the equilibrium point and some repel from it then the equilibrium point is *saddle*.

On the other hand, if the solutions end up in a closed orbits centering the equilibrium point then is termed as *center* [52]. An equilibrium point whose all eigen values of its jacobian matrix have non-zero real part is called Hyperbolic. The qualitative behavior of the solution near to degenerate fixed points which has at least one eigen value with zero real part are highly vulnerable tof bifurcation since such nodes changes their properties like stability or even existence by a small perturbation. Stability of degenerate fixed points is determined by Lyapunov function which is not the focus of this studies.

The study of stability can be also extended to a broader type of solutions, namely orbit. Next we give some definitions for the stability of the orbit which would be referred as orbital stability.

Definition 1.1.4. [57] An orbit $\mathbf{x}(t)$ with initial condition $\mathbf{x}(0) = \mathbf{x}_0$ is orbitally stable if all orbits $\hat{\mathbf{x}}(t)$ with nearby initial points $\hat{\mathbf{x}}_0 = \mathbf{x}_0 + \Delta x_0$ remain close to it forever. By definition $\mathbf{x}(t)$ is orbitally stable if for any $\epsilon > 0$ there exist a $\delta > 0$ such that $\|\mathbf{x}_0(t) - \hat{\mathbf{x}}_0(t)\| < \delta$ then $\|\mathbf{x}(t) - \hat{\mathbf{x}}(t)\| < \epsilon$ for $t \geq 0$.

It is important to emphasize that, the exponential separation rate of two initially close orbits can be quantified by the so called Lyapunov exponent λ which is defined for continuous systems as

$$\lambda = \lim_{t\to\infty} \lim_{\Delta x_0 \to 0} \frac{1}{t} \ln \frac{\Delta x(x_0, t)}{\Delta x_0} \tag{1.7}$$

while for discrete time system $x_{n+1} = f(x_n)$ the equation would be translated as

$$\lambda = \lim_{k\to\infty} \frac{1}{k} \sum_{i=0}^{k-1} \ln |f'(x_i)| \tag{1.8}$$

It is important to emphasize that for a linearized system about a equilibrium point, the Lyapunov exponents coincide with the eigen values of its Jacobian matrix.

Similarly to the linear case, stability of the orbits are classified according to the sign of the Lyapunov exponent. Specifically, if the Lyapunov exponent is negative, that is, $\lambda < 0$ indicates the the orbit or equilibrium point is stable, while $\lambda = 0$ indicates a conservative system without dissipation with the state of Lyapunov stability. Finally, $\lambda > 0$ shows the unstability of the orbit.

To determine whether a system is chaotic, degree of divergence of its solution in the presence of tiny error in initial condition can be measured using Lyapunov Exponents. This identifies the sensitive dependence of a system. Positive Lyapunov Exponent verifies the state of chaos in dynamical system (i.e. diverging to a completely different solution even if two trajectories have started from very close initial conditions) and a system with all negative Lyapunov exponent will have either an attracting fixed point or a periodic cycle and will not behave chaotically [2].

1.1.2 Bifurcations

As previously mentioned, bifurcation is the transition of the structure of the system's dynamic when the system's parameter has been perturbed. In fact changing bifurcation parameter changes the system property qualitatively such as number of system's fixed points or their stability. Creation or destruction of fixed point due to changing a system parameter is known as saddle node bifurcation and when fixed points appear or disappear in a symmetrical pairs the term changes to pitchfork bifurcation. Fixed points can remain while their stability might changes which is called Hopf bifurcation where in the close vicinity of those fixed points their stability is determined via eigen values of the Jacobian matrix [52]. Hopf bifurcation will be recalled when Chua's characteristic is explained.In general those bifurcations which occurs by changes in the stability of eqilibrium points are classified as local bifurcations in which the bifurcations mentioned above are included.

1.2. Chua's circuit as a paradigm for chaos

Analysis and control of non-linear systems are more complicated than linear ones and necessitate a deep understanding of their dynamics. Accordingly the need to study and manipulate such systems has been a motivation for the invention of autonomous Chua's circuit in 1983 as the first physical platform for reproducing chaos and nonlinear dynamics. This chaotic circuit is the simplest electronic circuit which can be realized at low cost, producing rich dynamic from the periodic

one by cascade of double period bifurcation and ending to chaos as the result of varying its bifurcation parameters. Chua's circuit has been used for decades and is still a unique tool for understanding and analyzing nonlinear dynamics and chaos. The schematic of Chua's circuit is shown in figure 1.1a. Chua's circuit is

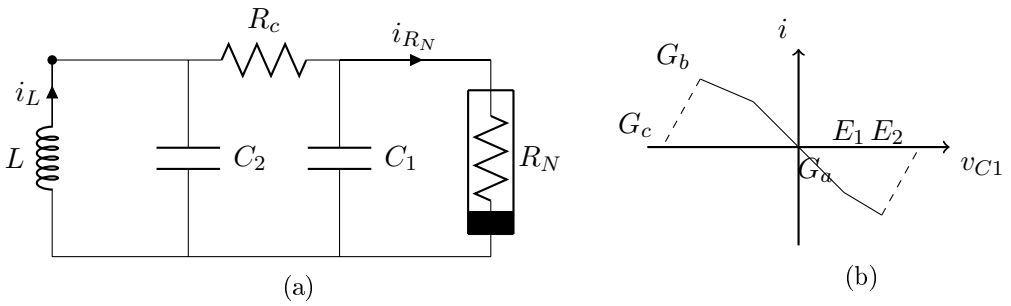

Figure 1.1: (a) Schematic of Chua's circuit, (b) Chua's diode characteristic

described by a set of ordinary differential equations as

$$\begin{cases} \dfrac{di_L}{dt} = -\dfrac{1}{L} v_{C2} \\ \dfrac{dv_{C2}}{dt} = \dfrac{G}{C_2}[v_{C1} - v_{C2}] + \dfrac{1}{C_2} i_L \\ \dfrac{dv_{C1}}{dt} = \dfrac{G}{C_1}[v_{C2} - v_{C1}] - \dfrac{1}{C_1} i(v_{C1}) \end{cases} \tag{1.9}$$

where i_L, v_{C1}, v_{C2} are the state variables corresponding to the inductor's current and voltages on the capacitors C_1 and C_2 respectively.$G = 1/R_c$. It's noteworthy that since the first realization of Chua's circuit, several efforts has been carried out to generalize the circuit aiming to have the simplest synthesis which generates the most complex dynamic. As a result among all Chua's circuit families a canonical form of it is realized so far by adding a resistors in series with inductor and is called Chua's oscillator to distinguish it from the original Chua's circuit [9]. Chua's oscillator is prototypical since it can reproduce any dynamics generated by systems of continuous odd symmetric three regions piecewise linear vector field.

1.2.1 Piecewise linear classical model

Birth of Chaos is the result of infinitely continuous stretching and folding of dynamical system's trajectories. In particular, piecewise-linear circuits can generate chaos they have at least two unstable equilibrium points to provide stretching by one and folding trajectories by the other equilibrium point [19, 28]. Such conditions are feasible for autonomous circuits if they satisfy three fundamental properties listed below

(i) presence of at least one nonlinear element

(ii) having a locally active asymptotically passive resistor

(iii) presence of at least three energy storage elements (third order system).

Presence of an ad hoc voltage-controlled nonlinear locally active resistor known as Chua's diode as well as three storage elements facilitate Chua's circuit by this properties and create the possibility of generating chaos steady state solution by this circuit. Chua's diode driving point characteristic shown in figure 1.1b is characterized in such a way to exist at least two unstable equilibrium points to satisfy the condition of generating chaos. Chua's diode characteristic is described by the following equations:

$$i(v_{C1}) = \begin{cases} G_c v_{C1} + E_1(G_a - G_b) + E_2(G_b - G_c) & E_2 < v_{C1} \\ G_b v_{C1} + E_1(G_a - G_b) & E_1 < v_{C1} \leq E_2 \\ G_a v_{C1} & |v_{C1}| \leq E_1 \\ G_b v_{C1} + E_1(G_b - G_a) & -E_2 \leq v_{C1} < -E_1 \\ G_c v_{C1} + E_1(G_b - G_a) + E_2(G_c - G_b) & v_{C1} < -E_2 \end{cases} \tag{1.10}$$

where $G_a\,, G_b < 0$ and $G_c > 0$. The outer parts G_c would guarantee the eventually passivity of the element since for the large enough voltage across the real resistor its absorbed power $P = v * i$ is positive and characteristic must locate in the first and third quadrant of the $v - i$ plane. However on the condition that Chua's attractor is bounded in the active region those outer segments will not influence on Chua's circuit dynamics. The normalized dimensionless form of Chua's equations aiming to reduce the number of parameters and scaling them to ease the numerical analysis the equations, can be obtained by rescaling the state variables and defining new parameters as

$$x = \frac{v_{C1}}{E_1} \qquad y = \frac{v_{C2}}{E_1} \qquad z = \frac{i_L}{E_1 G} \qquad \tau = \frac{tG}{C_2}$$
$$\alpha = \frac{C_2}{C_1} \qquad \beta = \frac{C_2}{LG^2} \qquad a = \frac{G_a}{G} \qquad b = \frac{G_b}{G} \qquad c = \frac{G_c}{G}$$

$$\begin{cases} \dfrac{dz}{d\tau} = -\beta y \\ \dfrac{dy}{d\tau} = x - y + z \\ \dfrac{dx}{d\tau} = \alpha(y - x) - \alpha i(x) \end{cases} \tag{1.11}$$

where

$$i(x) = \begin{cases} cx + a - b + \dfrac{E_2}{E_1}(b-c) & \dfrac{E_2}{E_1} < x \\ bx + a - b & 1 < x \leq \dfrac{E_2}{E_1} \\ ax & |x| \leq 1 \\ bx + b - a & -\dfrac{E_2}{E_1} \leq x < -1 \\ cx + b - a + \dfrac{E_2}{E_1}(c-b) & x < -\dfrac{E_2}{E_1} \end{cases} \tag{1.12}$$

Chua's circuit has three equilibrium points; $\mathbf{x}^*_-$ and $\mathbf{x}^*_+$ on the outer negative and positive regions respectively, and $\mathbf{x}^*_0$ in the origin, which are

$$\mathbf{x}^*_- = \begin{bmatrix} \dfrac{G(G_b - G_a)}{G + G_b} E_1 \\ 0 \\ \dfrac{G_a - G_b}{G + G_b} E_1 \end{bmatrix} \qquad \mathbf{x}^*_0 = \begin{bmatrix} 0 \\ 0 \\ 0 \end{bmatrix} \qquad \mathbf{x}^*_+ = \begin{bmatrix} \dfrac{G(G_a - G_b)}{G + G_b} E_1 \\ 0 \\ \dfrac{G_b - G_a}{G + G_b} E_1 \end{bmatrix}$$

All the eigenvalues of equilibrium points are shown in figure 1.2 for R_{chua} ranged from 1500Ω to 2000Ω where the arrows point toward the direction of increasing R_c. By increasing R_c the stability of outer equilibrium points changes since the sign of the real part of their complex eigenvalue become positive and unstable and results in Hopf bifurcation.

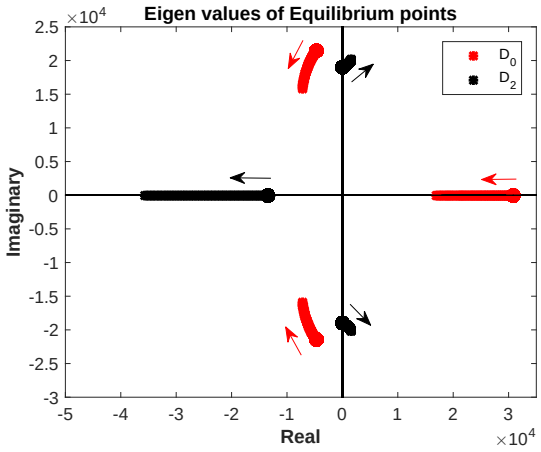

Figure 1.2: Eigen values of Chua's circuit's equilibrium points (D_0 indicates the eigenvalues belong to the equilibrium point in the origin and D_2 corresponds to the equilibrium points of the outer regions whose eigenvalues are the same.)

1.2.2 Typical complex dynamics

To find Chua's circuit solution, piece-wise linear characteristic of Chua's circuit allow us to analyze each region separately, then the overall solution can be found by putting together all of them. The first step to study system's dynamic is calculating the equilibrium points. Then in each region the system is linearized about its equilibrium point where the stability of dynamics nearby the equilibrium point is determined by calculating the eigenvalues of the system Jacobian matrix $\mathbf{A}$. We wish to emphasize that $\mathbf{A}$ has one real eigenvalue λ associated to the the eigenvector $\mathbf{E}^r$ and a pair of complex conjugate $\sigma \pm j\omega$ spanning the corresponding eigen-plane $\mathbf{E}^c$. Therefore, the solution of the circuit can be expressed as the the sum of two solutions $\mathbf{x}_r(t)$ belonging to $\mathbf{E}^r$ and $\mathbf{x}_c(t)$ to $\mathbf{E}^c$ as

$$\mathbf{x}_r(t) = C_r e^{\lambda t}\mathbf{x}_\lambda \tag{1.13}$$

$$\mathbf{x}_c(t) = 2C_c e^{\sigma t}[cos(\omega t + \phi)\mathbf{x}_{cr} - sin(\omega t + \phi)\mathbf{x}_{ci}] \tag{1.14}$$

Then if $\lambda > 0, \mathbf{x}_r(t)$ grows exponentially other wise if $\lambda < 0, \mathbf{x}_r(t)$ converge asymptotically to zero both in direction of $\mathbf{E}^r$. For the complex conjugate pair if $\sigma > 0$ and $\omega \neq 0, \mathbf{x}_c(t)$ spirals away from the corresponding equilibrium point along the complex eigen-plane and in the opposite case i.e. $\sigma < 0, \mathbf{x}_c(t)$ spirals toward equilibrium point along the eigen-plane $\mathbf{E}^c$. Table 1.1 shows Chua's simulated circuit solutions when R_c decreases from 1970Ω to 1965Ω, 1945Ω and 1915Ω. Note that by decreasing R_c the Chua's circuit's dynamic undergoes structural changes ranging from limit cycles to chaotic double scroll due to the changes of the stability of the equilibrium points.

Table 1.1: Simulated Chua's circuit dynamics for $R_c = 1970\Omega, 1965\Omega$, 1945Ω and 1915Ω

Inductor model	
1970Ω	1965Ω
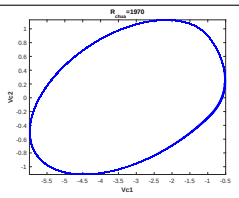	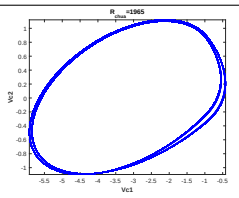
1945Ω	1915Ω
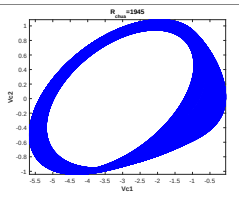	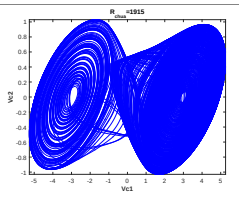

For the sake of completeness we also calculate a bifurcation diagram and Lyapunov exponent diagram of Chua's circuit when R_c is varied in a decreasingly manner from 2000Ω to 1600Ω. The results are shown in figure 1.3.

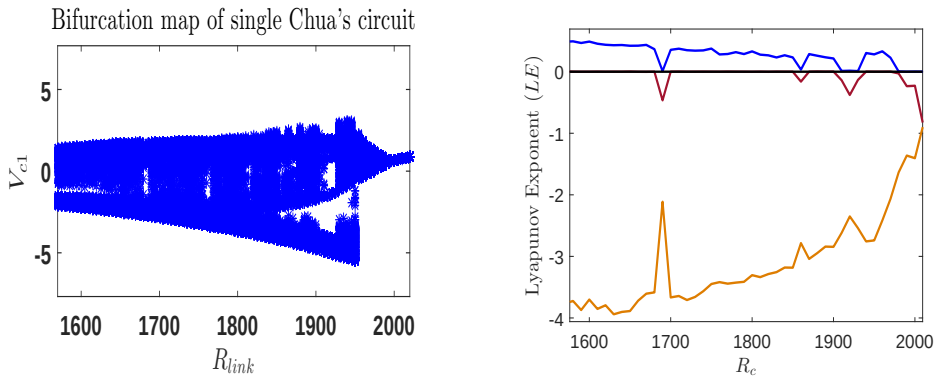

(a) (b)

Figure 1.3: Single Chua's circuit a)bifurcation diagram b)Lyapunov exponents diagram

1.3. Complex networks

Real world systems are mainly characterized by being the integration of interacting components whose collective behavior can significantly differ from their individuals. Underlying those complex systems there is an intricate structure of interconnections that affects its behavior. In figure 1.4 some examples of complex networks are shown. It is no a secret that complex systems have great benefits

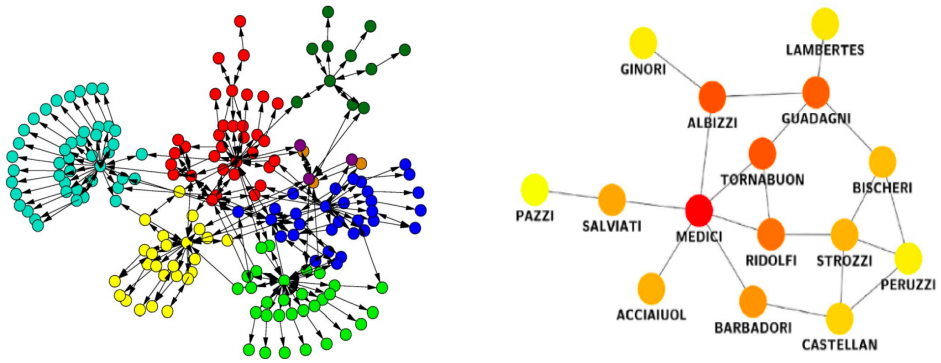

(a) (b)

Figure 1.4: Examples of complex networks: (a) Pages on a web site and the hyperlinks between them [35] (b) Florentine marriages network [3]

in many aspects such as spreading information in world wide web or flow of energy in power distribution networks [4]. Nevertheless these systems are highly vulnerable and delicate since a single interacting component can have impact in all the network and failure in one part of the systems can be spread all over the network through the inter-connectivity and cause to black out and significant defragmentation of the whole complex systems. Therefore it is of great importance to inspect the structure and configuration through which all the sub-

systems interact as well as collective behavior and properties of the members of the network. In this regard the connectivity of each complex system can be described efficiently by a complex network $\{N, L\}$ where nodes (N) represent the subsystems and connections are modeled by links (L).

Complex networks are strong representations of complex systems for the purpose of inspecting the structure of interaction so that possibly approaching a description of collective behavior emerging from complex systems which has been a scientific challenge for decades in network science and all the involved disciplines. Complexity in complex Networks can be described from different standpoints ranging from the mode and number of inter-communications among subsystems to their intricate character. Complex networks connectivity structure can be complicated or change over the time where some links might appear, disappear or their features might vary. Moreover system's components might interact differently when the links which connect them are different in features like weight and direction. Additionally components can be nonlinear systems or diverse and network might be composed by non-identical systems.

1.3.1 Modeling network structure and graph theory

Different types of complex network (structured interactions) from economical to biological and many more are being studied using graph theory by which any of them can be modeled effectively by a graph as a mathematical description.
Graphs $\mathscr{G} = (V, L)$ are mathematical structures composed by two sets of elements; set of N vertices $V = \{n_1, n_2, n_N\}$ as individual units and set of k edges $L = \{l_1, l_2, l_k\}$, for $0 < k < N(N-1)/2$ representing the link among each pair of nodes. l_{ij} is the link connecting a pair of adjacent nodes i and j. For example a network of four interconnected computers is shown in figure 1.5a, while in figure 1.5b it is shown the the graph representation $\mathscr{G}$ with four nodes and four vertices.

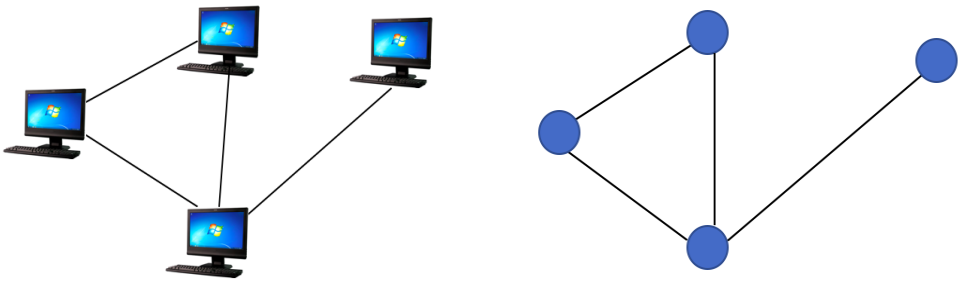

(a) (b)

Figure 1.5: Examples of (a) a network of computers, and (b) its graph representation.

When a graph $\mathscr{G}$ is *undirected* the incident connection between each two nodes is mutual and bidirectional (see figure 1.4b), while in *directed* graphs two connected nodes are sequentially ordered i.e. $l_{ij} \neq l_{ji}$ (see figure 1.4a). Connection from

a node to itself (loop) and more that one link between two nodes are beyond definition of graph and such structure is called multi-graph. Each node can be characterized by its size which is the number of connected links to it.
Graphs can be classified by different criteria. One is the number of links in the graph i.e. k. A graph is *sparse* if $k \ll N$ and is dense if number of links is close to the maximum number of links. A graph whose number of links $k = N(N-1)/2$ i.e there is link between every pair of nodes, is called complete.
If for every pair of distinct nodes there exist a path linking all the nodes in the network; then, then the graph is called *connected*; otherwise, it is *disconnected*. We can also associate to every every link in a graph a weight, in this case the graph is called *weighted graph*.
The connectivity in an un-weighted graph is represented by the *Adjacency matrix* $\mathbf{A}_{N\times N}$ whose elements $a_{ij} = 1$ if nodes i and j are connected; otherwise, $a_{ij} = 0$. For undirected graphs matrix $\mathbf{A}$ is symmetrical, while it might be asymmetrical if the graph is directed. Instead a weighted graph is represented by a connectivity matrix W whose entries $\sigma_{ij} > 0$ if nodes i and j are connected and $\sigma_{ij} = 0$ otherwise.
Both connectivity and node's degree of a graph are captured by the *Laplacian matrix* $L \in \mathbb{R}^{N\times N}$ whose off-diagonal entries are given by $L_{ij} = -a_{ij}\sigma_{ij}, \quad \text{for} \quad i \neq j$, while diagonal entries $L_{ii} = \sum_{j=1}^{N} a_{ij}\sigma_{ij}$. It is important to emphasize that Laplacian matrix representing undirected graphs $\mathscr{G}$ are symmetric and positive semi-definite matrices whose eigenvalues can be sorted in ascending order $\lambda_1 \leqslant \lambda_2 \leqslant \cdots \leqslant \lambda_N$. Note that the sum of rows and columns of the Laplacian matrix are always zero.

1.3.2 Emerging dynamics

As mentioned earlier interacting systems behave differently from their individual dynamics when they are isolated. As a matter of fact collective behavior is not only a function of subsystem's dynamic but also of the structure of the network through which they interact. Consider a network composed by N coupled oscillators which can be described as

$$\frac{d\mathbf{x}_i}{dt} = \mathbf{F}_i(\mathbf{x}_i(t)) + \sum_{j=1}^{N} \sigma_{ij} a_{ij} \mathbf{H}(\mathbf{x}_i, \mathbf{x}_j) \qquad i \in \{1, \cdots, N\} \tag{1.15}$$

where $\mathbf{x}_i = [x_1, \cdots, x_n]$ and $\mathbf{F}_i(\mathbf{x}_i(t)) = [f_1(\mathbf{x}_i(t)), \cdots, f_n(\mathbf{x}_i(t))]$ are the n-dimensional state vector and vector field of the i_{th} oscillator respectively. Vector field $\mathbf{F}_i(\mathbf{x}_i(t))$ describe the dynamic of the ith node. The coupling strength of each link is denoted by σ_{ij} which is associated to nodes i and j. The coupling matrix $\mathbf{A} = [a_{ij}] \in \mathbb{R}^{N\times N}$ describes the connectivity between nodes where $a_{ij} = 1$ if nodes i and j are connected and $a_{ij} = 0$ otherwise. $\mathbf{H}(\mathbf{x}_i, \mathbf{x}_j)$ denotes the coupling function between nodes i and j i.e the operator which connect each two nodes.

Aiming to studying of collective behavior as a function of network parameters like structure, coupling strength as well as node's dynamics, it is often consid-

ered a simplified model by assuming a homogeneous networks whose nodes are nominally identical i.e. $\mathbf{F}_1(\mathbf{x}_1(t)) = \mathbf{F}_2(\mathbf{x}_2(t)) = \cdots = \mathbf{F}_N(\mathbf{x}_N(t)) = \mathbf{F}(\mathbf{x}_i(t))$. We further assume the coupling between nodes to be bidirectional with identical coupling strengths, that is $\sigma_{ij} = \sigma$ for all $i, j \in \{1, \cdots, N\}$. In this case the adjacency matrix $\mathbf{A}$ is symmetric whose entries are either zero or one and are scaled by the coupling strength σ. The simplified model of network (4.1) reads

$$\frac{d\mathbf{x}_i}{dt} = \mathbf{F}(\mathbf{x}_i(t)) + \sigma \sum_{j=1}^{N} a_{ij}\mathbf{H}(\mathbf{x}_i, \mathbf{x}_j) \qquad i \in 1, \cdots, N \tag{1.16}$$

This model is used to described many coupled oscillators [33, 51]. Depending on the network's features such as topology, coupling strength and dynamic of nodes, the behavior of subsystems and their coherency respect to other members with which they interact direct or indirect varies. Components can evolve equally and synchronously as they pass through a transient time or keep different types of relativity such as phase locking in oscillators known as phase synchronization. Contrarily systems can be connected in the network but evolve in a way if they are not physically connected to any other node.

1.3.3 Synchronization

One important collective behavior which has been the focus of many network studies is synchronization, which is widely seen in natural and artificial networks. Synchronization can be as an essential property for proper functioning of many networks when coordination is required such as power distribution networks and neural network of the brain for information processing [51]. There are several definitions for synchronization regarding to the types of coordination among nodes and some of them are been reviewed here.
Two nodes i and j are considered to be completely synchronized if they converge to the same solution as they evolve in time, i.e

$$\lim_{t\to\infty} ||\mathbf{x}_i(t) - \mathbf{x}_j(t)|| = 0 \tag{1.17}$$

Similarly the state of complete or asymptotic synchronization in a network happens if all nodes of a network converge to the same solution $\mathbf{x}_s(t)$, i.e. $\mathbf{x}_1(t) = \mathbf{x}_2(t) = \cdots = \mathbf{x}_N(t) = \mathbf{x}_s(t)$. This subspace is termed as *synchronization manifold* $\mathcal{S}$ and is defined as

$$\mathcal{S} := \{\mathbf{x} \in \mathbb{R}^N | \quad ||\mathbf{x}_i(t) - \mathbf{x}_j(t)|| = 0 \ \forall i, j \in 1, \cdots, N\} \tag{1.18}$$

where $\mathbf{x}_i(t)$ belongs to this synchronous manifold if

$$\lim_{t\to\infty} ||\mathbf{x}_i(t) - \mathbf{x}_s(t)|| = 0$$

Complete synchronization can be seen for networks with identical nodes otherwise in the presence of any parameter mismatch nodes can tend to a very close vicinity

of synchronization manifold but not to the exact manifold. This tendency is termed as *Bounded synchronization* which can be defined as

$$\lim_{t\to\infty} ||\mathbf{x}_i(t) - \mathbf{x}_j(t)|| \leq \epsilon \quad \text{for} \quad \epsilon > 0, \forall i \in \{1, \cdots, N\} \tag{1.19}$$

In addition to complete and bounded synchronizations the members of a network can reach to the same synchronization manifold by delay respect to one another, the state known as lag synchronization i.e.

$$\mathbf{x}_i(t+\tau) = \mathbf{x}_j(t)$$

In the coupled oscillators synchronization might appear among only oscillators phases where all remain identical or nearly identical in phase while they are weakly or not correlated in the amplitude [7]. All discussed synchronous states have been studied and observed in this experimental studies which will be reported in the corresponding chapter.

1.3.4 Clustering and group theory

In spite of the complete synchronization importance, transition to its opposite state is the introduction to intricate diversities. This transition mechanism in the network is strongly influenced by different network parameters. However the phenomena is not completely understood yet. Recent studies have tried to shed light on the network behavior beyond the complete synchronization [21, 42, 50]. It has been observed in many complex networks that by loosing complete synchronization state, network nodes start diverging from the manifold of complete synchronizations while partitioning into patterns of several so called clusters. Those nodes belonging to the same clusters are synchronized while the ones from different clusters are loosely or not correlated. We denote the synchronous trajectory of each cluster as $\mathbf{x}_{s'_m}(t)$. In particular, the synchronous manifold of the m_{th} cluster can be defined as

$$\mathcal{S}'_m := \{\mathbf{x} \in \mathbb{R}^{M_k} | \quad ||\mathbf{x}_j(t) - \mathbf{x}_i(t)|| = 0 \quad \forall\, i, j \in M_k\} \tag{1.20}$$

where $\sum_{k=1}^{m} M_k = N$ and m is the number of clusters and i_{th} node belongs to m_{th} cluster if

$$\lim_{t\to\infty} ||\mathbf{x}_i(t) - \mathbf{x}_{s'_m}(t)|| = 0$$

It has been revealed such clustering is closely related to the structure of the network in particular when the structure is symmetric [42]. Fortunately, with the aid of tools such as group theory the network elements tendency to diverge from the global synchronous manifold and partition in sub-synchronous manifold has been partially inferred.

1.3.4.1 Group theory

In this section the introductory group theory is reviewed following by the concept of symmetry.
A group $< G, * >$ is a non-empty set G with a binary operation $(*)$ which satisfies the following axioms:

(i) Closure; $\forall x, y \in G \Rightarrow x * y \in G$

(ii) Associativity; $\forall x, y, z \in G \Rightarrow x * (y * z) = (x * y) * z$

(iii) Identity $\forall x \in G \; \exists e \in G \ni x * e = e * x = x$

(iv) Inverse $\forall x \in G \exists x^{-1} \in G \ni x * x^{-1} = x^{-1} * x = e$

For a group $(G, *)$ identity and inverse elements are unique.

Definition 1.3.1. In addition Abelian group is a group which satisfies commutativity i.e. $\forall x, y \in G \Rightarrow xy = yx$.

Definition 1.3.2. Definition 2. For a group $< G, * >$, Number of elements in the group is called order of the group denoting by $|G|$.

Definition 1.3.3. Definition 3. For a group $(G, *)$ if there exist a non-empty subset H of G such that $(H, *)$ is also a group then H is a subgroup of G . The trivial subgroup of any group is formed by a set formed by identity element only. Order of the subgroup is always is smaller or equal to its corresponding group i.e. $|H| < |G|$

Definition 1.3.4. Definition 4. The order of an element g denoted by $|g|$ in a group G is the smallest positive integer k such that $g^k = e$ where e is the identity element. If such k does not exist then the order of the element g is infinite.

Generally groups are classified into two groups of finite and infinite; A group G is finite if it contains finite number of elements otherwise the group is Infinite . Set of real numbers, rational numbers, integer numbers and complex numbers each one under addition form a group denoted by $< R, + >, < Q, + >, < Z, + >$ and $< C, + >$ respectively as examples of infinite groups. $< R^+, . >$ represents the infinite group of positive real numbers under multiplication. The finite cyclic groups and symmetric groups are the well-known examples of finite groups.
If A group $< G, * >$ with finite number of elements where $|G| = n$ contains an element g with $|g| = n$ where there is no $k > 0$ smaller such that $g^k = e$. Then the group is described as $\{e, g, g^2, \cdots, g^{n-1}\}$ where g is called a generator of the group $< G, * >$ and is written as $G =< g >$. Such a group is called cyclic group which is an abelian group and is generated by single element g. symmetric groups: All permutations of a set <G> composed by n elements form a group under composition which is called symmetric group denoted by S_n. The order of S_n is $n!$ where n is the number of elements in the group. $|S_n| = n!$ group of network symmetries. All those symmetry operations on the network of N nodes which leaves the network structure and dynamical equations unchanged form a group G under composition. Symmetry operations can be identity I; where just leave the structure unchanged, mirror reflection M, rotations of different angles

r, or combination of these operations Group representation: Representation of a group is a set of invertible linear transformations of vector spaces which is a tool to represent the group elements in terms of matrices consequently indicating the group operations by matrix multiplications [22]. Group representation is important since it facilitates the problems of group theory by linear algebra. Irreducible representation. If representation of a group can not be reduced to a subspace linear transformations then is called irreducible in the other words a group representation that has no nontrivial invariant subspaces.
Each symmetry operation g of the network can be presented by a permutation matrix $\mathbf{P}_g$; an N dimensional binary matrix having an entry of $p_{ij} = 1$ in each row where the exchange of nodes i and j does not vary the structure and 0 anywhere else. By symmetry $p_{ij} = p_{ji} = 1$ which implies that this $\mathbf{P}_g$ is symmetric where $\mathbf{P}\mathbf{P}^{-1} = \mathbf{P}^2 = \mathbf{I}_{N\times N}$. The permutation matrices can be decomposed if there exist a similar matrix $\mathbf{M}$ such that $\mathbf{M}^{-1}\mathbf{P}_g\mathbf{M} = \mathbf{P}'_g$ where $\mathbf{P}'_g$ is the equivalent representation of $\mathbf{P}$ which is decomposed to k matrices given by

$$\mathbf{P}'_g = \begin{bmatrix} \mathbf{P}_g^1 & 0 & \cdots & 0 \\ 0 & \mathbf{P}_g^2 & \cdots & 1 \\ \vdots & \vdots & \ddots & \vdots \\ 0 & 0 & \cdots & \mathbf{P}_g^k \end{bmatrix} \tag{1.21}$$

dimension of $\mathbf{P}_g$ is the sum of dimensions of sub-matrices of $\mathbf{P}'_g$ i.e. The orbit of a node $\mathbf{x}_i$ in the network topology is the set of all nodes in the network by which *ith* node can be permuted leaving the topology unchanged. Consequently the clusters in the network are identified by finding all the orbits in all representations of symmetry groups of the network.

$$dim(\mathbf{P}_g) = \sum_{l=1}^{k} dim(\mathbf{P}_g^l)$$

Each cluster is characterized by its corresponding synchronous manifold $\mathcal{S}'_k$ ($k = 1, \cdots, \mathrm{M}$ where M is the number of clusters) to which all the nodes dynamics belonging to that cluster converge. If N is considered as the number of nodes $M = N$ when there is not any pair of synchronized nodes. In this work different topology has been examined and the role of network symmetry has been explored as well as changing parameters such as connectivity and coupling strength in the transition from or toward global synchronization.

1.4. Metrics for detecting synchronization

Synchronization among corresponding state variables of each node can be quantified by evaluating the correlation between them where depending on the network properties, node's correlations can vary. In a network of oscillators complete synchronization occurs when all network's components oscillate with identical amplitude and phase. We consider network (1.16) and we assume that only there is available a scalar measurement $y_i(t) = \Gamma\mathbf{x}_i(t)$ for each node $i \in \{1, \cdots, N\}$, where Γ is the output matrix.

In this study two indexes have been used to compute the level of synchronization termed as "cross correlation index (I_{CC})" and "synchronization index (I_S)" which are described below

(i) Cross correlation index (I_{cc}) has been applied to quantify the degree of synchronization particularly the correspondence among oscillator's phase.

$$I_{cc}(y_i, y_j) = \frac{\sum_{k=1}^{N_s} [y_i(k) - \overline{y_i}]\,[y_j(k) - \overline{y_j}]}{\sqrt{\sum_{k=1}^{N_s} [y_i(k) - \overline{y_i}]^2\,[y_j(k) - \overline{y_j}]^2}} \tag{1.22}$$

where $\overline{y_i} = \frac{1}{N_s}\sum_{k=1}^{N_s} y_i(k) \quad i = 1, \cdots, N$ is the mean value of the dynamic of the i_{th} node. If $y_i = y_j$ which means y_i, y_j are synchronized then

$$I_{cc}(y_i, y_j) = \frac{\sum_{k=1}^{N_s} [y_i(k) - \overline{y_i}]^2}{\sqrt{\sum_{k=1}^{N_s} [y_i(k) - \overline{y_i}]^4}} = 1 \tag{1.23}$$

Similarly $I_{cc} = -1$ when two signals are opposite and $I_{cc} = 0$ shows no correlation among two signals. The general form of I_{cc} for $N > 2$ signals is:

$$I_{cc} = \frac{1}{N}\sum_{i=1}^{N} I_{cc}(x_i, \overline{x}) \tag{1.24}$$

where $\overline{y(k)} = \frac{1}{N}\sum_{i=1}^{N}(y_i(k) - \overline{y_i})$

(ii) Synchronization index (I_s) measures the rms distance of trajectories $y_i(t)$ at ith node from the "average" trajectory $\langle y(t)\rangle$ expressed in percentage

$$I_s = 100\sqrt{(\frac{1}{NN_s}\sum_{i=1}^{N}\sum_{k=1}^{N_s}(\frac{|y_i^k - \langle y(t)\rangle|}{|y_{max} - y_{min}|})} \tag{1.25}$$

where N is the number of nodes (Chua's circuits), N_S the number of (measured) samples and $y_{max} - y_{min}$ is a normalizing factor for each set of measurements. Such percent distance index approaches zero when all traces are fully synchronized, and 100% when they are completely uncorrelated, and synchronization is completely lost in phase and amplitude.

1.5. Stability analysis of synchronous solutions

1.5.1 Master stability function approach (MSF)

It is of the great importance to characterize synchronous behavior of the network and to know when and under what conditions respect to network parameters, network is able to keep the coordination among its nodes. Answering to this question

necessitate the stability analysis of the network. A well-known approach to carry such analysis of linearly coupled networks is Master stability function (MSF) [41] which is a tool for stability analysis of synchronization as a function of network topology, coupling strength, coupling function and nodes dynamics knowing only the individual dynamic of nodes and network coupling function. This approach is based on measuring the evolution or exponential growth rate of an infinitesimal perturbation on the transverse subspace to synchronization manifold. The common criterion to obtain MSF is measuring the maximum Lyapunov exponent of small fluttering of those solutions transverse to synchronization manifold. Master stability function requires the following assumptions:

(i) the coupled nodes of the network are all identical.

(ii) all node's output are coupled with the others through the same function.

(iii) the manifold of synchronization is invariant; any node initiate evolving from synchronous manifold will remain in the manifold for all time t.

(iv) the coupling between nodes is arbitrary and is approximately linear in the vicinity of synchronous state.

Considering equation (1.16) for a network of identical nodes which are coupled via equal coupling strength the adjacency matrix can be replaced by laplacian matrix $L = [l_{ij}] \in \mathbb{R}^{N\times N}$ as

$$\frac{d\mathbf{x}_i}{dt} = \mathbf{F}(x_i) + \sigma \sum_{j=1}^{N} L_{ij}\mathbf{H}(\mathbf{x}_j),\ i = \{1, \cdots, N\} \tag{1.26}$$

where $\mathbf{L}$ is symmetric and every row sum and column of Laplacian matrix is zero i.e.

$$\sum_{j=1}^{N} L_{ij} = 0 \qquad \text{which means} \qquad \sum_{j=1, j\neq i}^{N} L_{ij} = -L_{ii} \tag{1.27}$$

For the system described by equation (1.26), it is assumed that there exists a synchronous solution $\mathbf{x}_s(t)$ which is the same as nodes' individual solution i.e $\mathbf{x}_s(t) = \mathbf{x}_1(t) = \mathbf{x}_2(t) = ...\mathbf{x}_N(t)$ such that $\dot{\mathbf{x}}_s = \mathbf{F}(\mathbf{x}_s)$. By applying an infinitesimal perturbation on synchronous manifold $\delta\mathbf{x}_i = \mathbf{x}_i - \mathbf{x}_s$ and substituting the equation 1.26, the variational equation of this time evolving perturbation $\delta\dot{\mathbf{x}}_i = \dot{\mathbf{x}}_i - \dot{\mathbf{x}}_s$ is

$$\frac{d\delta\mathbf{x}_i}{dt} = \mathbf{F}(\mathbf{x}_i(t)) + \sigma \sum_{j=1}^{N} L_{ij} \Big(\mathbf{H}(\mathbf{x}_j) - \mathbf{F}(\mathbf{x}_s)\Big) \qquad i = \{1, \cdots, N\} \tag{1.28}$$

applying Taylor series expansion at $\mathbf{x}_s$ yields

$$\frac{d\delta\mathbf{x}_i}{dt} = \mathrm{D}\mathbf{F}(\mathbf{x}_s)(\mathbf{x}_i - \mathbf{x}_s) + \sigma \sum_{j=1}^{N} L_{ij} \left(D\mathbf{H}(\mathbf{x}_s) + \mathrm{D}\mathbf{H}(\mathbf{x}_s)(\mathbf{x}_j - \mathbf{x}_s)\right) \tag{1.29}$$

which results in,

$$\frac{d\mathbf{x}_i}{dt} = \mathrm{D}\mathbf{F}(\mathbf{x}_s)\delta\mathbf{x}_i + \sigma \sum_{j=1}^{N} L_{ij}\mathrm{D}(\mathbf{H}(\mathbf{x}_s))\delta\mathbf{x}_j,\ i = \{1, \cdots, N\} \tag{1.30}$$

where $\mathrm{D}\mathbf{F}(\mathbf{x}_s)$ and $\mathrm{D}\mathbf{H}(\mathbf{x}_s)$ are the Jacobian matrices of the corresponding vector field and coupling functions evaluated at $\mathbf{x}_s$. The general form of the equation is:

$$\frac{d\mathbf{x}}{dt} = (\mathbf{I}_{N\times N} \otimes \mathrm{D}\mathbf{F}(\mathbf{x}_s) + \sigma\mathbf{L} \otimes \mathbf{H}(\mathbf{x}_s))\delta\mathbf{x}, \tag{1.31}$$

where $\otimes$ is the Kronecker product. $\delta\mathbf{x} \in \mathbb{R}^{nN}$ dimensional vector of all the perturbations of the network i.e. $\delta\mathbf{x} = (\delta\mathbf{x}_1, \delta\mathbf{x}_2, \cdots, \delta\mathbf{x}_N)$. $\mathbf{L}$ is the symmetric Laplacian matrix whose eigenvector matrix is $\mathbf{Q}$ and satisfyies $\mathbf{L} = \mathbf{Q}\mathbf{\Lambda}\mathbf{Q}^{-1}$ where $\mathbf{\Lambda}$ is diagonal matrix of its eigenvectors. It is straight-forward to write $\mathbf{Q}\mathbf{Q}^T = \mathbf{Q}^T\mathbf{Q} = \mathbf{I}$ since $\mathbf{Q}$ is orthogonal matrix. By projecting variations $\delta\mathbf{x}$ into the eigen-space spanned by eigen vectors of coupling matrix $\mathbf{L}$ i.e. $(\mathbf{Q}^T \otimes \mathrm{I}_{n\times n})\delta\mathbf{x} = \delta\mathbf{y}$, the block diagonalized form of the variational equation is

$$\frac{d\mathbf{y}}{dt} = \left(I_{N\times N} \otimes \mathrm{D}\mathbf{F}(\mathbf{x}_s) + \sigma\Lambda \otimes \mathrm{D}\mathbf{H}(\mathbf{x}_s)\right)\delta\mathbf{y} \tag{1.32}$$

The generic form of equation for each can be written as

$$\frac{d\mathbf{y}}{dt} = \left(\mathrm{D}\mathbf{F}(\mathbf{x}_s) + kD\mathbf{H}(\mathbf{x}_s)\right)\delta\mathbf{y}, \tag{1.33}$$

for $k = \sigma\lambda_i$ for $i = \{1, \ldots, N\}$ where $\lambda_i = \{\lambda_1, \lambda_2, \cdots, \lambda_N\}$ are the eigenvalues of Laplacian matrix. The 1st block in equation associates with $\lambda_1 = 0$ which denotes the motion parallel to synchronous manifold i.e. trajectory of an uncoupled oscillator, whereas $\lambda_i \geqslant \lambda_2$ corresponds to the perturbed motions on the transverse synchronization manifold which are concerned for stability analysis. It is notable that the purpose of block-diagonalization is to isolate the synchronous motion from the transverse ones in order to ease the manipulating of those transverse manifolds and analyzing their stability. By evaluation maximum Lyapunov exponent $\bigwedge_i$ of equation 17 for $i \geqslant 2$ and for k in the interval $k_a < k < k_b$ the synchronous manifold would be stable if all those transverse motions damped down i.e for all those the maximum Lyapunov exponent would be negative $\bigwedge_i \leqslant 0$ otherwise if $\bigwedge_i > 0$ the synchronization manifold is unstable.

1.5.2 Extended master stability function (EMSF)

The synchronization which is treated by Master Stability approach is base on the assumption of network of identical nodes. However, in practice, due to noise and slight parameter mismatches of the network's members, they tend close to the synchronization manifold but not exactly lying in this manifold. Loss of asymptotic synchronization toward nearly synchronous state, respect to the scale of parameter mismatch has been treated by Extended master stability function,

an approach for studying synchronization in nodes with nearly identical parameters. In this method a more general model of equation (1.45) has been considered which as:

$$\frac{d\mathbf{x}_i}{dt} = \mathbf{F}(\mathbf{x}_i(t), \mu_i) + \sigma \sum_{j=1}^{N} L_{ij}\mathbf{H}(\mathbf{x}_j),\ i = \{1, \cdots, N\} \tag{1.34}$$

where μ_i is the parameter of i_{th} node and in the case of asymptotic synchronization is uniform i.e. $\mu_1 = \mu_2 = \cdots = \mu_N$. The parameter mismatch $\delta\mu_i$ can be considered as $\mu_i - \bar{\mu}$ where $\bar{\mu} = \frac{1}{N}\sum_{i=1}^{N}\mu_i$. The the system is expected to stay in a near synchronous state for some values of coupling σ and configuration L where $\lim_{t\to\infty}||\mathbf{x}_i - \mathbf{x}_j|| \leq \epsilon$ for $\epsilon > 0$. The near synchronous state $\bar{x}$ is considered as the average of all individual nodes's solutions i.e. $\bar{\mathbf{x}} = \frac{1}{N}\sum_{i=1}^{N}\mathbf{x}_i$. The small variation of each node's dynamic from the state $\bar{\mathbf{x}}$ is defined as $\delta\mathbf{x}_i = \mathbf{x}_i - \bar{\mathbf{x}}$. Consequently the variational equation will be governed by $\delta\dot{\mathbf{x}}_i = \dot{\mathbf{x}}_i - \dot{\bar{\mathbf{x}}}$ where by substituting the corresponding equation for each term for the specific case of Laplacian coupling the equation will be

$$\frac{d\delta\mathbf{x}_i}{dt} = \mathbf{F}(\mathbf{x}_i(t), \mu_i) - \frac{1}{N}\sum_{j=1}^{N}\mathbf{F}(\mathbf{x}_i(t), \mu_i)\sigma\sum_{j=1}^{N}L_{ij}\mathbf{H}(\mathbf{x}_j) \tag{1.35}$$

Using again Taylor expansion about the near synchronous state yields

$$\begin{aligned}\frac{d\delta\mathbf{x}_i}{dt} &= \mathbf{F}(\mathbf{x}, \bar{\mu}) + D\mathbf{F}_{\bar{\mathbf{x}}}(\mathbf{x}_i, \mu_i)(\mathbf{x}_i - \bar{\mathbf{x}}) + D\mathbf{F}_{\bar{\mu}}(\mathbf{x}_i, \mu_i)(\mu_i - \bar{\mu}) \\ &\quad -\frac{1}{N}\sum_{j=1}^{N}[\mathbf{F}(\bar{x}, \bar{\mu}) + D\mathbf{F}_{\bar{\mathbf{x}}}(\mathbf{x}_i, \mu_i)(\mathbf{x}_i - \bar{\mathbf{x}}) + D\mathbf{F}_{\bar{\mu}}(\mathbf{x}_i, \mu_i)(\mu_i - \bar{\mu})] \\ &\quad -\sigma\sum_{j=1}^{N}L_{ij}(\mathbf{H}(\bar{\mathbf{x}}) + D\mathbf{H}_{\bar{\mathbf{x}}}(\mathbf{x}_i)(\mathbf{x}_i - \bar{\mathbf{x}}))\end{aligned} \tag{1.36}$$

where $D\mathbf{F}_{\bar{\mathbf{x}}}$ and $D\mathbf{F}_{\bar{\mu}}$ are the Jacobian matrices evaluated on the average trajectory and average parameter respectively. Equation (1.36) can be rewritten as

$$\frac{d\delta\mathbf{x}_i}{dt} = D\mathbf{F}_{\bar{\mathbf{x}}}(\bar{\mathbf{x}}, \bar{\mu})\delta\mathbf{x}_i + D\mathbf{F}_{\bar{\mu}}(\bar{\mathbf{x}}, \bar{\mu})\delta\mu_i - \sigma\sum_{j=1}^{N}L_{ij}D\mathbf{H}(\bar{\mathbf{x}})\delta\mathbf{x}_i \tag{1.37}$$

From the fact that $\sum_{i=1}^{N}\delta\mathbf{x}_i = \sum_{i=1}^{N}\mathbf{x}_i - N\bar{\mathbf{x}} = 0$, $\sum_{i=1}^{N}\delta\mu_i = \sum_{i=1}^{N}\mu_i - N\bar{\mu} = 0$, and $\sum_{i=1}^{N}l_{ij} = 0$ we have that the vector form of the variational equation reads

$$\delta\dot{\mathbf{x}} = [\mathbf{I}_{N\times N}\otimes D\mathbf{F}_{\bar{\mathbf{x}}}(\bar{\mathbf{x}}, \bar{\mu}) - \sigma L\otimes D\mathbf{H}(\bar{\mathbf{x}})]\delta\mathbf{x} + \mathbf{I}_{N\times N}\otimes D\mathbf{F}_{\bar{\mu}}(\bar{\mathbf{x}}, \bar{\mu})\delta\mu. \tag{1.38}$$

If the system does not have parameter mismatch then the variational equation is the same as the one of MSF (1.45). Next, by block-diagonalizing, yields

$$\frac{d\delta\mathbf{y}}{dt} = [\mathbf{I}_{N\times N}\otimes D\mathbf{F}_{\bar{\mathbf{x}}}(\bar{\mathbf{x}}, \bar{\mu}) - \sigma\mathbf{P}\otimes D\mathbf{H}(\bar{\mathbf{x}})]\delta\mathbf{y} + \mathbf{Q}^T\otimes D\mathbf{F}_{\bar{\mu}}(\bar{\mathbf{x}}, \bar{\mu})\delta\mu. \tag{1.39}$$

For each node we have that

$$\frac{d\delta\mathbf{y}_i}{dt} = [D\mathbf{F}_{\bar{\mathbf{x}}}(\bar{\mathbf{x}},\bar{\mu}) - \sigma\lambda_k D\mathbf{H}(\bar{\mathbf{x}})]\delta\mathbf{y}_i + D\mathbf{F}_{\bar{\mu}}(\bar{\mathbf{x}},\bar{\mu})\sum_{j=1}^{N} Q_{ij}\delta\mu_j. \tag{1.40}$$

where $\mathbf{Q}^T = [Q_{ij}]$ is the transverse of the eigenvector matrix and $k \geq 2$.
The variational equation would be in the following form:

$$\frac{d\delta\mathbf{y}_i}{dt} = [D\mathbf{F}_{\bar{\mathbf{x}}}(\bar{\mathbf{x}},\bar{\mu}) - \epsilon D\mathbf{H}(\bar{\mathbf{x}})]\delta\mathbf{y}_i + D\mathbf{F}_{\bar{\mu}}(\bar{\mathbf{x}},\bar{\mu})\Phi. \tag{1.41}$$

The extended master stability function is then a function of, individual dynamic, coupling function, structure of the network and parameter mismatch. The stability of the system will be obtained by the sign of its maximum Lyapunov exponent and then by substituting $\Phi = \sum_{j=1}^{N} q_{ij}\delta\mu_j$ and $\epsilon = \sigma\lambda_k$ the stability will be obtained for a specific topology and parameter mismatch

1.5.3 Proportional derivative master stability function (PDMSF)

Stability analysis of network coupled by dynamic component such as capacitor and inductor has been studied by PD master stability function. In this case we consider the network (1.16) setting the coupling function $\mathbf{H}(\mathbf{x}_i) = \mathbf{\Gamma}\mathbf{x}_i$, where $\mathbf{\Gamma} \in \mathbb{R}^{N\times N}$ is the inner coupling matrix representing interconnections between the state variables of each node. Then the dynamics of the network with dynamic links can be written as

$$\frac{d\mathbf{x}_i}{dt} = \mathbf{F}(\mathbf{x}_i(t)) + \sigma_1\sum_{j=1}^{N} L_{ij}\mathbf{\Gamma}\mathbf{x}_j + \sigma_2\sum_{j=1}^{N} L_{ij}\mathbf{\Gamma}\mathbf{x}_j,\ i \in \{1,\cdots,N\} \tag{1.42}$$

which can be written in compact form as

$$\frac{d\mathbf{x}}{dt} = \mathbf{I}_{N\times N} \otimes\ \mathbf{F}(\mathbf{x}) - \sigma_1(\mathbf{L}\otimes\mathbf{\Gamma})\mathbf{x} - \sigma_2\left(\mathbf{L}\otimes\mathbf{\Gamma}\left(\frac{d\mathbf{x}_j}{dt}\right)\right), \tag{1.43}$$

similarly to master stability function the system would be linearized around the synchronous state followed by a diagonalization which results in the following variational equation

$$\frac{d\delta\mathbf{y}}{dt} = (\mathbf{I}_{N\times N} - \sigma_2\mathbf{\Lambda}\otimes\mathbf{\Gamma})^{-1}[\mathbf{I}_{N\times N} + \sigma_1\mathbf{\Lambda}\otimes\mathbf{\Gamma}]\delta\mathbf{y}, \tag{1.44}$$

where $\mathbf{\Lambda}$ is the matrix of eigenvalues of the Laplacian matrix L. Hence the states equations are decoupled and the variational equation for state ith node reads

$$\frac{d\delta\mathbf{y}_i}{dt} = (\mathbf{I}_{n\times n} - \sigma_2\lambda_k\mathbf{\Gamma})^{-1}[\mathrm{DF}(\mathbf{x}_s) + \sigma_1\lambda_k\mathbf{\Gamma}]\delta\mathbf{y}, \qquad k \in \{2,\cdots,N\} \tag{1.45}$$

Therefore, the maximum Lyapunov exponent of the variational equation (1.45) determines the stability of the synchronous state. If it would be negative the state is stable otherwise is unstable.

1.5.4 Stability of clusters

Earlier the stability of complete synchronization using the MSF approach has been introduced. Master stability diagram shows the transition and network parameter's threshold by which complete synchronization remain stable for a generic network network. Furthermore, it has been explained how by loosing synchronization networks tend to form clusters where a single synchronous manifold $\mathbf{x}_s$ bifurcate to M synchronous manifold where $2 \leq M \leq N$ depends on network parameters. N represents number of nodes and $M = N$ is the extreme condition where there are no synchronized nodes. Stability analysis of such states can not be analyzed with MSF since the analysis in master stability function is based on a single state synchronous manifold which is kept apart through diagonalization to manipulate those states transverse to it.

However by clusters there are multi-state manifolds of synchronization for which there should be considered M variational equations and study all transverse to each synchronous manifold as It is discussed in [42]. It has to be considered also that dimension of synchronous manifold in this case is more than that of compete synchronization. The variational equations for the Laplacian coupled oscillators described by equation (1.26) about the synchronous manifold of clusters is defined as:

$$\frac{d\delta\mathbf{x}}{dt} = \left[\sum_{m=1}^{M} \mathbf{E}^m \otimes D\mathbf{F}(\mathbf{x}_{sm}(t)) + \sigma\mathbf{L}\sum_{m=1}^{M}(\mathbf{E}^m) \otimes D\mathbf{H}(\mathbf{x}_{sm}(t))\right]\delta\mathbf{x}(t) \quad (1.46)$$

where $\mathbf{E}^m$ is an N dimensional matrix whose diagonal entries $E^m_{ii} = 1$ if i_{th} node belongs to cluster m_{th} otherwise $E^m_{ii} = 0$. $\sum_{m=1}^{M} E(m) = I_N$. Using the advantage of group theory the equation can be block diagonalized [42] corresponding to the cluster structure using a matrix $\mathbf{T}$. The resulted block diagonalized matrix is

$$\mathbf{L}' = \mathbf{T}^{-1}\mathbf{L}\mathbf{T} = \begin{bmatrix} \mathbf{L}_{tran} & 0 \\ 0 & \mathbf{L}_{syn} \end{bmatrix} \quad (1.47)$$

In this way the set of eigenvalues of $\mathbf{L}$ $(0 = \lambda_1 < \lambda_2 < \cdots < \lambda_N)$ is divided into two groups, each belonging to one diagonal block, $\mathbf{L}_{syn}$, with dimension n_2, representing the synchronous subspace and $\mathbf{L}_{tran}$, with dimension n_1, indicating the subspace of transverse motions (with 0 eigenvalue belonging to $\mathbf{L}_{syn}$), satisfying the sorting relations $(0 = \lambda_{1syn} < \lambda_{2syn} < \cdots < \lambda_{n2syn})$, $(\lambda_{1tran} < \lambda_{2tran} < \cdots < \lambda_{n1tran})$ with $N = n_1 + n_2$ [21]. The matrix $\mathbf{M}$ of eigenvectors of the permutation matrix can be used as the matrix $\mathbf{T}$ so that

$$\mathbf{M} : \mathbf{M}^{-1}\mathbf{P}_g\mathbf{M} = \hat{\mathbf{P}} = \text{diagonal}$$

By projecting the state variables on space spanned by vectors of $\mathbf{P}_g$ (defined in (1.21)) i.e. $\delta\mathbf{y} = (\mathbf{T} \otimes \mathbf{I}_n)\delta\mathbf{x}$, the variational equation is

$$\frac{d\delta\mathbf{y}}{dt} = \left[\sum_{m=1}^{M} \mathbf{J}^m \otimes D\mathbf{F}(\mathbf{x}_{sm}(t)) + \sigma\mathbf{L}'\mathbf{J}^m \otimes D\mathbf{H}(\mathbf{x}_{sm}(t))\right]\delta\mathbf{y}(t) \quad (1.48)$$

where $\mathbf{J}^m$ is the projection of $\mathbf{E}^m$. Therefore linearization about synchronized cluster states $\{\mathbf{x}_{s1}(t), \mathbf{x}_{s2}(t), \cdots, \mathbf{x}_{sm}(t)\}$ Therefore, cluster synchronization is stable if

1. All maximum Lyapunov exponents corresponding to transverse mode would be negative which means the stability of transverse modes.

2. The asymptotic synchronous pattern would exist in the steady state.

Chapter. 2

Description and characterization of the experimental setup

Networks of chaotic oscillators and their complex dynamics have been widely considered in the literature; in particular, networks with Chua's circuits as nodes have been commonly used to study synchronization emerging in networks of dynamical systems. However, most of the available results are of theoretical and numerical nature, whereas relatively few experimental studies have been presented. This is mainly due to difficulties in the realization and operation of networks with a large number of nodes. Indeed, most of the available experimental results have been obtained for networks of two or three nodes. A larger scalable setup has been proposed to study higher dimensional networks with a nearest neighbor structure in the context of Cellular Neural Networks (CNNs) but few are available for networks with a general reconfigurable structure. Moreover, most experiments have been dedicated to investigate the complete synchronization phenomenon, where all states of the nodes synchronize asymptotically. Few examples are available of experimental efforts in the study of other interesting phenomena such as phase synchronization, clustering formation, the emergence of patterns and waves within the ensemble of oscillators. In order to overcome such limitations, and test complex networks of chaotic oscillators having a high number of nodes (up to 48) and having a general and reconfigurable structure, an experimental test-bed has been realized in the Circuit Laboratory of the Department of Electrical Engineering and Information Technology (DIETI) of the University of Naples Federico II. The present chapter is dedicated to the complete description and characterization of the setup. Its peculiarity, with respect to other experimental arrangements, resides in: (i) the full and direct control of the network structure, the link type and coupling strength; (ii) the possibility of selecting each node main parameters; (iii) a modular high rate multichannel acquisition section for the simultaneous analysis of the large number of variables under observation. Figure 2.1 shows the schematic of the experimental setup which is composed of three main modules:

(i) a set of N nodes, that are Chua's circuits, whose parameters can be set individually;

(ii) an interconnection module through which the nodes are coupled;

(iii) a data acquisition system which allows the continuous monitoring of the variables of interest.

The first version of the test-bed dates back to the beginning of 2011 and in the following will be addressed as NetV11 (figure 2.2a). A newer version (NetV16) has been completed in 2016 (figure 2.2b). The main difference between these two versions resides in the interconnection module: in version NetV11 the links among the nodes were established manually by properly placing a set of jumpers; in version NetV16 the connections are fully automated and controlled directly via Personal Computer.

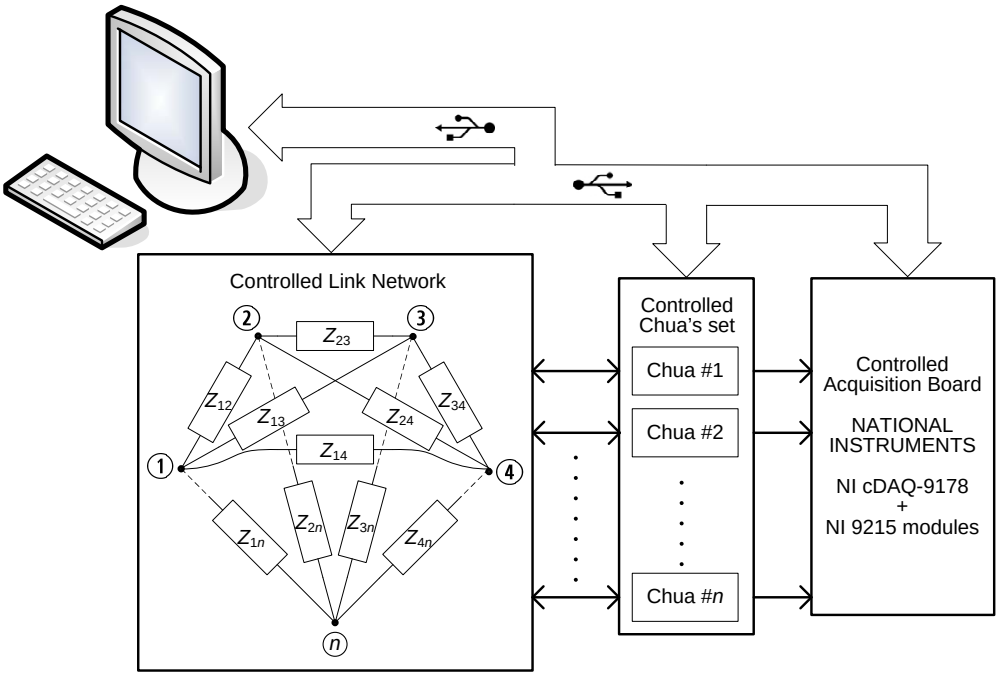

Figure 2.1: schematic of experimental setup

Both setups are adapted for testing dynamically coupled networks as well where coupling capacitors are paralled to coupling resistors. Figure 2.3 shows both setups equipped by capacitive links where in both the capacitor values are adjustable manually through DIP switches. We have characterized a wide range of capacitive links for the setup NetV16 which will be reported in the following relative section.

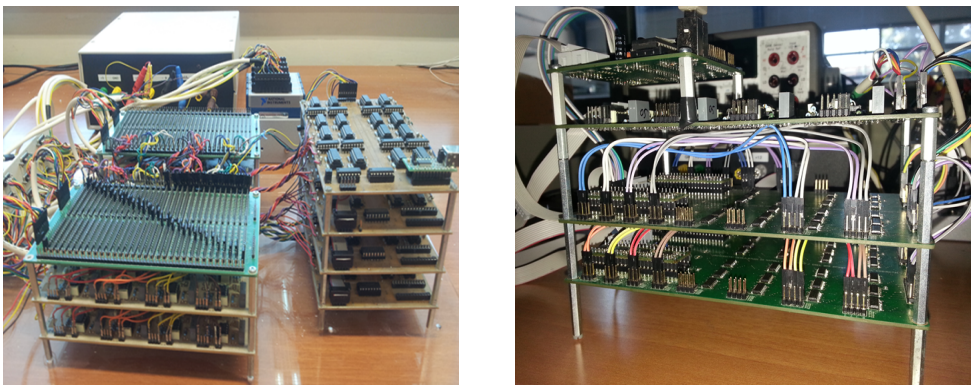

(a) (b)

Figure 2.2: experimental setups coupled by resistors (static coupling) a) NetV11-partially automatized b) NetV11-Fully automatic

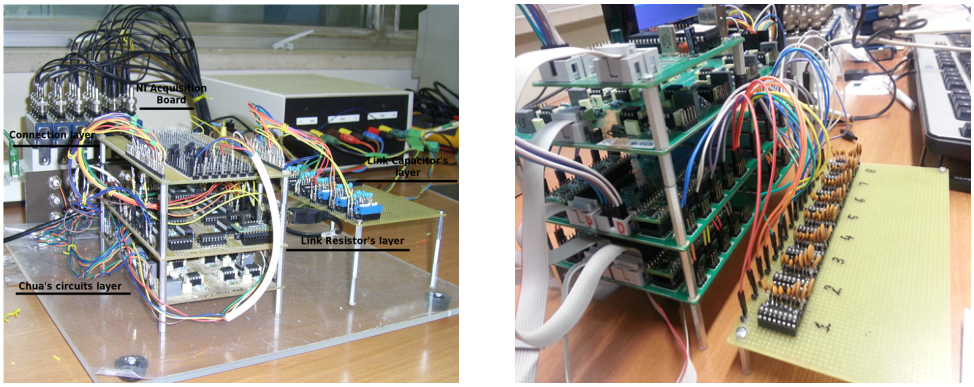

(a) (b)

Figure 2.3: experimental setups equipped by capacitive links a) NetV11 b) NetV16

2.1. Description

2.1.1 Chua's circuits as network's nodes

For the sake of robustness and accuracy all Chua's circuits have been realized following the implementation proposed in [27] which results in a robust and economical assembling of Chua's circuits. Moreover the inductor is replaced by the synthesis presented in [1] using inductance gyrator composed by 2 operational amplifiers, one capacitor and 4 resistors. This implementation provides a more accurate systems for the practical purposes such as data measurement, tolerance and parasitic parameters' control since the commercial capacitors are closer to the ideal ones than those of inductors.
Figure 2.4 shows the schematic of the realized Chua's circuit, on which the values of components are indicated for NetV11. Table 2.1 shows the elements' values of Chua's circuits applied in the second version NetV16. The equivalent inductor

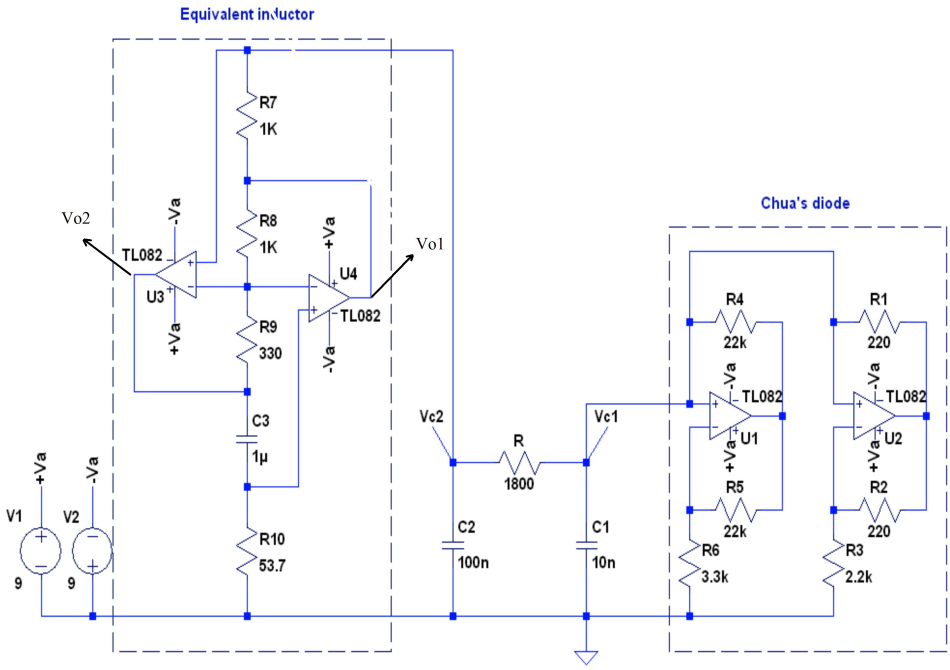

Figure 2.4: schematic of experimentally implemented Chua's circuits

synthesized by gyrator can be computed as

$$Leq = R_7 R_9 R10 C3 / R8$$

Table 2.1: Elements' values of Chua's circuit installed in second version of setup

Element	value
R_1	219.79Ω
R_2	219.83Ω
R_3	2200Ω
R_4	$22k\Omega$
R_5	$22k\Omega$
R_6	3296.25Ω
R_7	1Ω
R_8	1Ω
R_9	329.75Ω
R_10	54.60Ω
C_1	$10.05nF$
C_2	$100.65nF$
C_3	$1.03F$

2.1.2 Interconnection network

The coupling links are realized by resistors (static links) as well as capacitors or parallel resistors and capacitors (dynamic links) with separately adjustable type and strength. This module has been realized differently for the mentioned setup versions which is described in the following.

1. The coupling resistive configurations for NetV11 are composed of set of physical resistors adjustable through USB controllable digital switches DG412DJZ and a matrix of manually controllable interconnections where two nodes can be coupled though a coupling resistor by placing jumpers (JP) as figure 2.5a shows. Each static coupling link consists of two digital switches DG412DJZ

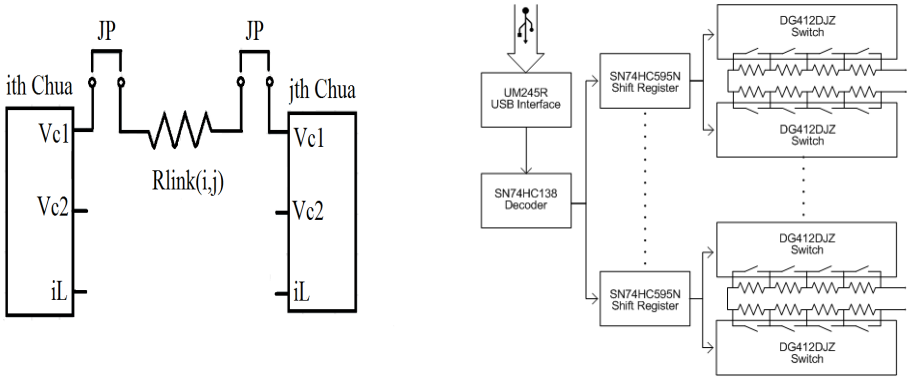

(a) (b)

Figure 2.5: a) schematic of manual connection among two Chua's circuits using jumpers (JP) b) schematic of USB controllable digital switches adjusting physical coupling resistors

connecting to 8 resistors which can provide 8 bit of resolution. Therefore each coupling link can vary among $2^8 = 256$ different scalable values. On a single PCB, 8 coupling resistors are mounted along with their corresponding switches. For each coupling resistor one shift register SN74HC595N is mounted on the same PCB where two of shift registers are connected to a decoder SN74HC138 for individual setting of each coupling though USB interface UM245R. Figure 2.5b depicts an schematic of two coupling resistors controlled by UM245R. Figures 2.6a and 2.6b show interconnection matrix providing 16 connections and 8 coupling resistors on a single PCB, respectively. 4 PCBs on each 8 static coupling links are mounted, are accessible through one USB interface UM245R for the purpose of control.

2. In the second version NetV16, physical coupling resistors are replaced by digital potentiometers AD5293 for each, with maximum nominal resistor of 20 and 50 $k\Omega$. End-to-end resistor tolerance error is $< 1\%$. Figure 2.10a shows the schematic of the potentiometer. The AD5293 shift register has 16 bits data-word consisting of two unused bits, which are set to 0, followed by four control bits (to choose the function of the software command for

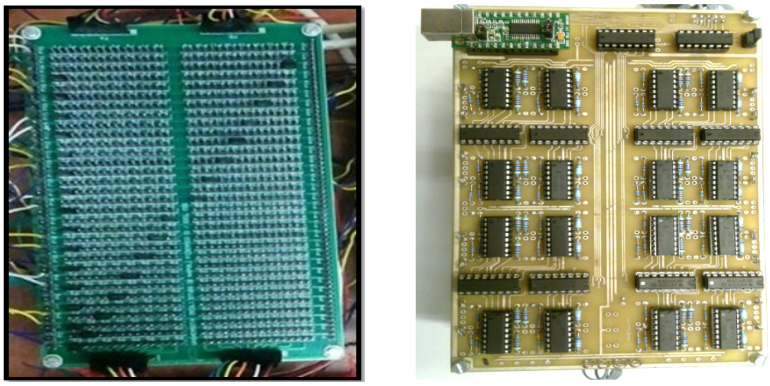

(a) (b)

Figure 2.6: experimental setup a) interconnection matrix for 16 links b) 8 coupling resistors mounted in a single PCB

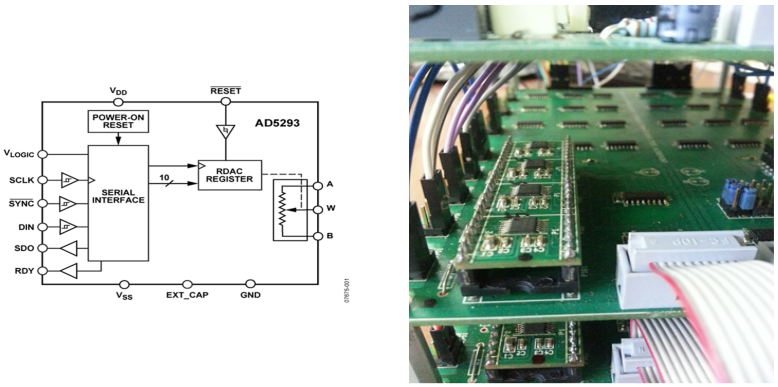

(a) (b)

Figure 2.7: a) schematic of potentiometer AD5293 b) potentiometers applied in the setup

example writing or reading) and 10 RDAC data bits. The RDAC register shown in schematic controls directly the position of digital potentiometer wiper (W). The 10-bit data in the RDAC latch is decoded to select one of the 1024 possible settings available in potentiometer accessed by wiper terminal. Digital programmed output resistance between the W terminal and B terminal is obtained as,

$$R_{WB}(D) = \frac{D}{1024} \times R_{AB}$$

where D is decimal equivalent of the binary code loaded in the 10-bit RDAC register and R_{AB} is the end-to-end resistance. Resistance of R_{WA} is a digitally controlled complementary like mechanical potentiometer which can be calibrated to give a maximum of 1% absolute resistance error. R_{AB} is calculate as,

$$R_{WA}(D) = \frac{1024 - D}{1024} \times R_{AB}$$

In the zero-scale condition, a finite total wiper resistance of 120 Ω is present. In the current setup version NetV16, maximum number of coupling resistors are 16 realized by 16 potentiometers, each group of 8 mounted on a single PCB.

2.1.3 Data acquisition real time analysis and control

For simultaneous, multiple data acquisition and real time processing of large sets of electrical measured data in complex network, currently 64 variables, National Instrument compactDAQ series instruments, as well as the LabVIEW software for implementing the real time data processing and system control have been used. Moreover additional to labview the system is accessible through matlab as well.
In labview program after sampling data whose rate is 60k samples in a second, there are two possible modes; visual and scan. In visual mode data is monitored and coupling resistors can be changed step by step by operator while in the scan mode operator choose a range for coupling resistors and then within that range automatically all the values are scanned and data is saved and monitored simultaneously. a sample of front panel of visual mode of labview is shown in figure 2.8. As figure shows through labview the phase diagram of any single chua

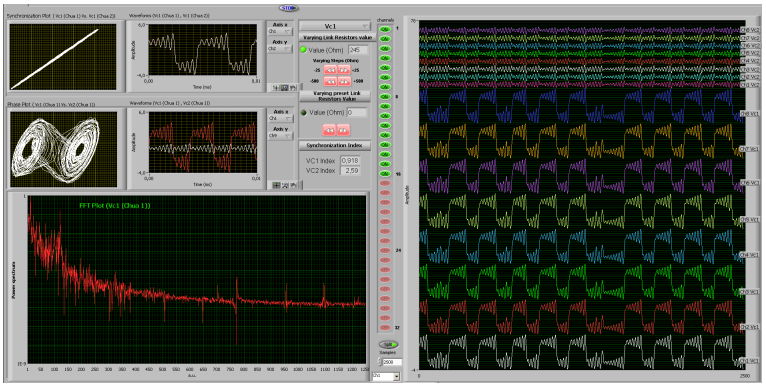

Figure 2.8: monitoring data in labview-front panel

as well as relative phase diagram among chua's state variables are monitored. Frequency response, as a representation of dynamic structure is shown as well. all the waveforms of Chua's circuits upto 32 can be shown individually or merged in order to distinguish better the state of complete synchronization. The resolution of observing waveforms can also be changed which is useful for observing clusters.

2.2. Characterization

2.2.1 Node's Parasitics and Tolerances

As the early step, for Chua's diode and the op-amp equivalent inductor, an accurate experimental characterization has been carried out in order to assess that the tolerances and parasitic elements were within the prescribed ranges. Chua's

diode, implemented as in figure 2.4 with nominal values as therein indicated, should theoretically give a symmetrical piecewise linear characteristic as shown already in figure 1.1b, with the parameters reported in table 2.2.

Table 2.2: Experimental and theoretical parameters of Chua's characteristic

Description				
$G_a[S]$	Conductance	$-7.56.10^{-4}$	$-6.89.10^{-4}$	$-6.88.10^{-4}$
$G_b[S]$	Conductance	$-4.09.10^{-4}$	$-3.77.10^{-4}$	$-3.76.10^{-4}$
$G_c[S]$	Conductance	0.0046	0.0019	0.002
$E_1[V]$	Break voltage	± 0.97	-0.988	1.008
E_2 [V]	Break voltage	± 6.79	-5.72	6.27
v_{sat} [V]	Saturation voltage	± 7.47	-7.03	7.59

The nonlinear characteristic (v, i) of the Chua's diode has been experimentally measured with a simple characterization scheme. In figure 2.9, a comparison between the theoretical expectation and measured samples is reported. The characteristic is almost symmetric in the range $[+5.7, +5.7]V$ (changes are lower than 2%), while sensible changes (of about 5%) can be found in the break voltage E_2, in the slope G_c and the saturation voltage V_{sat}. These values are also different from the theoretical nominal values that were previously calculated. The differences can be ascribed to the adopted operational amplifiers that do not provide, in the needed tolerance range, a symmetric output and whose positive and negative saturation voltages slightly differ from one another. We remark that such differences do not affect significantly our experiments because the regime $|v_d| \geq 5V$ was never explored.

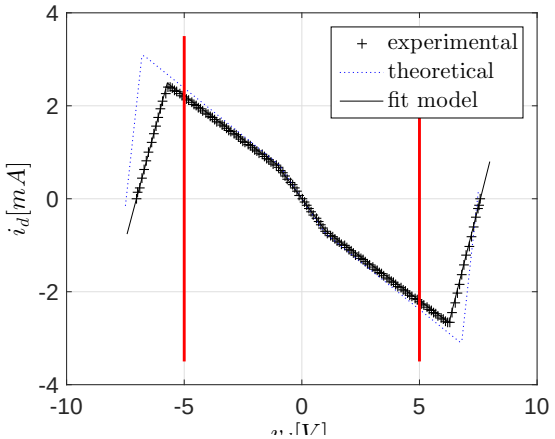

Figure 2.9: Chua diode characteristic

2.2.2 Characterization of node's dynamics

Aiming to construct a physical implementation of a reconfigurable complex network, to be used as prototypical model of different real complex systems, a pre-

liminary goal has been the evaluation of the realized system when compared with simulations. A detailed characterization of the single node dynamics as a function of the Chua's resistor R_c value has been carried out, following the methodology suggested in [46] for an automated experimental campaign. Typical problems in bifurcation analysis as period evaluation, transition to chaos and attractor discriminations have been faced in the automated evaluation of the observed waveforms. A global assessment of the node's behavior has been pursued by comparing the experimental bifurcation diagram with accurate PSpice simulations, taking into account real measured components values, parasitics and the nonlinear element modeled by a piecewise linear resistor as described in the previous section. The Chua resistor R is chosen as the bifurcation parameter and the value of voltage v_{c1} (at crossing points $v_{c2} = 0$) as dependent variable. Figure 2.10 shows the simulated (a) and experimental (b) bifurcation diagrams obtained, respectively, in the case in which the voltage v_{C2} reaches zero with positive slope. The two maps compare satisfactorily, with major bifurcation points in good agreement with respect to the bifurcation parameter R_c.

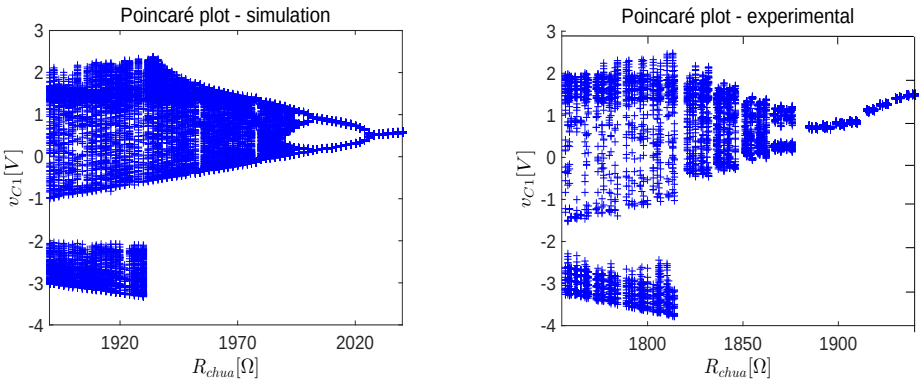

(a) (b)

Figure 2.10: poincarè map of Chua's circuit a) simulation result b) experimental result

A coarse classification of the observed experimental behavior of an isolated node as a function of R_{chua} is given in Table 2.3 (starting from periodic behavior (limit cycle), a transition is observed to a double scroll attractor followed by a single scroll one, and finally a transition back to periodic behavior).

The recorded, experimental and simulated dynamics can be observed in figure 2.11 where some representative phase portraits are shown.

Table 2.3: Observed dynamics of an isolated node

Asymptotic behavior	R_{chua} range [Ω]
Limit cycle	$1667 \leq R_{chua} \leq 1685$
Limit cycle	$1885 \leq R_{chua} \leq 1940$
Double scroll	$1690 \leq R_{chua} \leq 1814$
Single scroll	$1821 \leq R_{chua} \leq 1943$
Single scroll	$1846 \leq R_{chua} \leq 1854$
Single scroll	$1858 \leq R_{chua} \leq 1862$
Period adding ($T = 2$)	$R_{chua} = 1866, 1872$
Period adding ($T = 3$)	$R_{chua} = 1855, 1875$
Period adding ($T = 4$)	$R_{chua} = 1845, 1867, 1868, 1873, 1876$

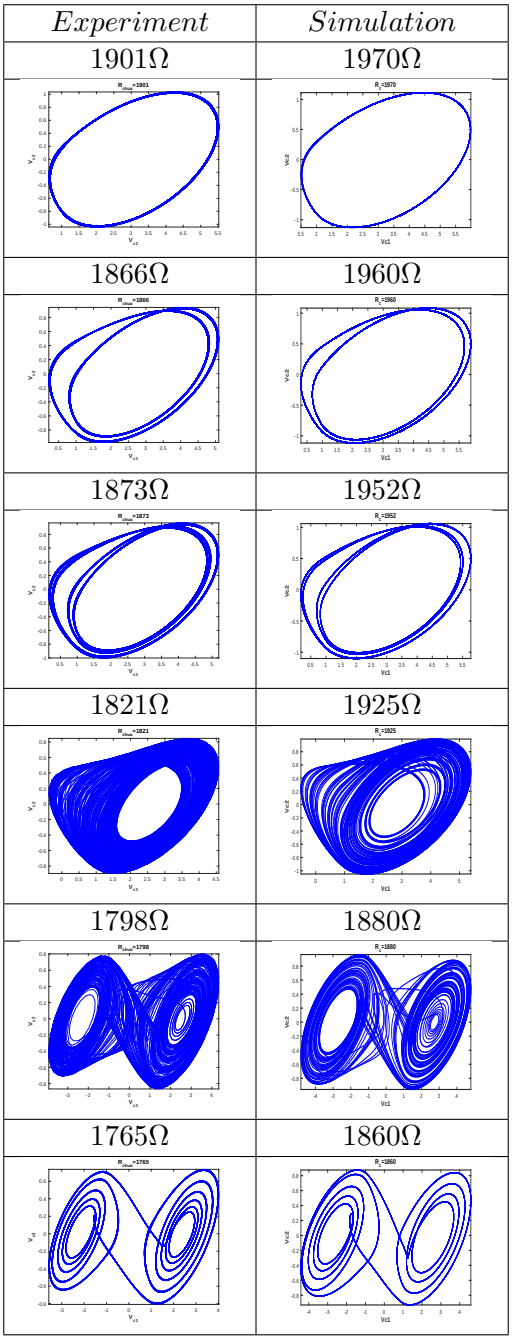

Figure 2.11: experimental and simulated Chua's circuits' dynamics

In this study, probing the collective dynamics of the networks for simplicity all the Chua's circuits are set nominally identical with $R_c = 1800\Omega$ and 1796Ω in NetV11 and NetV16 respectively where they generate chaotic double scroll attractors. The tolerance among Chua's circuits elements is 1%. Circuit's are coupled through the output extracted from their state variable v_{C1}.

2.2.2.1 Modified Chua's circuit model to reveal clusters

As it is mentioned the inductorless experimental setup has been realized by implementing inductive gyrator composed of opamps. The output voltages of opamps apply a constraint on V_{C2} which is not considered in the commonly used model of Chua's circuit recalled in chapter 1. We have realized that, in the absence of this constraint, the numerical results diverge after the network looses complete synchronization. Consequently by increasing V_{C2}, the voltage V_{C1} increase over saturation voltage and therefore it saturates for all Chua's circuits. This results in a significant disagreement among experimental and simulation results of emerged dynamic after the network looses complete synchronization. Even considerable disagreement appears with predicted MSF threshold which agrees with experiment. When Chua's circuit saturate the patterns generated by physical setup after loosing complete synchrony cannot be seen in the simulation. For the agreement among experimental and simulation results it is necessary to consider all the real conditions and constraints. For this purpose the Chua's model is modified taking in to account the gyrator restricted saturation voltage as the following:

$$\begin{cases} \dfrac{dv_{C3}}{dt} = -\dfrac{G_{10}}{C_3} v_{C2} \\ \dfrac{dv_{C2}}{dt} = \dfrac{G}{C_2}[v_{C1} - v_{C2}] + \dfrac{G_7}{C_2}[v_{O2} - v_{C2}] \\ \dfrac{dv_{C1}}{dt} = \dfrac{G}{C_1}[v_{C2} - v_{C1}] - \dfrac{1}{C_1} i(V_{R_N}) \end{cases} \tag{2.1}$$

$$v_{O2} = \begin{cases} v_{sat}, & : V_{O_2} \geqslant v_{sat} \\ V_{O_2}, & :\mid V_{O_2} \mid < v_{sat} \\ -v_{sat}, & : V_{O_2} \leqslant -v_{sat} \end{cases} \qquad v_{O1} = \begin{cases} v_{sat}, & : V_{O_1} \geqslant v_{sat} \\ V_{O_1}, & :\mid V_{O_1} \mid < v_{sat} \\ -v_{sat}, & : V_{O_1} \leqslant -v_{sat} \end{cases}$$

Where $V_{O_2} = -\dfrac{R_8}{R_9} v_{O1} + (1 + \dfrac{R_8}{R_9}) v_{C2}$ and $V_{O_1} = v_{C2} - v_{C3}$

The corresponding $i_L = i_{R_7} = \dfrac{R_8}{R_7 R_9} V_{C3}$ since the opamp is considered as ideal one. Dimensionless equations can be obtained by changing the parameters as before except z, β, g_7

$$\begin{cases} \dfrac{dz}{d\tau} = -\beta y \\ \dfrac{dy}{d\tau} = g_7 v_{O2}(y,z) - (1+g_7)y + x \\ \dfrac{dx}{d\tau} = \alpha(y-x) - \alpha I(x) \end{cases}$$

$$z = \frac{v_{C3}}{E_1} \quad , \quad \beta = \frac{C_2 G_{10}}{C_3 G} \quad , \quad g_7 = \frac{G_7}{G}$$

$$v_{O2}(y,z) = \begin{cases} \dfrac{v_{sat}}{E_1}, & : V_{O_2} \geqslant \dfrac{v_{sat}}{E_1} \\ V_{O_2}, & :\mid V_{O_2} \mid < \dfrac{v_{sat}}{E_1} \\ -\dfrac{v_{sat}}{E_1}, & : V_{O_2} \leqslant -\dfrac{v_{sat}}{E_1} \end{cases} \qquad v_{O1}(y,z) = \begin{cases} \dfrac{v_{sat}}{E_1}, & : V_{O_1} \geqslant \dfrac{v_{sat}}{E_1} \\ V_{O_1}, & :\mid V_{O_1} \mid < \dfrac{v_{sat}}{E_1} \\ -\dfrac{v_{sat}}{E_1}, & : V_{O_1} \leqslant -\dfrac{v_{sat}}{E_1} \end{cases}$$

$$\text{where} \qquad V_{O_2} = -\frac{R_8}{R_9} v_{O1}(y,z) + (1 + \frac{R_8}{R_9})y \qquad \text{and} \qquad V_{O_1} = y - z$$

The three equilibrium points of the circuit are as the following,

$$X^*_- = \begin{bmatrix} \dfrac{GR_9(G_b - G_a)}{R_8 G_7 (G+G_b)} E_1 \\ 0 \\ \dfrac{G_a - G_b}{G+G_b} E_1 \end{bmatrix} \qquad X^*_0 = \begin{bmatrix} 0 \\ 0 \\ 0 \end{bmatrix} \qquad X^*_+ = \begin{bmatrix} \dfrac{GR_9(G_a - G_b)}{R_8 G_7 (G+G_b)} E_1 \\ 0 \\ \dfrac{G_b - G_a}{G+G_b} E_1 \end{bmatrix}$$

Table 1 shows the Characteristic of this model for a single Chua's circuit. Figure 2.12 shows all the eigen values of equilibrium points for R_{chua} varying from 1500Ω to 2000Ω where the arrows are toward the direction of increasing R_{chua}. As it is shown in the figure by increasing R_{chua} the stability of equilibrium points changes according to the change on the sign of real part of complex eigen values which verifies the hopf bifurcaion. The characteristic of this mode is similar to the one has reported in chapter 1 as well as the experimental results. The results show

that as long as we are seeking the behavior of a single Chua's circuit which is uncoupled from any network or we are interested in the global synchronization threshold, both models are applicable, however in order to simulate the network of Chua's circuit beyond synchronization threshold and reveal the patterns of cluster generated by the present experimental setup, the constraint on the applied opamps of gyrator has to be considered for which in this work the modified Chua's circuit has been proposed. In this model the real applied capacitor in gyrator has been directly modeled and then the equivalent current to the inductor has been obtained in a relation with V_{C3}. This is the current flowing on R_7 since the opamps are considered ideal. Later in chapter 4 the simulation results of emergent

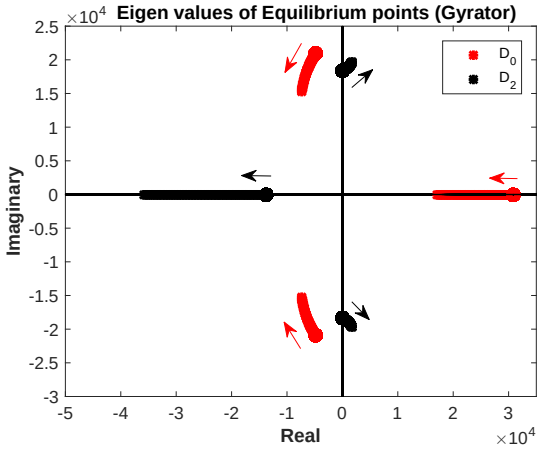

Figure 2.12: Real and complex eigen values of equilibrium points in D_0 origin and D_1 outer region; direction of arrows are toward increasing R_{chua}

dynamics produced by both model when the network has lost synchronization will be shown and compared.

2.2.3 Characterization of interconnection links

For the sake of accuracy all resistors ($R_1 - R_{16}$) realized by potentiometers for both nominal resistors $20k\Omega$ and $50k\Omega$ have been characterized and the tolerance has been calculated as:

$$\%Error(k) = \frac{max(R_{av}) - min(R_{av}) * 100}{R_{av}(k)}$$

$$R^k_{ave} = \frac{1}{r}\sum_{j=1}^{r} R^k_{mean}(j)$$

$$R^{k,r}_{mean} = \frac{1}{n_s}\sum_{i=1}^{n_s} R^{k,r}(j)$$

$$n_s = 1, \cdots, 3 \quad k = 1, \cdots, 1024 \quad r = 1, \cdots, 16$$

where $n_s = 3$ is the number of measured samples for each of coupling resistors $(R_1 - R_{16})$, r is the number of available realized resistors by potentiometer whose maximum is 16 currently and k is range of all resistor values generated by potentiometer with maximum of 1024. Figure 2.13a shows the error measured for all potentiometers with nominal resistor $R_{AB} = 20, 50k\Omega$. The measurement has been accomplished in 2 different ways for all; first the resistors are measured when all are decoupled from multiplexers; through which they are coupled with Chua's circuits, second the resistors are measured when they are all connected to multiplexers. The result are shown in figure 2.13a. Using these potentiometers has brought the advantage of accuracy in terms of wiring where the networks' nodes and their interconnection have become more compact. However compared with the first setup version for which physical resistors are used the error is not linear. The error is more that 3% for $R < 1082\Omega$, between 3% and 1% for $1082\Omega < R < 2639\Omega$ and less than 1% for $R > 2639\Omega$. We have chosen the potentiometer of $50k\Omega$ to explore the network dynamic according to better accuracy as figure 2.13a shows and wider range it provides. To avoid destruction, the

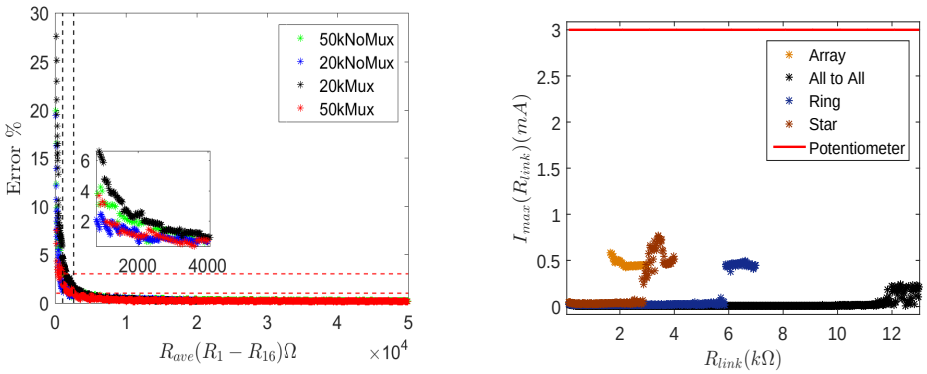

(a) (b)

Figure 2.13: a) potentiometer characterization b) maximum current passing through R_{link} when the network is coupled through specific configuraations

current flowing among terminal A and B, terminal W and A, and terminal W and B has to be limited to the maximum continuous current of ±3 mA. In order to ensure that the current passing through resistors in the coupling are within the accepted range, the maximum current passing through when the network is configured is measured for configurations all to all (all node are connected to each other), star (all nodes connected to one common node and not any other), ring and array among which all to all was expected to be the most crucial because of stronger connection. Figure 2.13b shows the results where the red line is indicating the limit current passing through potentiometer and has to stay below $3mA$. For all configurations the minimum current passing though the coupling resistors realized by potentiometer R_{link} is zero when all nodes in any configuration are synchronized and most dramatic current passes though (where the jump happen in diagram) when they loos synchronization (synchronization is explained in chapter 3).

It is important to mention that the output resistor generated by each potentiometer is not exactly equal to the one which is set as an input because of its formula for decimal conversion. Each coupling resistor is physically connected to multiplexer MPC508A whose pair of switches are connected at one side to a coupling resistor and in the other side each one to a Chua's circuit output (v_{C1}). Through shift register 74HC595 the corresponding multiplexer and their switches are selected to connect a pair of Chua's circuits. shift registers are controlled by decoder and the whole interconnection module is addressed and controlled though a micro-controller PIC18F4550 and USB interface by an ad hoc Labview program as well as matlab.

Similar to the first version, we have realized dynamic links composed of capacitors or capacitors and resistors where each coupling capacitor consists of 8 capacitors parallel to each other through DIP switches and therefore providing 8 bit of resolution i.e 256 different values ranging from $125pF$ to $34nF$ with the step of $125pF$. Figure 2.14a depicts the schematic of coupling capacitors representing a dynamic link which can be parallel to coupling resistors. The practical implementation of coupling capacitors are shown in figure 2.14b which are maximum 8 currently. All the capacitors composers of each link have been selected in such

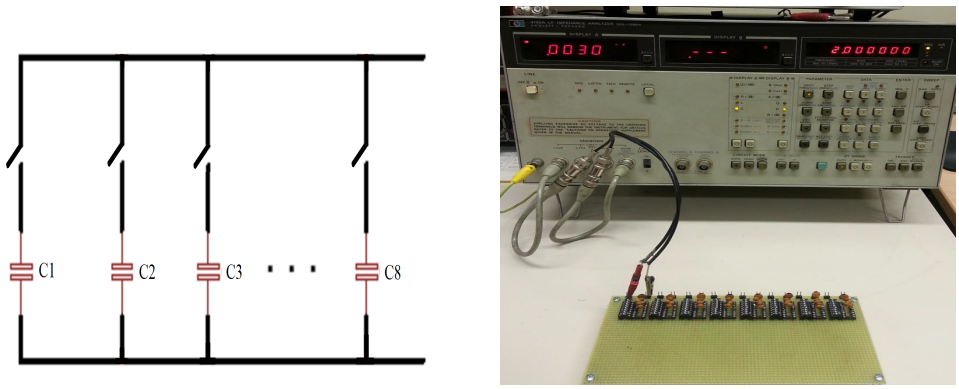

(a) (b)

Figure 2.14: coupling capacitors a) schematic b) practical implementation

a way to cover mentioned desired range. Figure 2.15 shows the characterization result with the error has been computed as the following

$$Error = \frac{max(C_i) - min(C_i)}{max(C_i)} \qquad i = 1, \cdots 8$$

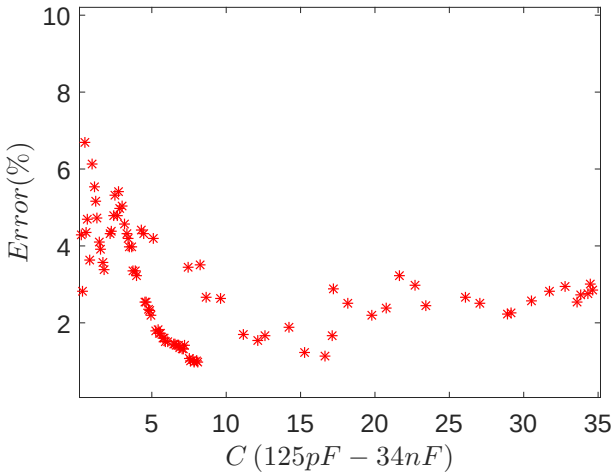

Figure 2.15: coupling capacitors characterization

As figure shows the maximum error among all 8 coupling capacitors is 6.7% in very low values and the rest remain below 4% which is acceptable for our experiments. It is worth noting that when all the capacitors are disconnected there is still a parasitic capacitor of DIP switches which is $2pF$.

Chapter. 3

Experiments on emergent dynamics: synchronization and beyond

Synchronization is a process observed in a wide range of systems, from natural ones such as fire flies lightning, biological and neural networks to artificial ones like power grids and etc. This behavior can play a key role in proper functioning of many systems such as power grids or information processing in the brain. However, on contrary, it can be related to disorders such as mental diseases [51, 54]. For all these reasons, among all emergent and collective dynamics of a complex network, several studies have been focused on synchronization of the network's components [5, 6, 24, 25, 41, 47, 53, 58, 60, 61].
Besides, it should not be forgotten the big challenge when collective behavior in the network differs significantly from the individual behaviors of its components. In this regard, studying synchronization of chaotic deterministic dynamical systems is of particular importance. Chaotic systems, when coupled in a network in addition to exhibit synchronization, might evolve in various emergent dynamics with different structures and patterns.
This study aims to explore emergent dynamics of coupled Chua's circuits; synchronization and beyond. Moreover, the robustness of synchronization as a function of coupling is studied. We have examined various network configurations for the purpose of inspecting synchronization mechanism as a function of network structure, node's number, coupling strength and parameter mismatch. Description of the work along with results can be found also in [31] . Studied networks are composed of nominally identical Chua's circuits coupled through interconnection layers classified in 3 groups:

(i) Networks coupled by nominally identical undirected resistive links, termed as diffusive static coupling with coupling function, that is network model (1.26) with $\mathbf{H}(\mathbf{x}_i) = \mathbf{\Gamma}\mathbf{x}_j$.

(ii) Networks coupled via nominally identical undirected links, composed of a pair of parallel resistor and capacitor named as dynamic coupling whose dynamics are described by (1.45).

(iii) Multiplex Networks, configured heterogeneously by static and dynamic

links.

This chapter will summarize the experimental results obtained through all the 3 classes of couplings discussed above. The chapter is organized in 5 sections. In the first section the behavior of an exemplary Chua's circuits influenced by coupling in the network is described and the simulation results are shown. The second section discusses the occurrence of complete synchronization in various examined networks of Chua's circuits. This section starts with describing the master stability function applied to network of Chua's circuits with different coupling functions and the calculated synchronization thresholds are compared with the experimental results followed by. In section 3, we have considered more complex models of interaction by using dynamic coupling (group (ii)) where the results of experiments are shown and compared with PDMSF approach. Section 4 explains the examined networks coupled by both static and dynamic links, named as multiplex networks, along with the acquired results in which we have observed significant improvement of synchronization level. The final section widely demonstrate the emerging dynamics and the mechanism that network goes through just after loosing synchronization in both statically and dynamically coupled networks where the results show a nontrivial patterns respect to configuration and type of coupling in the network.

3.1. Synchronization of prototypical chaotic systems

Consider 4 identical Chua's circuits each with its individual dynamic and governed by the following differential equation (1.9). Figure 3.1a shows the simulated phase diagram of each Chua's circuit. In the experiment the dynamic structure of all nodes are the same and chaotic single scroll, although they start from different initial conditions. Figure 3.2a depicts their waveforms in time domain $0 < t < 0.01$. We are interested in observing the impact of coupling

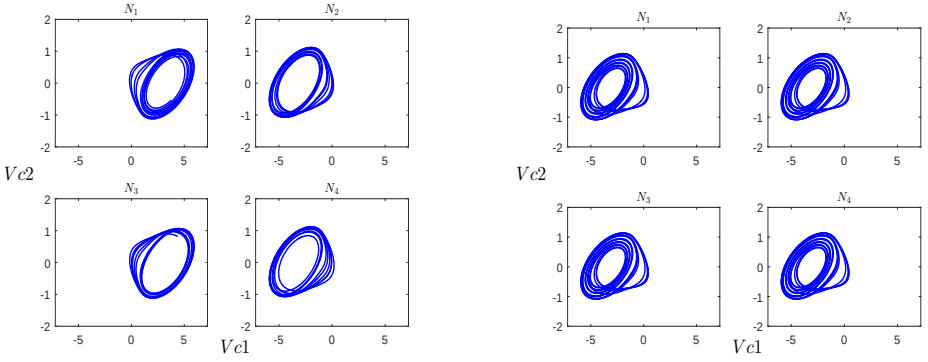

Figure 3.1: simulated phase diagram of 4 Chua's circuits a) decoupled b) coupled through resistors

on dynamics of network's node and emergence of synchronization. For this reason Chua's circuits are coupled in an array configuration as shown in figure 3.3

at time $t_1 = 0.01s$ with a high coupling strength implemented by a resistor of 1kΩ. After a transient time all the Chua's circuits converge to the same solution as it is shown in the figure 3.2a. By weakening the coupling strength at $t_2 = 0.03s$ through a 3kΩ resistor, Chua's circuits start loosing their agreement and finally they reach different solutions respect to each other. Figure 3.2b shows the steady state dynamic of all discussed intervals from the top respectively.

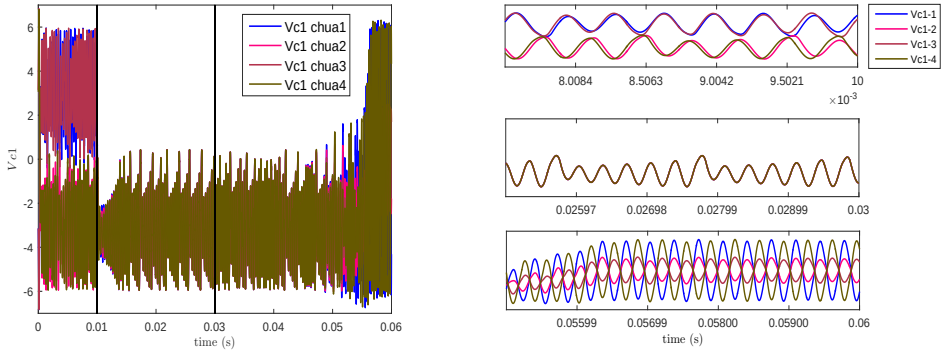

(a) (b)

Figure 3.2: a)waveforms of 4 Chua's circuits in three different conditions b) corresponding steady state waveforms

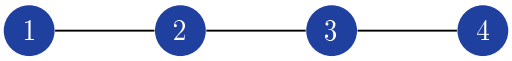

Figure 3.3: array configuration

The above example shows the impact of their interaction in the network with the result that their corresponding emergent dynamics can evolve completely different from their stand-alone behavior or can converge to the same solution for all the coupled systems. Network configuration, node's number and links type and strength are all network's parameters which strongly influence the collective or emergent dynamics of the network.

3.2. Experiments on networks of Chua's circuits with static coupling

The network discussed in the first section is coupled through un-directed, linear and static couplings implemented by resistors. The equation of motion can be written as

$$\frac{d\mathbf{x}}{dt} = \tilde{\mathbf{F}}(\mathbf{x}) - \varepsilon \mathbf{L} \otimes \mathbf{\Gamma} \mathbf{x} \tag{3.1}$$

where $\tilde{\mathbf{F}}(\mathbf{x}) := [\mathbf{F}^T(\mathbf{x}_1), \cdots, \mathbf{F}^T(\mathbf{x}_N)]^T$, and $\mathbf{x} := [\mathbf{x}_1^T, \cdots, \mathbf{x}_N^T]^T$ are the stack vectors of the vector fields and states of all Chua's circuits. $\mathbf{L}$ and $\mathbf{\Gamma}$ are the laplacian matrix and the coupling function matrix, respectively. The coupling strength is represented by ε which is uniform through all the network. As it

is discussed in chapter 1, using master stability function (MSF) [41], synchronization and its stability can be checked in such networks as a function of their parameters through the variational equation

$$\delta\dot{\mathbf{y}}_i = [\mathrm{D}\mathbf{F}(\mathbf{x}_i) - \varepsilon\lambda_i\Gamma]\delta\mathbf{y}_j \qquad i \geq 2 \tag{3.2}$$

Figure 3.4 shows the simulation results of master stability function for different coupling matrices $\mathbf{\Gamma}$ in the network of Chua's circuits where each individual evolves identically in chaotic double scroll attractor. The simulation is carried on using ode45 Matlab where the integration is run for long enough time considering $\frac{1}{3}$ of time to as transient. Each sub-figure shows the MSF characteristic as a

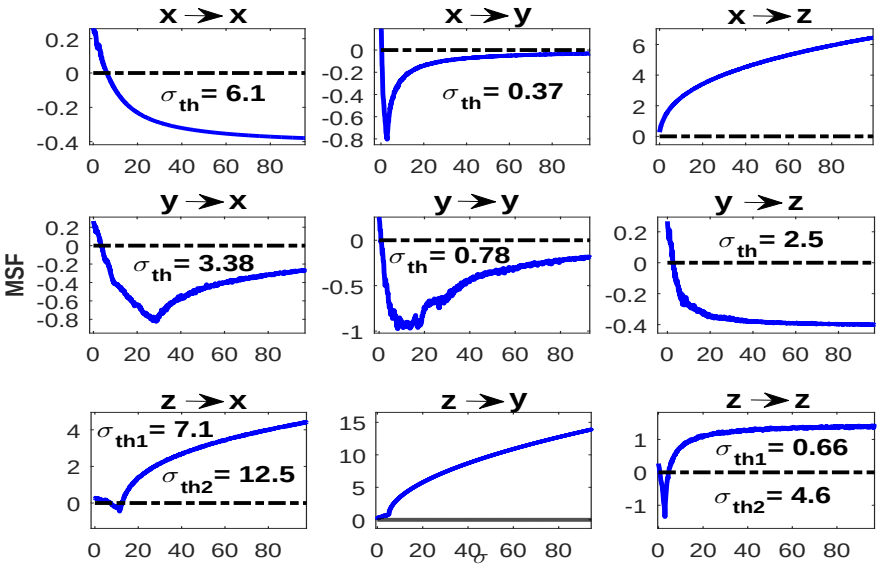

Figure 3.4: MSF diagram for simulated coupled Chua's circuits with various coupling functions and strengths

function of the coupling strength ($\sigma = \varepsilon\lambda$). Regions with negative maximum Lyapunov exponent verify the occurrence of the complete synchronization. MSF characteristic can vary among all 3 types classified as:

(i) Synchronization in the network occurs at σ_{th} and remain forever, e.g. the case $\mathbf{x} \to \mathbf{x}$ (figure 3.4).

(ii) Synchronization is reached at σ_{th1} and, by increasing the coupling strength, it is lost again at σ_{th2} and never is obtained again, e.g. the case $\mathbf{z} \to \mathbf{x}$ (figure 3.4).

(iii) Synchronization never occurs since the maximum Lyapunov exponent is always positive, e.g. the case $\mathbf{x} \to \mathbf{z}$ (figure 3.4).

$\sigma_{th} = \varepsilon\lambda_i$ is the threshold of synchronization. For coupled Chua's circuits the normalized coupling strength is given by $\varepsilon = (C_2R_C)/(C_1R_{link})$. In what follows we consider only the case where the Chua's circuits are coupled through their first state variable v_{C1} which is equivalent to consider the coupling matrix as

$$\mathbf{\Gamma} = \begin{bmatrix} 1 & 0 & 0 \\ 0 & 0 & 0 \\ 0 & 0 & 0 \end{bmatrix}$$

The first subfigure in 3.4 shows the MSF characteristic of this case where λ_2; the second eigen value of laplacian matrix, corresponds to σ_{th} i.e the value of the smallest coupling resistor R_{link} by which synchronization is lost.
The potential of our setup has allowed to investigate a wide range of network configurations with different number of nodes figure 3.5 and some of the notable results are summarized in this section.

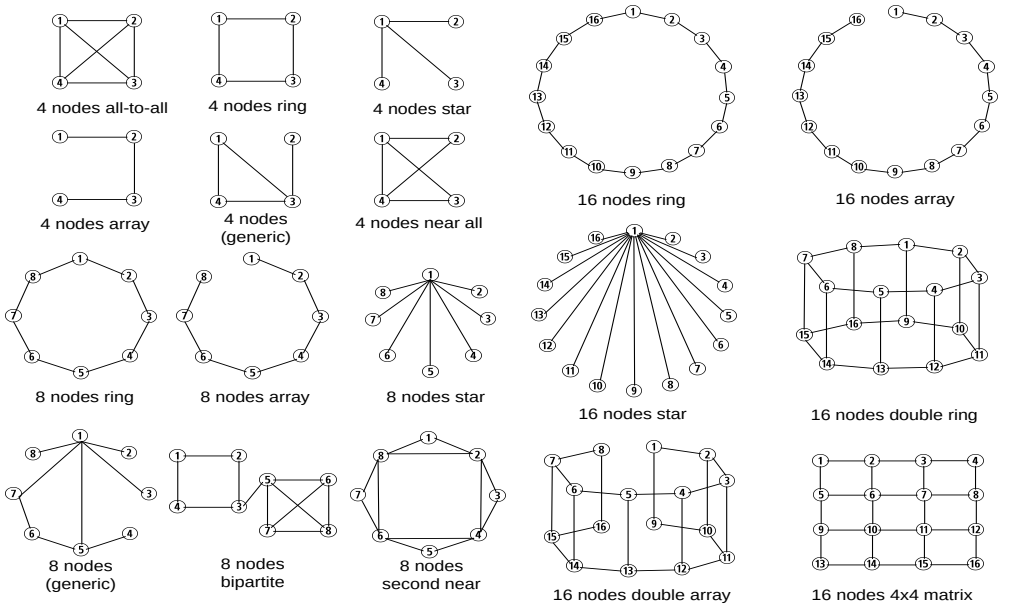

Figure 3.5: Different topologies implemented experimentally using the set up

As it is described in chapter 3, setup is available in two versions. As regards as the first version, the results of networks with 8,16,24,32 coupled Chua's circuits have been reported, all in array and ring configurations; additionally, star for networks of 8 and 16 Chua's circuits has been also configured. The second version of setup, whose maximum number of nodes is currently 8, has been used to examine networks of 4,5,6,7,8 Chua's circuits with various configurations exploring additionally the influence of non-local links (which connect non-adjacent nodes) in synchronization threshold. For all of the cases, coupled Chua's circuits are identical with chaotic double scroll as their individual dynamics; all couplings are uniform and undirected.

An experimental result in which the complete synchronization has formed is shown in figure 3.6a for the network of 8 Chua's circuits coupled in array structure with coupling resistor $R_{link} = 431\Omega$. The phase diagram of each node is depicted in figure 3.6b. Phase diagrams show all nodes are converging to chaotic double scroll solution which is the solution of decoupled nodes as well. Figure 3.6c shows the relative phase diagram where v_{C1} of the first node is plotted versus v_{C1} of all nodes. Relative cross correlation computed among v_{C1} of each pair of nodes i and j is shown in figure 3.6d. Poincarè map of all nodes is shown in figure 3.6e where the plane $v_{C2} = 0$ is considered as the poincarè section; results confirm the chaotic structure of nodes' dynamic as well as their agreement.

For the array, ring and star configurations, networks of 8,16,24 and 32 nodes have been scanned for coupling resistor R_{link} ranged from 120Ω to $3k\Omega$. Figure 3.7 shows their synchronization and cross correlation index diagram in the case of ring configuration. Vertical lines indicate theoretical threshold obtained by MSF (corresponding by color to each network) which highly agree with the experimental results. As figure shows, by increasing the number of Chua's circuits, the network synchronization come to be more fragile and is lost in lower coupling resistors. Similar scenario is happening for the array configuration which is shown in figure 3.8. Comparing figures 3.7 and 3.8 array configuration is more delicate and process of loosing synchronization is more abrupt.

The experimental results for the star configuration are depicted in figure 3.9 which is different from the other two configurations since, by increasing number of nodes, there is no shift in synchronization threshold and almost in all networks, synchronization shows very similar characteristic. This behavior is confirmed by MSF since the second eigen value of laplacian matrix λ_2 in star configuration is always 1 regardless of the number of nodes .

Table 3.1 shows the obtained synchronization threshold values both experimental and theoretical for discussed configurations. N represents the number of nodes, $R_{link_{th}}(MSF)$ and $R_{link_{th}}(exp)$ denote the threshold calculated through MSF and experiment respectively beyond which synchronization is lost. Considering that the minimum coupling resistor in the setup is 120Ω, for some networks (32-ring and array,16 and 24 both configured in array) which loose the synchronization below this value, the experiment result is not available.

Moreover in these experimental studies the role of non-local links (the link which connect two non-adjacent nodes) on synchronization level has been studied for several networks. Figure 3.10a shows several configurations of networks with 6 Chua's circuits.

Figure 3.10b shows the cross correlation index of all configurations. With regard to synchronization, the most robust is all to all configuration and the most fragile one is the array configuration. Configurations b and c and g in figure 3.10a show the same synchronization characteristic and all loose synchronization for the same value of the coupling strength. This results show the presence of nonlocal link

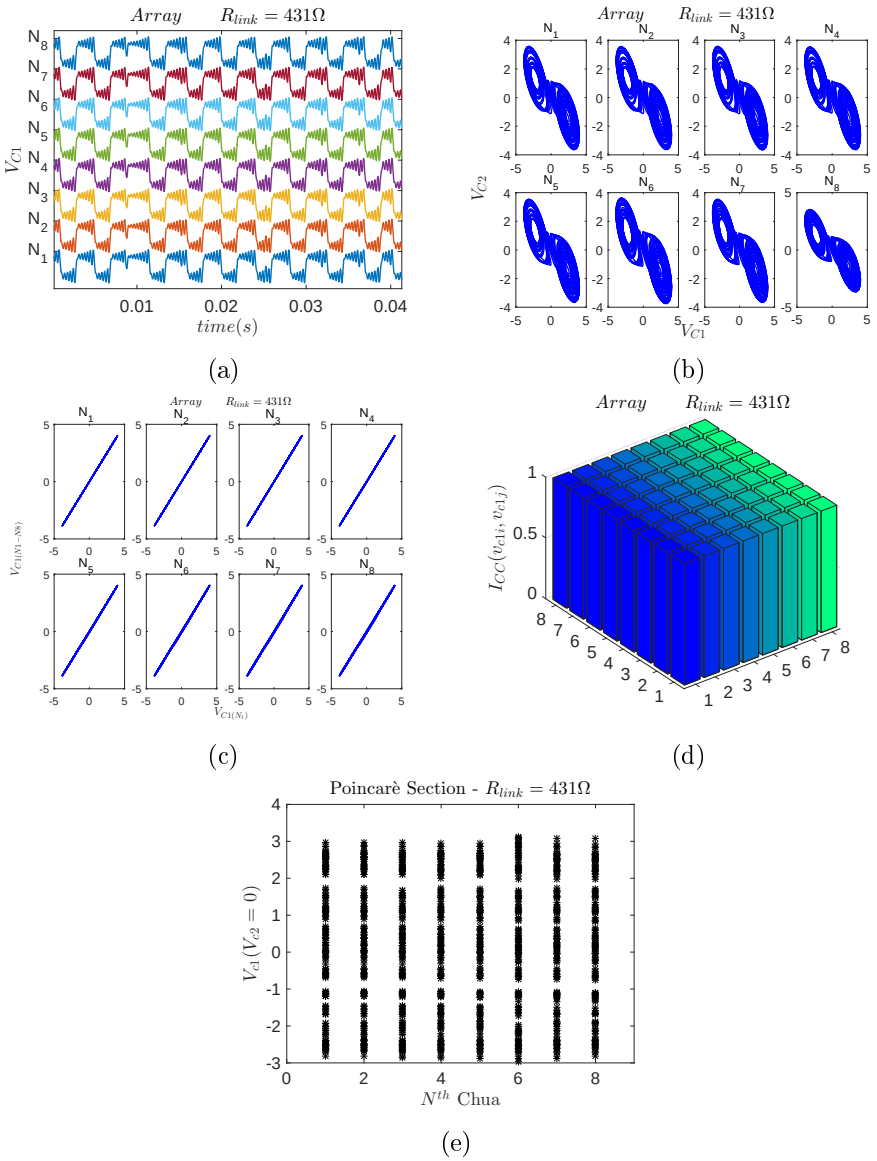

Figure 3.6: 8 coupled Chua's circuits at $R_{link} = 431\Omega$ reveal complete synchronization a) waveforms b) phase diagram (v_{C1i} vs. v_{C2i}) c) relative phase diagram (v_{C11} vs. v_{C1i}) d)relative cross correlation index $I_{cc}(v_{C1i}, v_{C1j})$ e)poincarè map

among nodes 2 and 5 in topology g has not improved the synchronization compare to configuration b in which no nonlocal links is implemented. However by adding the second nonlocal link among nodes 3 and 6 in topology f and further among nodes 1 and 4 in topology e, synchronization has kept improving each time.

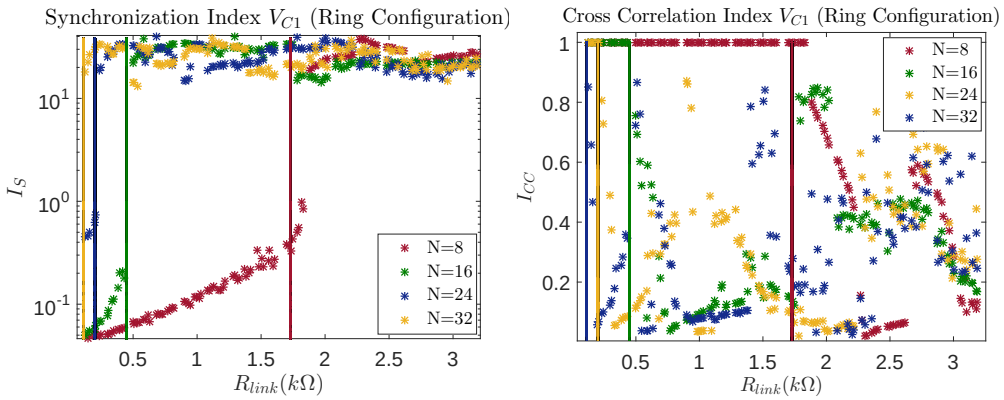

(a) (b)

Figure 3.7: 8 Chua's circuits configured in a ring a) synchronization index (I_S) b) cross correlation index (I_{CC})

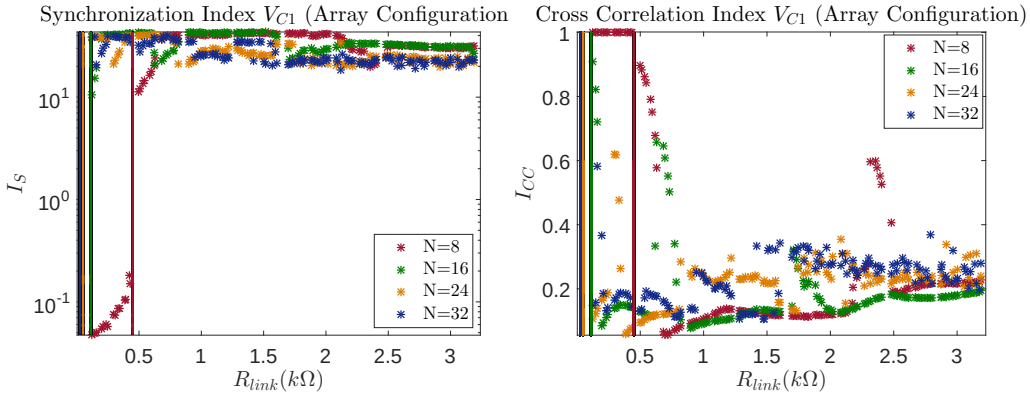

(a) (b)

Figure 3.8: array configuration of 8 Chua's circuits a) synchronization index (I_S) b) cross correlation index (I_{CC})

3.3. Experiments on networks of Chua's circuits with dynamic links

For the purpose of considering further complex model of interconnection, an additional dynamic term has been considered in the coupling of Chua's circuits by implementing coupling capacitors C_{link} parallel to coupling resistors R_{link}. The equation of motion for this network can be written as

$$\frac{d\mathbf{x}}{dt} = (\mathbf{I}_{nN\times nN} + \varepsilon_2 \mathbf{L} \otimes \mathbf{\Gamma})^{-1}(\tilde{\mathbf{F}}(\mathbf{x}) - \varepsilon_1 \mathbf{L} \otimes \mathbf{\Gamma}\mathbf{x}) \tag{3.3}$$

where $\mathbf{L}$ and $\mathbf{\Gamma}$ are the laplacian and coupling function matrix respectively. ε_1 and ε_2 are the coupling strengths of the proportional (resistive) and derivative

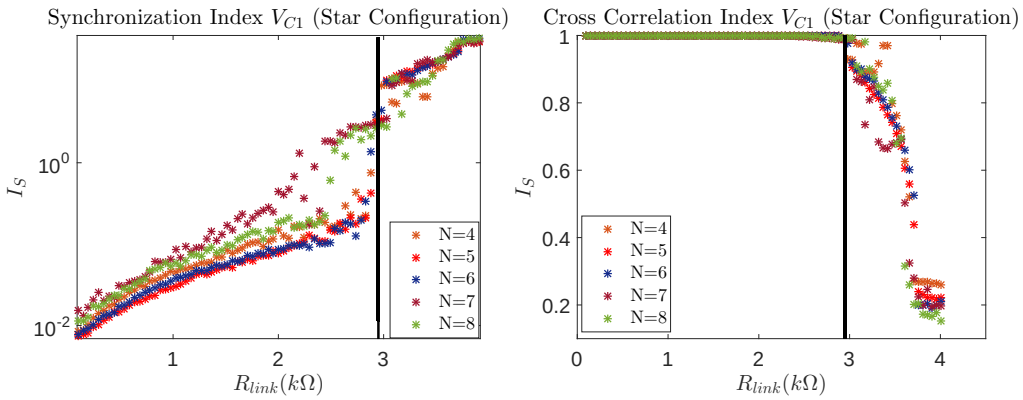

Figure 3.9: 8 Chua's circuits coupled in star a) synchronization index (I_S) b) cross correlation index (I_{CC})

Table 3.1: Synchronization threshold (experiment vs. MSF)

Configuration	N	λ_2	$R_{link_{th}(MSF)}$	$R_{link_{th}(exp)}$
Ring	8	0.5858	1729Ω	1831Ω
	16	0.1522	449Ω	431Ω
	24	0.0681	201Ω	209Ω
	32	0.0384	113Ω	–
Array	8	0.1522	449Ω	431Ω
	16	0.0384	113Ω	–
	24	0.0171	50Ω	–
	32	0.0096	28Ω	–
Star	4	1	2949Ω	2930Ω
	5	1	2949Ω	2979Ω
	6	1	2949Ω	2979Ω
	7	1	2949Ω	3027Ω
	8	1	2949Ω	3027Ω

(capacitive) contributions. Synchronization stability problem for this network can be solved by PDMSF approach [8] by finding the maximum Lyapunov exponent of the following variational equation

$$\frac{d\delta\mathbf{y}_i}{dt} = (\mathbf{I}_{n\times n} + \varepsilon_2\lambda_i\mathbf{\Gamma})^{-1}(D\mathbf{F}(\mathbf{x}) - \varepsilon_1\lambda_i\mathbf{\Gamma})\delta\mathbf{y}_i \quad for \quad i \geq 2 \tag{3.4}$$

where $k_1 = \varepsilon_1\lambda$ and $k_2 = \varepsilon_2\lambda$. The simulation results of PDMSF analysis for coupled Chua's circuits of this study is shown in figure 3.11 The black line shows the result when $k_2 = 0$ i.e. the value of capacitor in the coupling link is zero. The synchronization threshold is 6.1, which agrees with MSF result. The red line shows the condition where couplings in the links are composed of only capacitors. The threshold of gaining synchronization in the absence of R_{link} is 0.3. This result

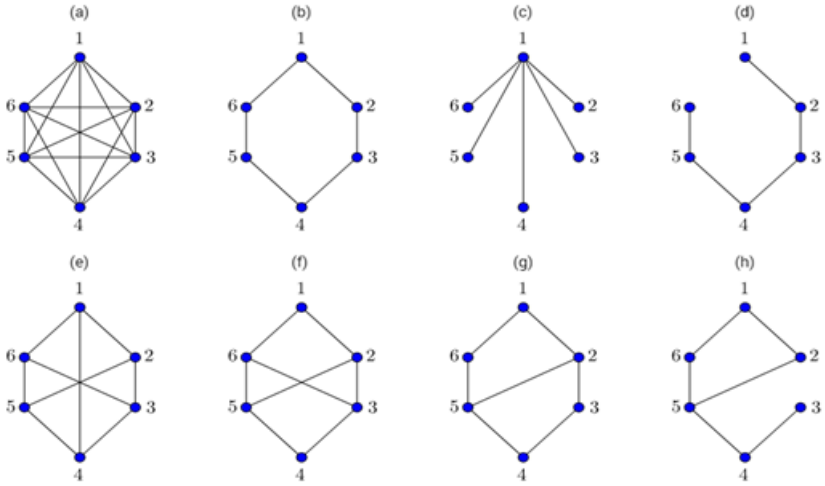

(a)

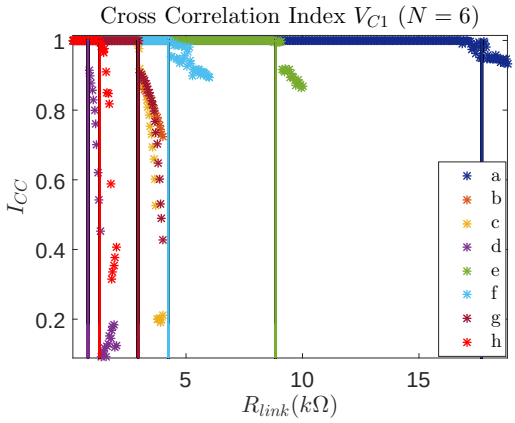

(b)

Figure 3.10: 6 coupled Chua's circuits a) examined configurations b) corresponding cross correlation indexes I_{CC} for all shown configurations

shows the strong impact of C_{link} in improving synchronization in the networks. The corresponding R_{link} and C_{link} to k_1 and k_2 respectively for Chua's circuit is calculated as

$$R_{link} = \frac{R_c C_2 \lambda_2}{C_1 k_1} \qquad C_{link} = \frac{k_2 C_1}{\lambda_2}$$

For the purpose of inspecting the effect of different configurations; coupled through dynamic links, in improving synchronization level, the two topologies shown in figure 3.12 have been implemented and their emergent dynamics have been explored. As figure shows, both topologies are composed of 8 identical nodes (Chua's circuits) and the coupling links are set to be uniform. Each link is realized by a pair of parallel coupling resistor R_{link} and capacitor C_{link}. The second eigen value of laplacian matrix λ_2 is 0.2509 for the first topology (a) and 0.2384

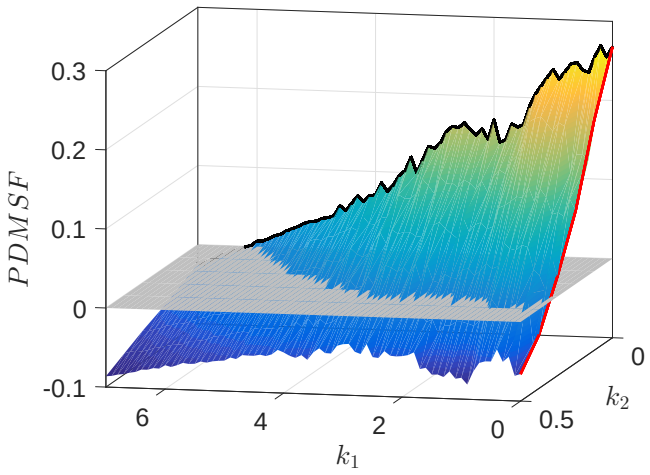

Figure 3.11: PDMSF diagram for k_1 varying from 0 to 7 and k_2 varying from 0 to 0.5

for the second one. Capacitors for all the links vary from $2pF$ to $20nF$ with the step of $500pF$ where for each capacitor coupling resistors are scanned from 120Ω to $20k\Omega$ with the step of 250Ω.

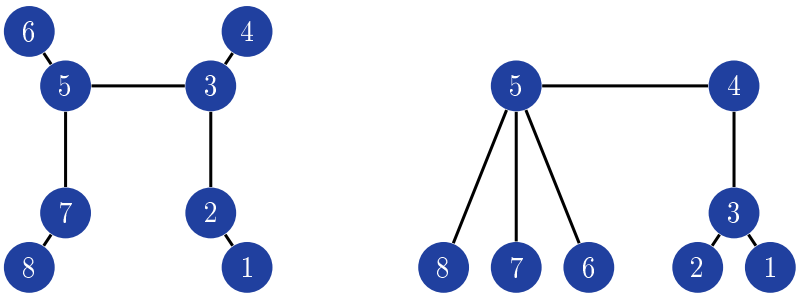

Figure 3.12: topologies implemented to dynamically coupled Chua's circuits

Two dimensional PDMSF diagrams are shown for both topologies in figure 3.13 where regions with positive maximum Lyapunov exponent show the ranges for which synchronized solution is unstable and cannot occur, whereas regions identified by negative maximum Lyapunov exponent are those with stable synchronous solution. The two networks are examined by the experimental setup for the coupling range mentioned above. Cross correlation and synchronization index of two experimentally tested networks are evaluated and the results are compared with the simulated ones as well as PDMSF diagram in figure 3.13. Figure 3.14 shows synchronization indexes for topology (a) obtained by simulation and experiment. Similarly for topology (b) synchronization indexes are shown in figure 3.15.

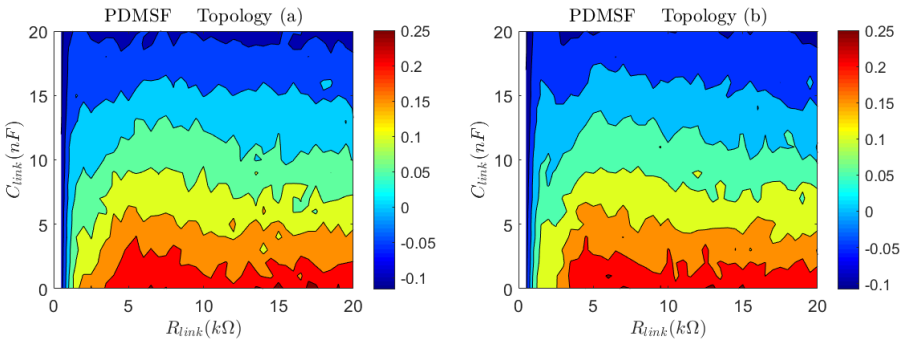

Figure 3.13: simulated PDMSF for a)topology a b)topology b

The simulation and experimental results show for both topologies that, when the coupling capacitors are very small, the synchronization threshold highly agrees with the threshold obtained by MSF approach in which the couplings are static i.e there are no capacitors in the links. Experimental threshold of loosing synchronization for both topologies (a) and (b) when $C_{link} = 2pF$ (This amount is the parasitic capacitor in the DIP switches which parallel the capacitors in each link to the coupling resistors) is 982Ω while the threshold obtained by MSF for $C_{link} = 0$ are 740Ω for topology (a) and 703Ω for topology (b). By further increasing the value of coupling capacitors the correlation level is improved according to the appearance of blue regions in I_S and I_{CC} which shows increasing of the synchronization level. Furthermore network topology (a) is showing better result since the blue region in synchronization diagram is wider.
It is worth noting, as it is already mentioned in chapter 1, that cross correlation index verifies the phase synchronization and it does not guarantee the equality of amplitudes, whereas synchronization index (I_S) measures both phase and amplitude agreement and this is the reason why in experimental I_{CC} diagram there are more uniformly colored blue regions compared to I_S.
Surprisingly, although the overall appearance of synchronization diagrams obtained by experiment is similar to simulation results, plotting the individual waveforms of chua's circuits reveals a poor agreement with theory and simulation. As an example, figure 3.16 shows both simulated and experimental waveforms of network topology (a) with $C_{link} = 18.19nF$ and $R_{link} = 6841\Omega$, located by pink arrow in both experimental I_S and I_{CC} diagrams of topology (a). Recalling PDMSF diagram in figure 3.14a the region with coupling capacitor $C_{link} = 18.19nF$ is a totally stable region far beyond threshold of gaining synchronization. According to theory in this region certainly, all chua's circuits' solutions have to synchronize completely in a chaotic double scroll solution of an individual node. However figure 3.16a obtained by experiment shows only phase correlated waveforms but not complete synchronization. For the same coupling, figure 3.16b obtained by simulation shows complete synchronization and chaotic double scroll solution which agrees with theoretical results. Such disagreement is

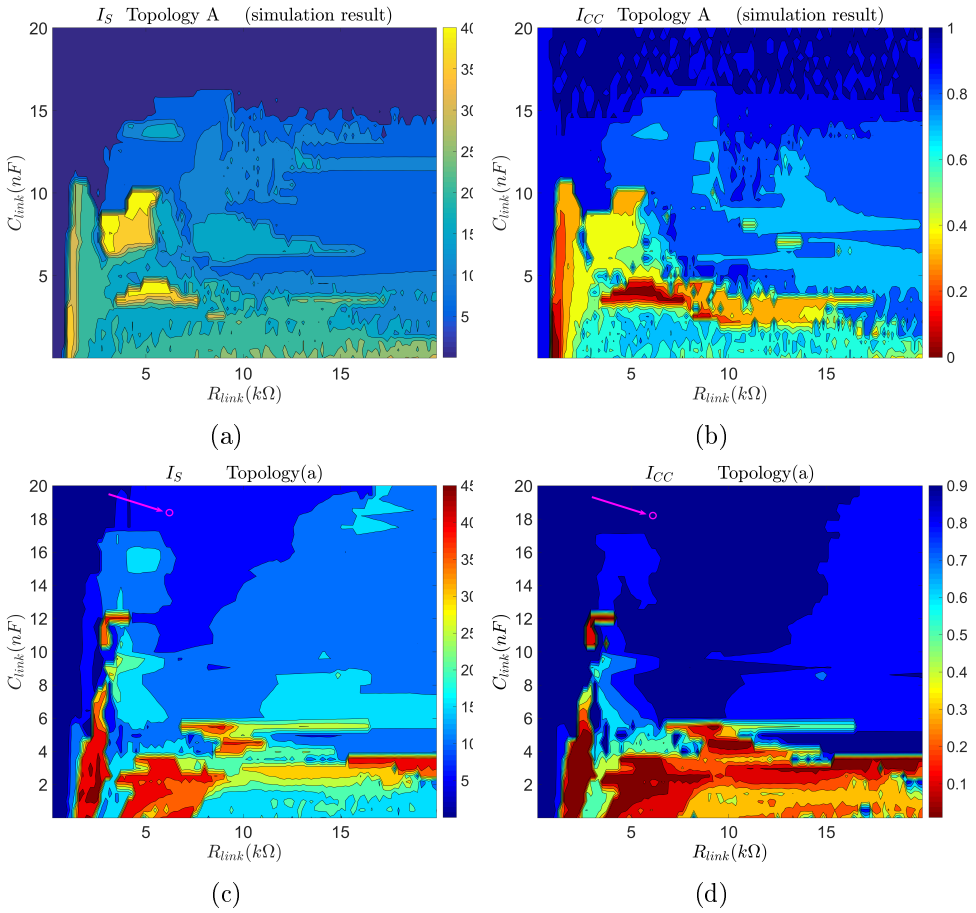

Figure 3.14: evaluated synchronization level for the topology shown in figure 3.18a a) synchronization index (I_S)-simulation results b) cross correlation index (I_{CC})-simulation results c)synchronization index (I_S)-experimental results d)cross correlation index (I_{CC})-experimental results

caused by super sensitivity of the system with respect to initial conditions: currently the initial condition of the state variables of the examined network cannot be controlled physically. For proving the high influence of initial conditions on network synchronization and solution structure we have examined the network topology (a) coupled through $C_{link} = 34nF$ (theoretically 100% stable synchronized region) and R_{link} being varied from 120Ω to $50k\Omega$ in two conditions: in the first test we have scanned all the resistors continuously whereas in the second test, before varying the coupling resistor in each step, the coupling links are isolated from the network automatically for 1 second (a time much bigger than time constant). We have seen that in the first test in some specific threshold the network looses synchronization and the dynamic immediately changes to periodic with significant partitioning: some nodes oscillate in positive region and some in negative region, as shown in figure 3.16a. In the second test, the network has

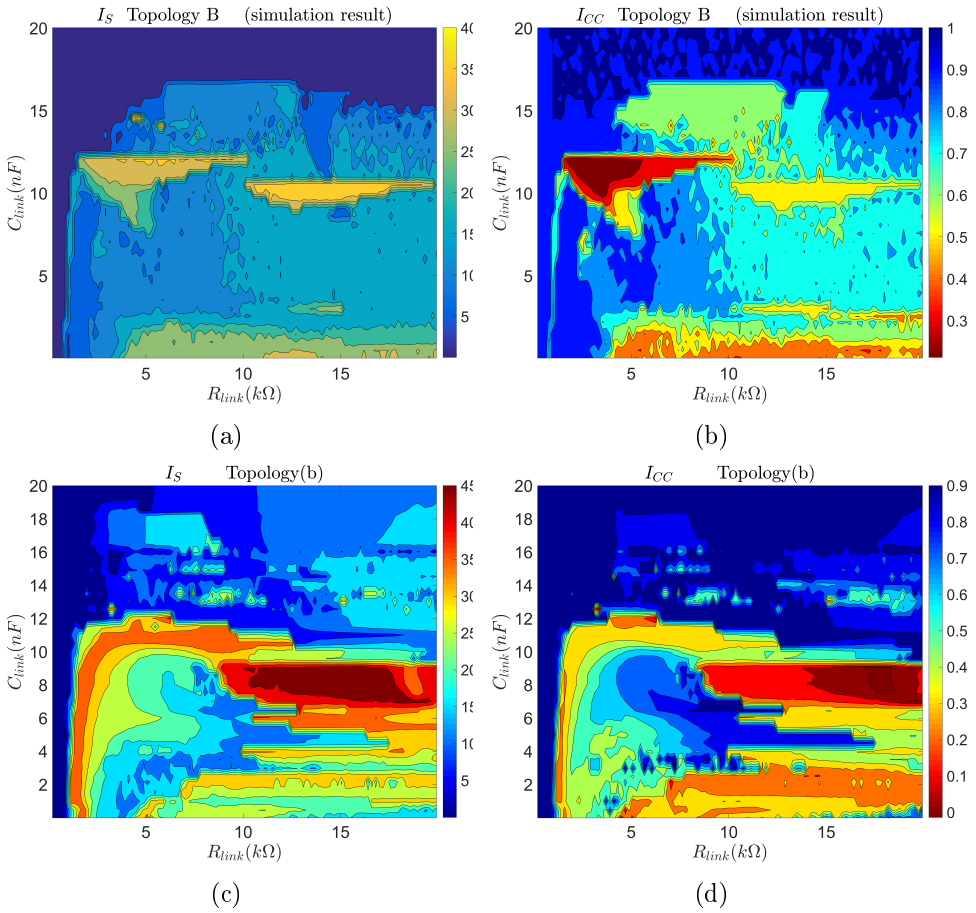

Figure 3.15: synchronization level evaluated for the topology shown in figure 3.18b a) synchronization index (I_S)-simulation results b) cross correlation index (I_{CC})-simulation results c)synchronization index (I_S)-experimental results d)cross correlation index (I_{CC})-experimental results

become more robust in keeping synchronization: eventually looses the synchrony and jumps to periodic solution but, immediately, recovers it. Figure 3.17 shows the cross correlation acquired from both tests. This results shows the coexistence of two solutions depending on initial conditions; such a result should be studied deeply by analyzing the basin of attraction for such network. Therefore, the presence of small parameter mismatches, parasitic terms and uncontrollable initial condition, which are not considered in PDMSF approach has narrowed experimental synchronization from complete to phase synchronization.

3.4. Experiments on networks with multiplex links

Networks in reality might be coupled through different types of links, leading to multiplex networks. In this study we refer to multiplex networks as those whose couplings do not have the same types in all over the network, i.e. laplacian matrix

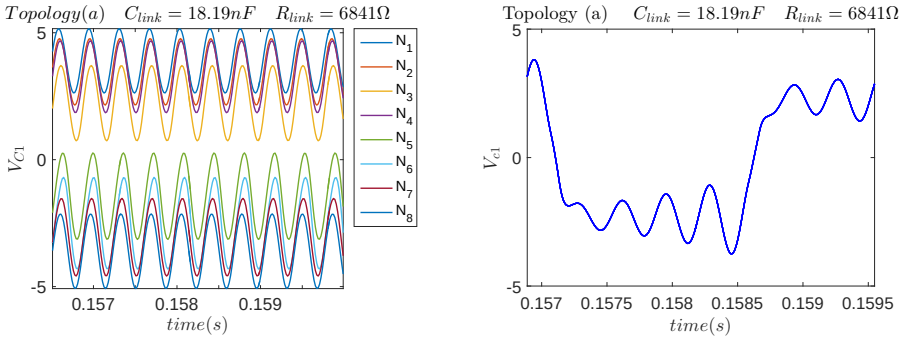

(a) (b)

Figure 3.16: waveforms of 8 coupled Chua's circuits with topology (a) coupled by $C_{link} = 18.19nF$ and $R_{link} = 6841\Omega$ a) experiment b)simulation

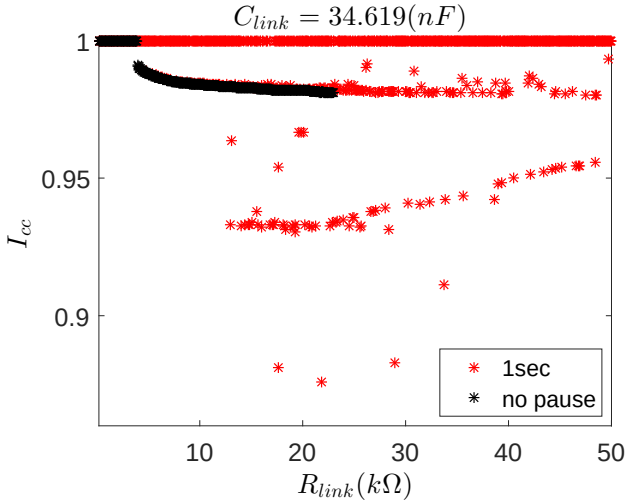

Figure 3.17: cross correlation index of topology a acquired under two text conditions; first the coupling resistor is scanned continuously and the second test is detaching all the coupling links for 1 second before each scan of coupling resistor

describing the resistive coupling (L_{Res}) is different from laplacian coupling matrix representing capacitive(dynamic) coupling among nodes (L_{Cap}). Therefore the equation of motion is governed by

$$\frac{d\mathbf{x}}{dt} = (\mathbf{I}_{nN\times nN} + \varepsilon_2 \mathbf{L}_{Cap} \otimes \mathbf{\Gamma})^{-1}(\tilde{\mathbf{F}}(\mathbf{x}) - \varepsilon_1 \mathbf{L}_{Res} \otimes \mathbf{\Gamma}\mathbf{x}) \tag{3.5}$$

The examined topologies are those shown in figure 3.12; topologies a and b can be combined in such a way that Chua's circuits are coupled by resistors through topology a and by capacitors through topology b and vice-versa. Figures 3.19 and 3.20 show the synchronization and cross correlation indexes for both cases obtained by experimental results. Figures show that the synchronization level

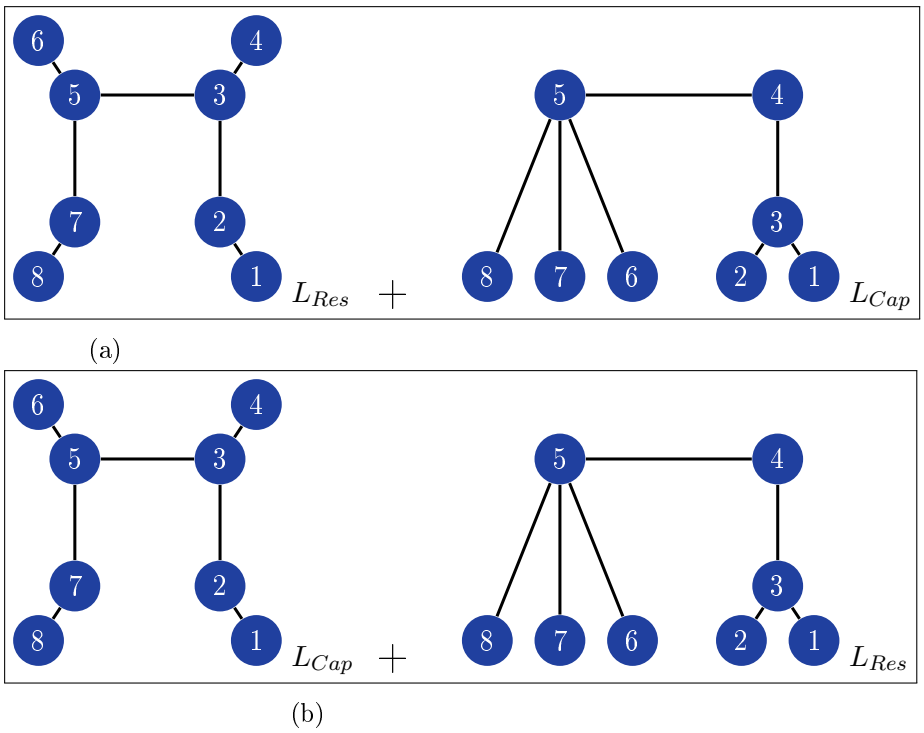

Figure 3.18: topologies implemented to multiplex coupled Chua's circuits a,b) 8 Chua's circuits are configured by resistors through topology represented by laplacian matrix L_{Res} and at the same time coupled by capacitors through L_{Cap}

compared to dynamically coupled network topologies a and b, is improved and multiplex topology a shows even a better results.

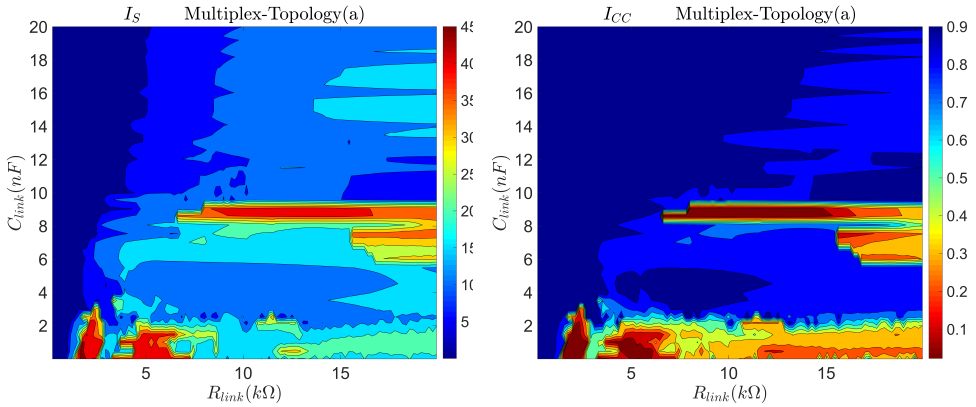

(a) (b)

Figure 3.19: multiplex network coupled via resistors and capacitors with topology a (L_{Res}) and b (L_{Cap}) respectively a) synchronization index I_S b) cross correlation index I_{CC}

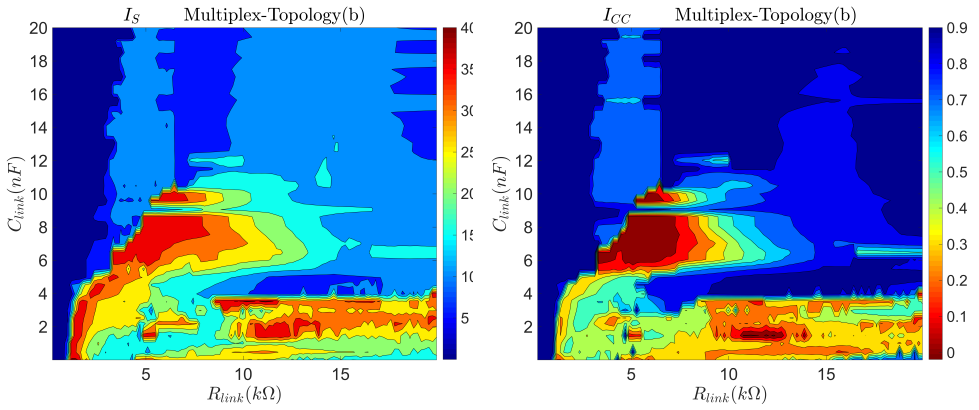

(a) (b)

Figure 3.20: multiplex network coupled via resistors and capacitors with topology b (L_{Res}) and a (L_{Cap}) respectively a) synchronization index I_S b) cross correlation index I_{CC}

This types of networks can be studied in network control and robustness problems. However they have not considered theoretically yet.

3.5. Further emergent dynamics: patterns and traveling waves

Beyond complete synchronization, interestingly the experiments show a non-trivial mechanism of synchronization loss which differs depending on the type of configurations and coupling links. Through this transition a rich variety of dynamical behaviors can be observed such as clustering and spatiotemporal periodic patterns and waves. Some of the results are reported and discussed in [17, 31, 43, 44] as well. In this section the most notable dynamics in the network with static couplings discussed in section 3.2 are presented.

The first reported case is nominally identical 24 chua's circuits configured in array with uniform static links. It is observed that, by loosing synchronization, nodes start partitioning into various clusters and converge to solutions different from complete synchronous solution. Figure 3.21 shows this network with two different coupling strength.

As figure 3.21a depicts each 2 nodes are in one partition or cluster. Moving from the center of network i.e. nodes 12 and 13, outwards, the amplitude of oscillation has increased. By varying the coupling resistor to 334Ω (figure 3.21b) number of nodes in each cluster is doubled. poincarè diagrams in figures 3.21 (c-d) show this partitioning clearly. This mechanism has been repeated for networks with array configuration with different numbers of nodes. In chapter 5 cluster synchronization is discussed more extensively.

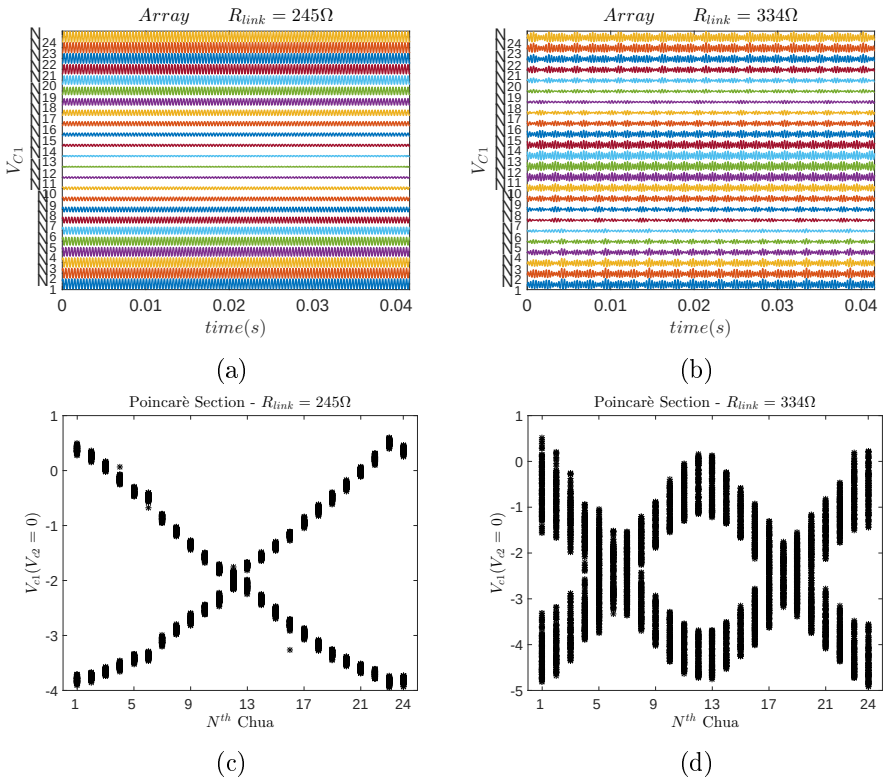

Figure 3.21: 24 Chua's circuits coupled in a ring a) waveform at coupling resistor $R_{link} = 245\Omega$ b) $R_{link} = 334\Omega$ c) poincarè diagram at $R_{link} = 225\Omega$ d) $R_{link} = 334\Omega$

Mechanism of synchronization loss in ring of 24 Chua's circuits is shown in figure 3.22. In this case all nodes keep a close correlation after loosing complete synchronization (figure 3.22a) which is termed as lag synchronization since the solution of all nodes will be the same after applying a suitable phase shift.

In figures 3.22(b-e) the emergent of spatiotemporal periodicity is shown. Figures 3.22(b-c) show travelling waves rotating clockwise and couter-clockwise. By further increasing the coupling resistance in figure 3.22(d) waveforms can be viewed as superposition of two waveforms of rotating clockwise and counter-clockwise 3.22(b-c). The similar patterns have formed by increasing the coupling resistance to 431Ω with increasing the frequency of rotation. Figure 3.23 shows Poincarè diagram, and relative cross correlation index for coupling resistors $R_{link} = 431\Omega$ where spatial periodicity is evidenced as well as node's clustering. Similar behavior has been observed in network with different number of nodes coupled in ring. Figure 3.24 shows mechanism of period doubling for ring of 24 nodes coupled with $R_{link} = 982\Omega$.

Distinctively in star configuration by loosing complete synchronization the central node's amplitude continues deteriorating as it is shown for star network of 8

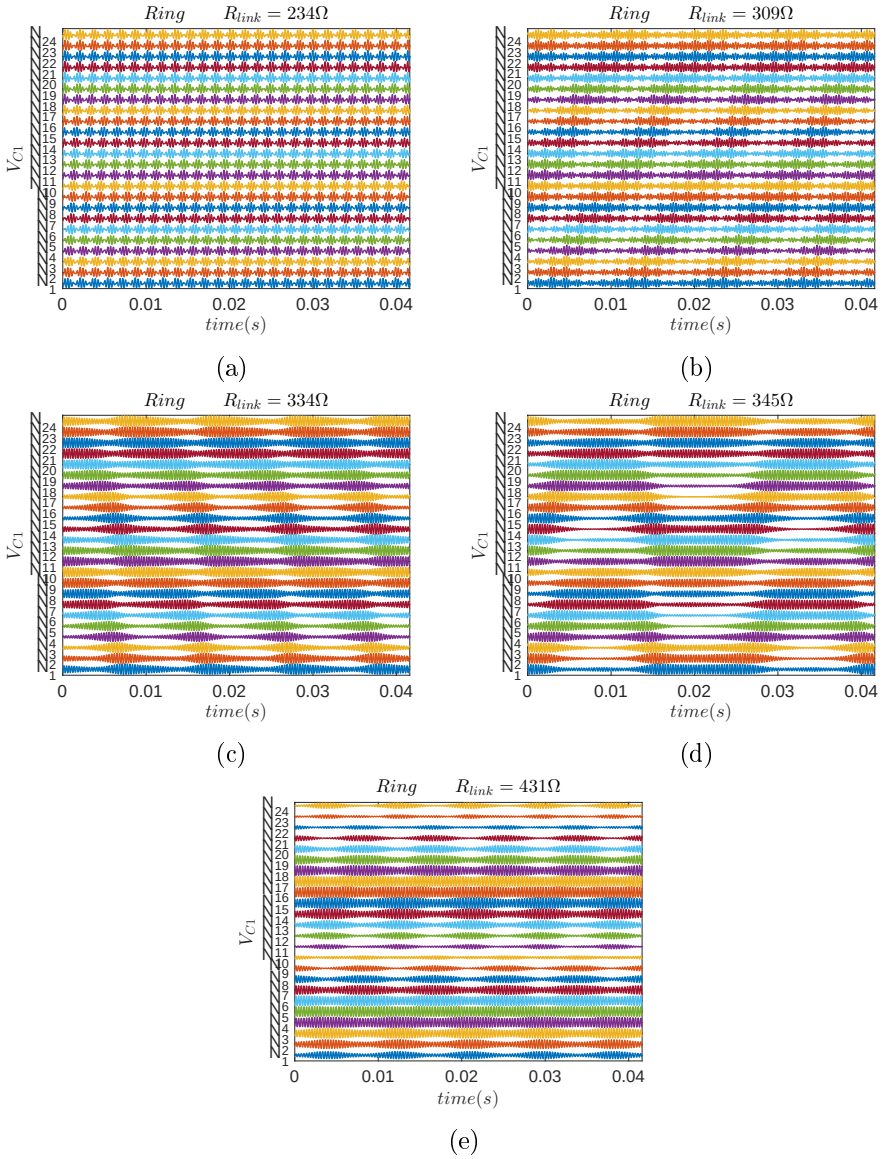

Figure 3.22: emergent dynamics of 24 coupled Chua's circuits in ring with R_{link} a) 234Ω b) 309Ω c) 334Ω d) 345Ω e) 431Ω

Chua's circuits in figure 3.25 which is along with varying the solution structure from chaotic to periodic.

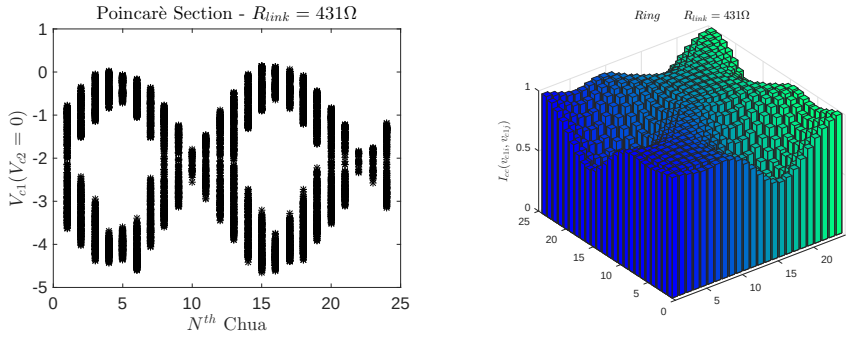

(a) (b)

Figure 3.23: ring of 24 Chua's circuits configured with $R_{link} = 431\Omega$ a)poincarè diagram b)relative cross correlation index

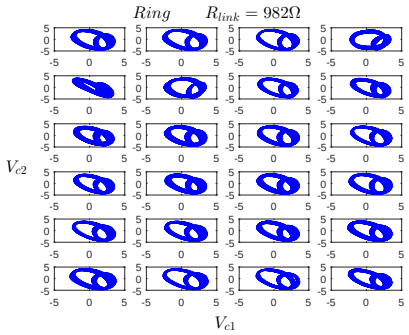

Figure 3.24: phase diagram of 24 Chua's circuits configured in ring with $R_{link} = 982\Omega$

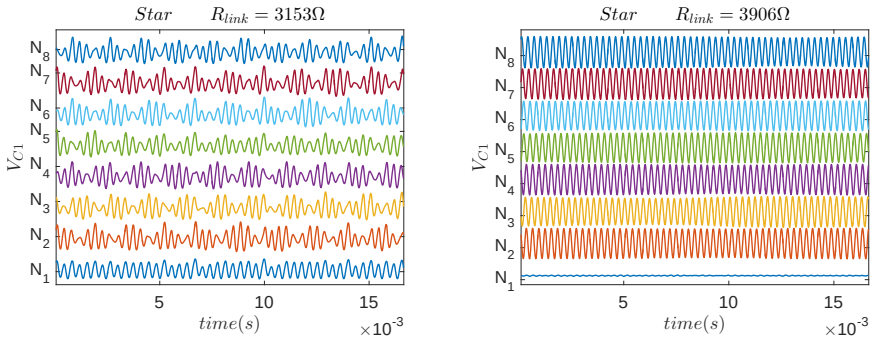

(a) (b)

Figure 3.25: waveforms of 8 Chua's circuits coupled in star configuration for different coupling resistors R_{link} a) 3153Ω b) 3906Ω

Chapter. 4

Experiments on cluster synchronization

Recent studies show that structural symmetry (automorphism) strongly affects the emergent dynamics of the network in the sense that structurally equivalent nodes in the network can synchronize and form clusters while diverging from other nodes belonging to different clusters [42]. This behavior is known as cluster synchronization.

Many of network structures are symmetric in which some specific nodes are topologically equivalent i.e. they can be mapped to each other without changing the network topology. The set of all structurally equivalent nodes of network's graph form an orbit [30]. On the other hand permutation of network's nodes which leaves the structure unchanged is called automorphism or symmetry. The set of all network's automorphisms form a group G under composition of permutations. Each automorphism or symmetry can be represented by a permutation matrix $\mathbf{P}$, a symmetric matrix with all row-sums and column-sums equal to 1. The entries of this matrix are 0 and 1 where $p_{ij} = p_{ji} = 1$ if nodes i and j can be mapped to each other without changing the structure otherwise $p_{ij} = 0$. It is straightforward to obtain $\mathbf{PP}^{-1} = \mathbf{P}^2 = \mathbf{I}$.

Using computational group theory all the automorphisms of a network can be computed. An important property of an automorphism is preserving the adjacency matrix i.e. $\mathbf{AP} = \mathbf{PA}$. This implies that nodes with the same equation of motion including the coupling term, if starting from a synchronized state, will remain synchronized. In this regard knowing the automorphism of a network graph can be helpful in predicting related patterns of clusters. However clusters might be unstable so that cannot be observed, which has motivated recent studies addressing the stability analysis of clusters. [42, 49].

This Chapter presents the experiment and simulation results of exploring cluster synchronization in various topologies based on the mentioned assumption that cluster formation is closely related to the symmetric structure of the network [20, 21, 42].
The examined networks are composed of nominally identical chaotic Chua's cir-

cuits coupled by resistors. Our aim is to investigate the emergence of clusters and the conditions for their persistence in real experimental conditions where the initial conditions of all nodes are random, without being controlled.
Such studies can be considered as further steps towards understanding the influence of network structure on its emergent behavior, specifically synchronization and failure mechanism in complex networks such as electrical power grids or neural networks in the brain and consequently network robustness.

For the sake of simplicity we have implemented a network composed of 5 nodes as the main topology which has gone through 4 different tests. In the first experiment all the coupling strengths of the main network have been varied equally and its dynamics has been monitored. In the second and third experiments, one link is removed to observe the effect of varying structural symmetries on the formation of clusters. Finally in the last experiment, one coupling strength has been changed while the remaining couplings have been kept fixed.

In the following section we report the first three examined cases mentioned above where we have investigated the influence of different structural symmetries on network dynamics. The second section will describe pattern control related to the last experiment, where we aim to probe the influence of varying one coupling link's strength on revealing all the possible patterns of clusters related to topological symmetry. In the last section we report the simulation results comparing the original model of Chua's circuit and the modified one as discussed in the second chapter.

4.1. Cluster synchronization and network structural symmetry

The networks of interest are those discussed in chapter 3.1 which are composed of nominally identical nodes evolving in double scroll chaotic regime when uncoupled. The couplings are static and identical, implemented by resistors which couple each pair of adjacent Chua's circuits through their v_{C1}. For the sake of simplicity the topology shown in figure 4.1a has been examined. This network has two orbits $\{1\}$ and $\{2,3,4,5\}$ which means that nodes 2,3,4 and 5 can be mapped to each other without changing the structure of the network and node 5 can be mapped to itself only. Consequently the axis shown by dashed red lines in figure 4.1b denotes two symmetry operations represented by permutation matrices $\mathbf{P}_1$ permuting nodes 2 and 5 as well as 3 and 4 and $\mathbf{P}_2$ permuting nodes 2 and 3 to each other and nodes 4 and 5, written as:

$$\mathbf{P}_1 = \begin{bmatrix} 1 & 0 & 0 & 0 & 0 \\ 0 & 0 & 0 & 0 & 1 \\ 0 & 0 & 0 & 1 & 0 \\ 0 & 0 & 1 & 0 & 0 \\ 0 & 1 & 0 & 0 & 0 \end{bmatrix} \qquad \mathbf{P}_2 = \begin{bmatrix} 1 & 0 & 0 & 0 & 0 \\ 0 & 0 & 1 & 0 & 0 \\ 0 & 1 & 0 & 0 & 0 \\ 0 & 0 & 0 & 0 & 1 \\ 0 & 0 & 0 & 1 & 0 \end{bmatrix}$$

Discussed network has been examined in four different ways: (i) varying all cou-

pling resistors R_{link} equally; (ii) and (iii) removing one link (figure 4.6(a,b)) and consequent change of the symmetries; (v) varying the coupling strength of only one link $R_{link(2-5)}$ and leave the rest of couplings fix in $10k\Omega$ (figure 4.9). In the first three cases network is unweighted (the coupling strength among nodes are considered identical) and the last case is weighted network(with heterogeneous coupling strength). Here we report the results of the first three tests. The unweighted networks' equation of motions is governed by equation (3.1)

Cluster formation of the network has been investigated by the resistors being scanned from 120Ω the region of complete synchronization to $50k\Omega$ where synchronization is lost. The correlation among nodes are quantified by the cross correlation index (I_{CC}) which is shown in figure 4.1c. Synchronization is lost experimentally at $R_{th(exp)} = 9033\Omega$. The vertical red line shows the theoretical threshold of synchronization calculated by MSF approach which is $R_{th(MSF)} = 8846\Omega$. The cross correlation index shows sudden jump just after loosing synchronization where its decrease shows the network transition towards the state of uncorrelation among Chua's circuits. Figure 4.2 shows the network's dynamic when all

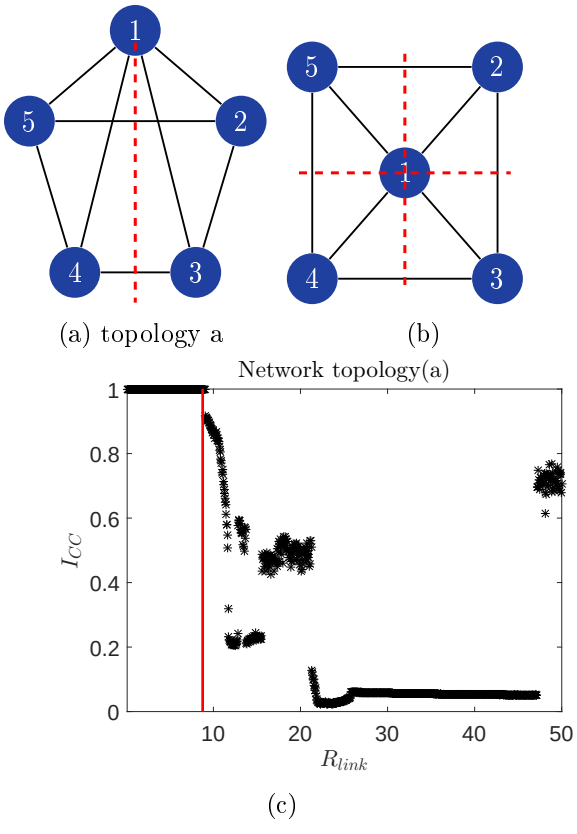

Figure 4.1: a-b) network topology c) cross correlation index

nodes are synchronized. Just after the threshold of loosing synchronization nodes $2, 3, 4$ and 5 remain correlated while dynamic of node 1 is sensibly different (figure 4.3a). By further increasing the coupling resistance other solutions, even with

different structure appear (Figure 4.3(b-d)). Although the network is structurally symmetric but no proper cluster synchronization corresponding to the mentioned symmetry axis appear. The proof can be seen through relative synchronization index shown in figure 4.4 among discussed expected clusters.

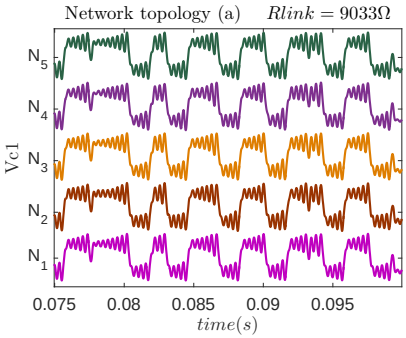

Figure 4.2: waveforms v_{C1} of Chua's circuits of network topology of figure 4.1 coupled by $R_{link} = 9033\Omega$

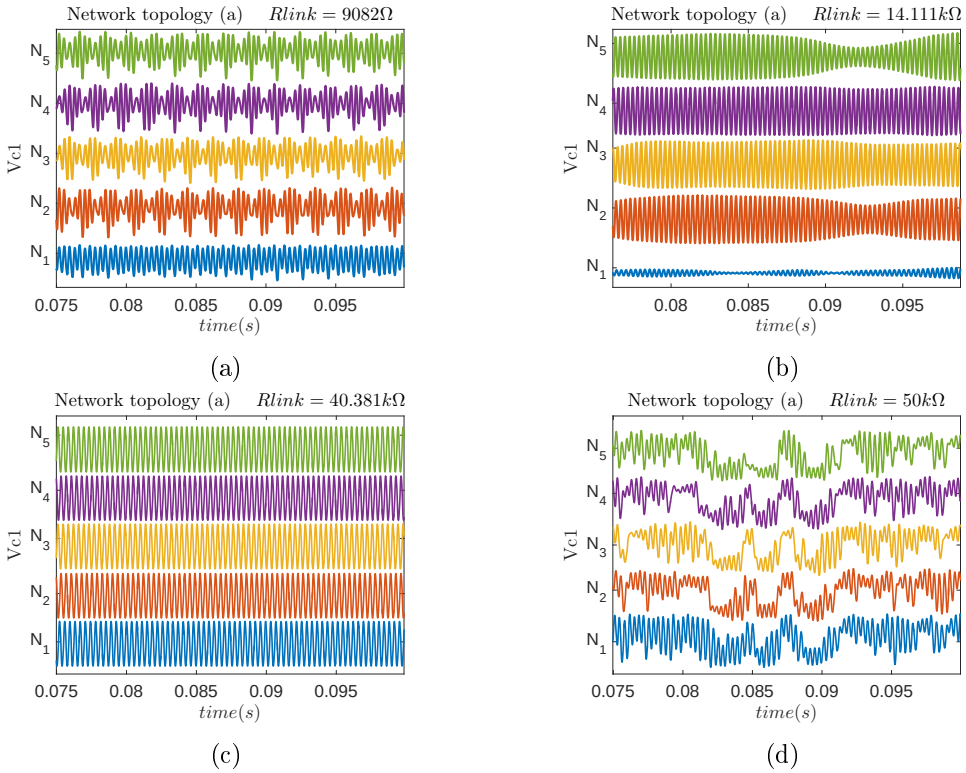

Figure 4.3: waveforms of Chua's circuits's state variables v_{C1} for network topology of figure 4.1 coupled by R_{link} a) 9082Ω b) $14.111k\Omega$ c) $40.381k\Omega$ d) $50k\Omega$

For theoretical investigation of synchronization mechanism (from stability to instability) additionally maximum Lyapunov exponent of all transverse modes $\delta\mathbf{y}_i \quad (i \geq 2)$ through MSF has been evaluated where the network is linearized

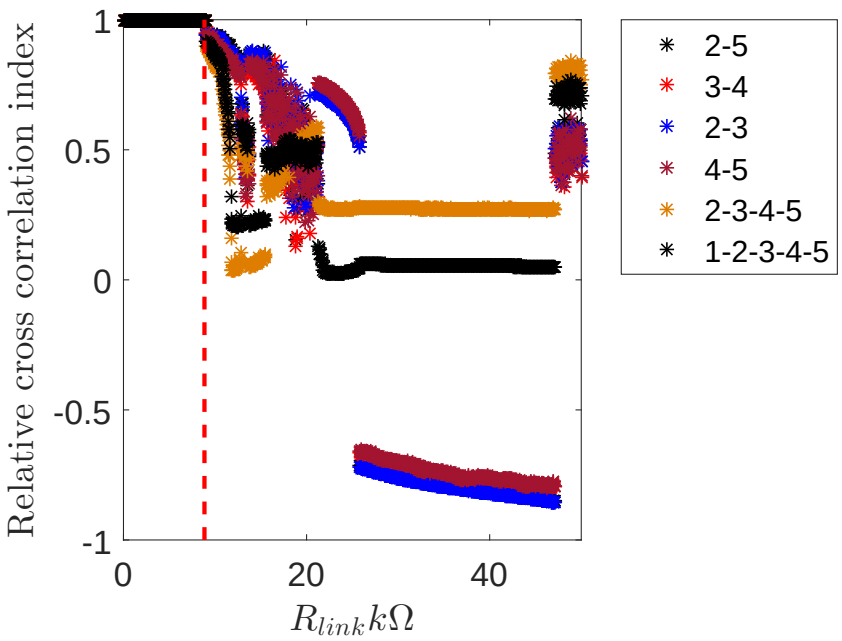

Figure 4.4: relative cross correlation index among symmetric pairs of nodes in topology of figure 4.1

about the complete synchronous state which is assumed to be the solution of an isolated node when is detached from the network i.e $\dot{\mathbf{x}}_S = \dot{\mathbf{x}}_i = \mathbf{F}(\mathbf{x}_i)$. Figure 4.5 depicts all maximum Lyapunov exponents corresponding to the transverse modes of the network i.e. $\delta\mathbf{y}_i \quad (i \geq 2)$ which are 4. The first mode represents the synchronous manifold $\delta\mathbf{y}_1$ whose maximum Lyapunov exponent is always positive due to the chaotic behavior of Chua's circuits. Black vertical dashed line R_{th} corresponds to the threshold of synchronization below which all the transverse modes damp due to negativity of their maximum Lyapunov exponents and therefore synchronous state is stable. Beyond threshold as figure shows third transverse mode first followed by the second one loose their stability and by further increasing R_{link} transverse modes 4 and then 5 loose their stability as well at $15k\Omega$ due to positive value of their maximum Lyapunov exponent. This means beyond R_{th} the dimension of the network solution increase since all nodes do not converge to the same solution anymore as shown in figure 4.3.

In the next experiment $R_{link(1-3)}$ has been disconnected as shown in figure 4.6a: Symmetry axis changes since now nodes 1-5 and 2-4 can be permuted without changing the structure. By switching $R_{link(1-3)}$ to $R_{link(1-4)}$, topology shown in figure 4.6b has been examined whose symmetry enables permuting of nodes 1-2 and 3-5 while topology remain unchanged. Figure 4.7 shows the cross correlation index of the two topologies where synchronization experimentally is lost at $R_{link} = 6396\Omega$. Unlike cross correlation index of the topology shown in figure 4.1a which decrease rapidly, the transition mechanism in both topologies in figure

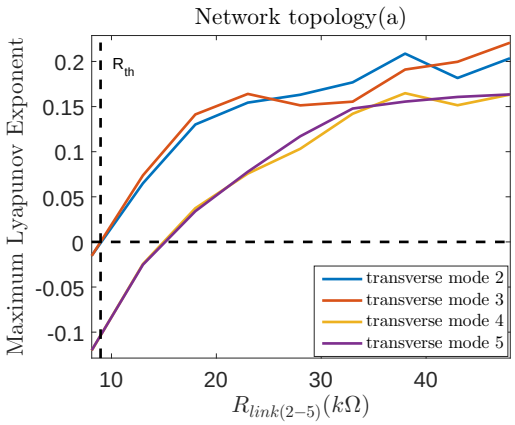

Figure 4.5: maximum Lyapunov exponent of all transverse modes $\delta \mathbf{y}_i \quad (i \geq 2)$ in network of figure 4.1

4.6 is smoother. The red vertical line corresponds to the theoretical threshold evaluated by MSF which is $5.896k\Omega$ for both networks since their connectivity matrix is similar i.e. their eigen values are the same. Relative cross correlation

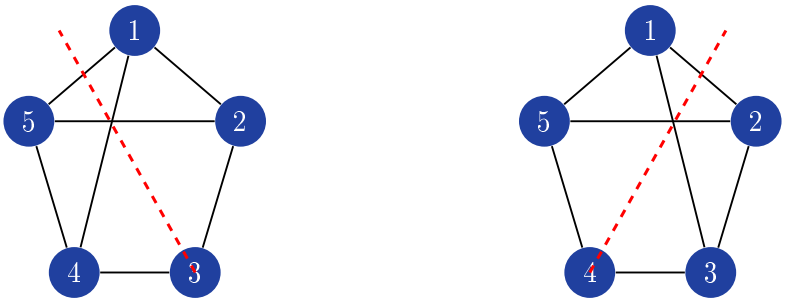

(a) topology b (b) topology c

Figure 4.6: a) network topology a with link $1-3$ disconnected b) network topology a with link $1-4$ disconnected

indexes of clusters corresponding to symmetries of topologies in figure 4.6 are shown in figure 4.8.

Relative cross correlation index among pairs of (1-5) and (2-4) is shown in figure 4.8a just after loss of global synchronization where both clusters have formed. By increasing the value of coupling resistance, cluster synchronization among nodes 1 and 5 is weakened at $9.483k\Omega$ without disturbing cluster of nodes 2 and 4. Cluster 1 and 5 is lost also at $10.5k\Omega$. By further increasing of coupling resistance cluster synchronization among nodes 2 and 4 is retained in a wide range from $21.29k\Omega$ to $36.13k\Omega$. Similarly in figure 4.8b it is observed the formation of symmetry related clusters where by increasing coupling resistor one cluster has been lost while other cluster has remained synchronized.

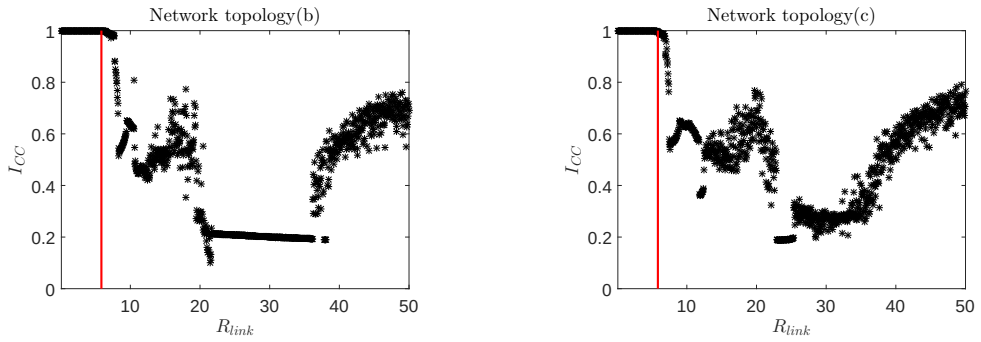

(a) (b)

Figure 4.7: cross correlation index (I_{CC}) a)network topology b b)network topology c

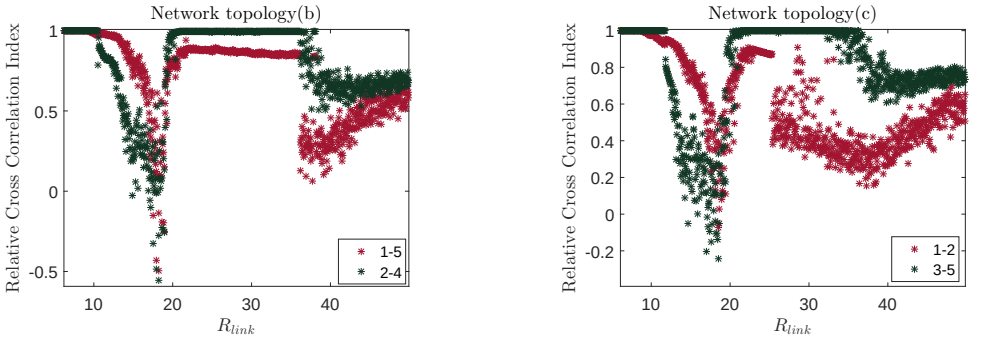

(a) (b)

Figure 4.8: relative cross correlation index (I_{CC}) a)network topology b b)network topology c

4.2. Cluster synchronization in weighted networks

As it was explained the expected clusters related to discussed symmetries in the main topology under the first test did not appear. Here we present an experiment through which by varying the strength of only one non-local link the network dynamic is scanned and clusters related to symmetry come to exist and remain stable in specific range of coupling. The network topology is shown in figure 4.9 where is the same as the main topology with keeping all the coupling strength fixed and identical at $10k\Omega$ and vary link $2-5$ i.e $\sigma_{25} \neq \sigma_{ij} \quad i,j \neq 2,5$. The coupling resistor $R_{link(2,5)}$ has been varied from 120Ω to $50k\Omega$, the link is dashed in figure 4.9. The equation of motion of this weighted network is

$$\frac{d\mathbf{x}_i}{dt} = \mathbf{F}(\mathbf{x}_i(t)) + \sum_{j=1}^{N} \sigma_{ij} a_{ij} L_{ij} \mathbf{H}(\mathbf{x}_j) \qquad i \in \{1, \cdots, N\} \tag{4.1}$$

where σ_{ij} and a_{ij} are the coupling strength and the adjacency indicator between nodes i and j.

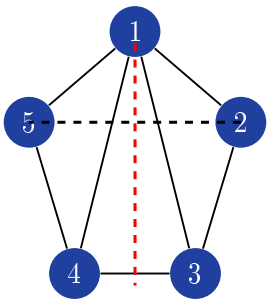

Figure 4.9: network topology (d) all the couplings are set at $10k\Omega$ except $R_{link(2-5)}$ which is varying from 120Ω to $50k\Omega$

This network never reaches complete synchronization since in the case of equal links the coupling strength is already beyond the complete synchronization threshold. Cross correlation index shown in figure 4.10a verify the absence of complete synchronization however still keeping high average value of 0.8 in a wide range (120Ω to $20k\Omega$).
Figure 4.10b shows the maximum Lyapunov exponents of all transverse modes of this network. The first transverse mode is always unstable which verifies that global (complete) synchronization never occurs in this configuration since for having complete synchronization according to MSF approach all the transverse modes have to be stable and negative. Therefore all the network nodes converge not to a single manifold of synchronization but to several. Figure 4.11 shows the dynamics of network nodes in $R_{link} = 98\Omega$ where node number 1 evolve in a solution different from the other 4 which have remained correlated. By further increasing the coupling resistance at 6530Ω indicated by L_1 in figure 4.10b the third transverse mode loose stability and this condition will remain. The modes 4 and 5 have remained stable for all coupling resistors, however their maximum Lyapunov exponent for high values of resistor tend to remain constant. To understand all the network behavior and solutions, network has to be linearized about all those cluster synchronous manifold. Here we obtain information only about the global synchronous manifold. It is worth noting that unlike the first three experiment in this experiment network is unweighted. By varying the link among nodes 2 and 5 the ordering of tranverse manifild obtained from block diagonalization of coupling matrix changes [62]. This is shown in figure 4.10(c,d) for both permutations $\mathbf{P}_1$ and $\mathbf{P}_2$.

Through figure 4.12 the complete synchronization and the cluster synchronization are compared. Cluster synchronization related to permutations $\mathbf{P}_1$ and $\mathbf{P}_2$ are shown separately in figure 4.13. Figure shows in the beginning, when the coupling resistance is low, cluster pattern of 3-4 and 2-5 form, by further increasing this cluster switch to other pattern 2-3 and 4-5 which can be seen in the zoomed subfigure. Increasing the resistance retain the first pattern of cluster i.e. 2-5 and 3-4. From 20 to 40 $k\Omega$ a sub cluster of the second pattern appear which are nodes 4-5 where 2 and 3 remain uncorrelated. Finally in very high resistance nodes 2 and 3 retain their synchronization stronger than 4 and 5 and so they keep the

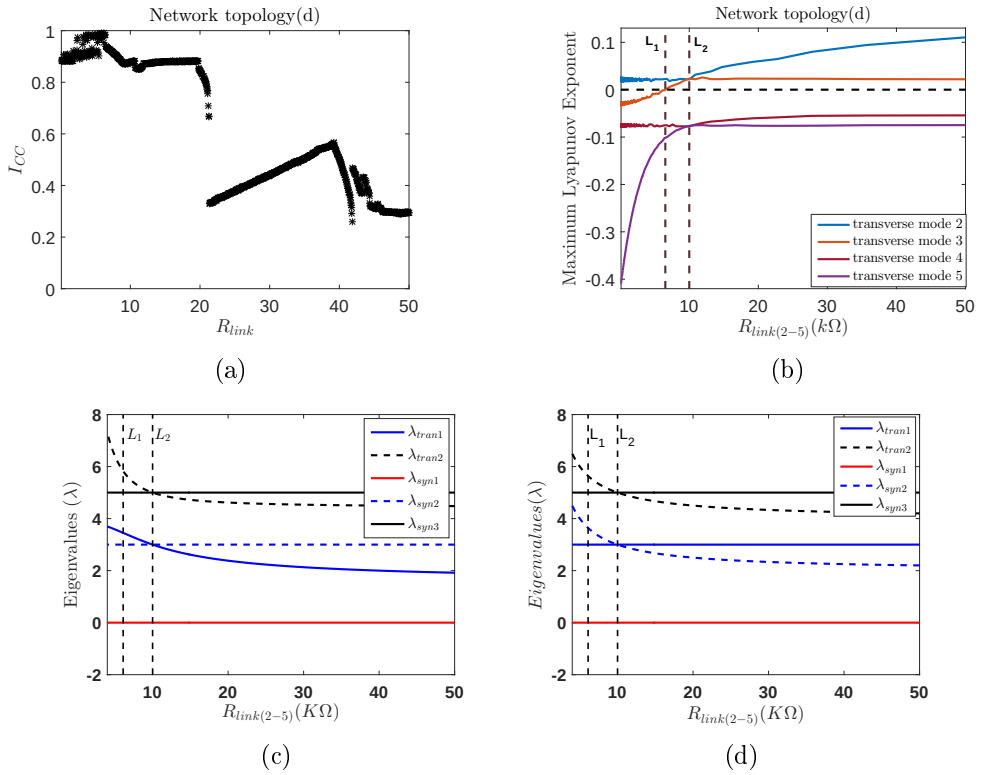

Figure 4.10: network topology (d) a) cross correlation index b)maximum Lyapunov exponent of all transverse modes c) ordering eigen values of block diagonalized Laplacian coupling matrix related to permutation P_1 d) ordering of eigen values of block diagonalized Laplacian coupling matrix related to permutation P_2

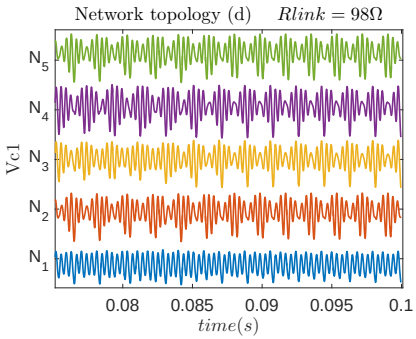

Figure 4.11: network topology (d) waveforms v_{C1} at $R_{link} = 98\Omega$

second pattern of cluster related to permutation $\mathbf{P}_2$.

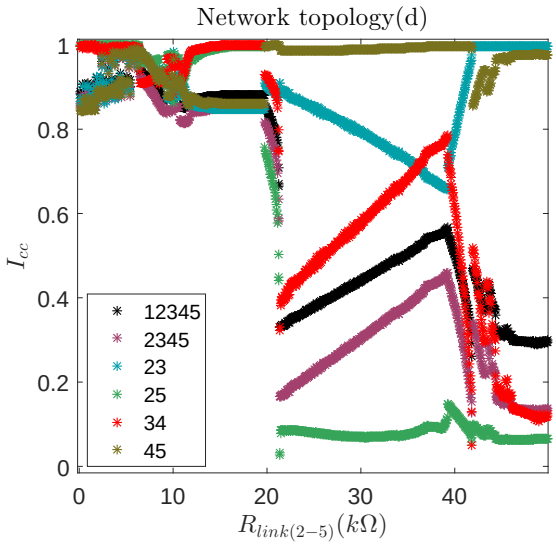

Figure 4.12: cross correlation index of complete and cluster synchronization in network topology (d)

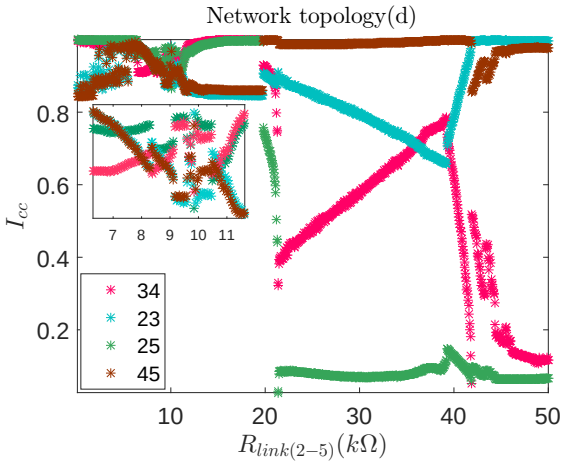

Figure 4.13: cross correlation index of cluster patterns $2-5, 3-4$ and $2-3, 4-5$ clusters in network topology (d)

4.3. Simulation results

Discussed networks have been simulated as well by adopting Chua's circuit model firstly introduced in chapter 1. The coupled differential equation of the network has been solved using matlab ode45 solver. The simulation results in unsynchronized region do not show any agreement with the experiment. Similarly ode15s, ode23s and ode23tb have failed to reach an agreement to the experiment since by loosing synchronization the amplitude of v_{c1} increase above saturation volt-

age for all nodes and as a result what appears is saturated v_{C1} and the patterns which appear in the experiment do not emerge. Figure 4.14 shows the waveforms of the network topology (a) simulated by chua's model shown in chapter 1 for $R_{link} = 8k\Omega$ when the network is synchronized and $R_{link} = 12k\Omega$ where the network is supposed to loose synchronization according to the threshold is reported in the previous section.

The network topology shown in figure 4.1 has been simulated for the same values

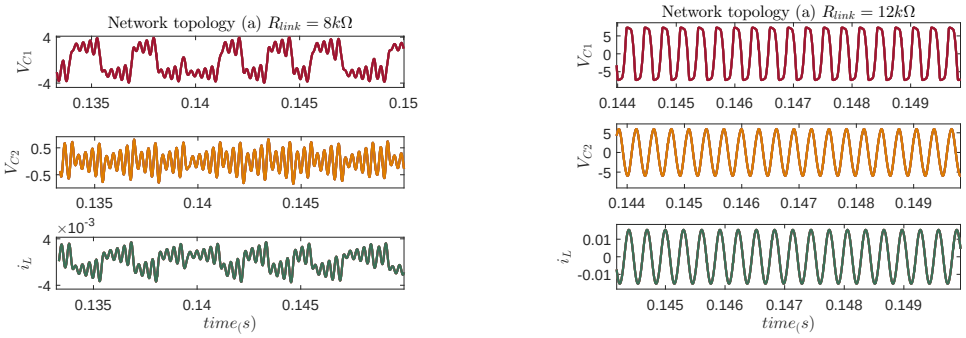

(a) (b)

Figure 4.14: network topology (a) simulation results using the 1st model of Chua's circuita) a) $R_{link} = 8k\Omega$ b) $R_{link} = 12k\Omega$

by the modified model of Chua's circuit which are shown in figure 4.15. Figure 4.16 depicts individually all the state variables of the network at $R_{link} = 12k\Omega$.

Simulated cross correlation indexes for topology a in figure 4.1, obtained by

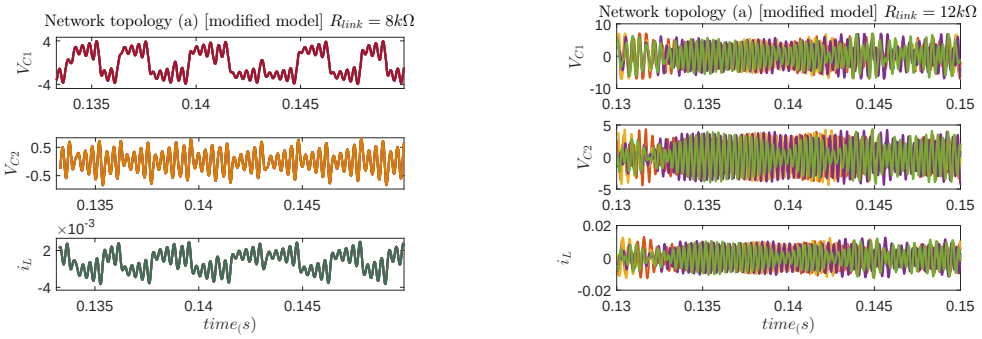

(a) (b)

Figure 4.15: network topology (a) simulation results using the the modified model of Chua's circuita) a) $R_{link} = 8k\Omega$ b) $R_{link} = 12k\Omega$

both classical and modified model, are shown in figure 4.17. According to cross correlation indexes in figure 4.17, clearly the classical model cannot reveal clusters and indicate synchronization for all values. In this regard the experimental setup has played an important role in showing the clusters and the necessity of modification in mathematical model of chua's circuit for revealing clusters.

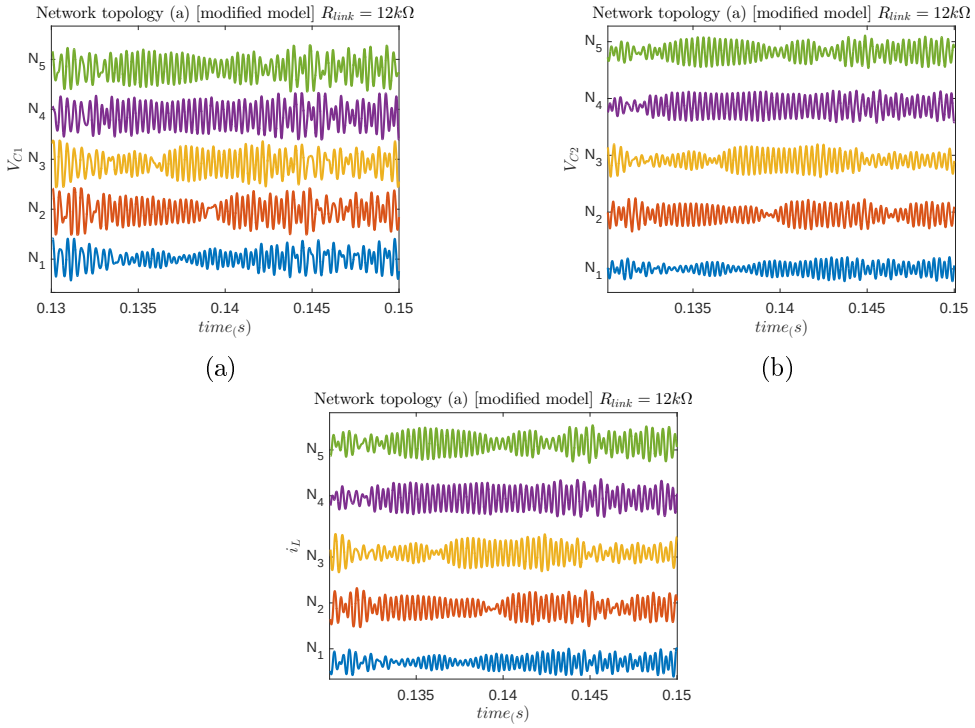

Figure 4.16: modified Chua's circuit simualtion result for $R_{link} = 12k\Omega$ a) v_{C1} b) v_{C2} c) i_L

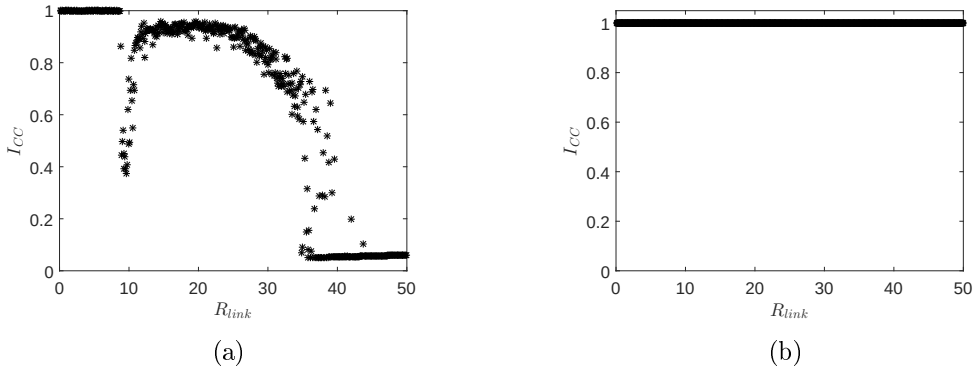

Figure 4.17: cross correlation index of network topology of figure 4.1 a) simulated by classic model of Chua's circuit b) simulated by modified model of Chua's circuit

Conclusions, discussion and research prospect

Contributions and notable achievements

We have presented novel experimental results of emerging dynamics in a complex network of interacting nonlinear oscillators, from a setup that has been recognized as a not trivial in the landscape of current research [16]. Collecting such results from a real physical implementation has been an important tool to demonstrate the robustness of many theoretically predicted phenomena, and at the same time a way to get them almost in real time, as compared to simulations. Moreover it has been demonstrated the feasibility, with present day data acquisition technology, to deal with the contemporaneous acquisition and control of relatively fast varying signals (up to 64 up to now) in this context.
Main contribution of this PhD work have been:

(i) the accurate characterization of the setup, both in the chaotic nodes and the interconnection network;

(ii) the contribution to the realization of updated version of the setup with new structure, range and resolution for the interconnection network;

(iii) the realization of extended measurement campaigns on synchronization thresholds for several topologies and both static and dynamic links;

(iv) the proposal and the effective use of the setup for new experimental studies on clustering;

(v) the proposal and the effective use of the setup for new experimental studies on PID and Multiplexed synchronization;

In particular, as consequence of the accurate characterization, in Chapter 2 some corrections to the Chua's circuit model have been proposed, required for better catching collective behaviors (beyond complete synchronization) in the network, whereas the previous standard model caused significant disagreement between simulation and experiment.

In chapter 3 we showed the experimental results of complete synchronization occurring in several topologies networks (statistically covering the range of possibilities) with homogeneous coupling, as a function of coupling strength and

network topology. The results evidenced a high agreement with MSF theoretical approach, validating the latter in a vast experimental range. Then such experimental range has been extended to even more realistic networks, by considering dynamic and complex links, with a more questionable agreement to theoretical predictions, which leaves open space to new research. We have also experimentally shown an improvement on synchronization level though using dynamic and complex coupling. In the same chapter we experimentally show a wide range of remarkable behaviors emerging in the network beyond complete synchronization. In fact through the experimental setup we have not restricted synchronization to the complete one and we have covered different types as lag and phase synchronization, as well as cluster formation in the network.

Finally, in chapter 4, we showed the physical implementation of symmetric networks where their symmetry cause partitioning networks' nodes correspondingly. It is shown how symmetries can be at the origin of different patterns, that (depending on coupling) result stable, and consequently can be formed and experimentally observed.

Open problems and future works

Apart from the above-described specific achievements, this study revealed the high potential of the considered experimental setup, that can be used in a plenty of exploratory multipurpose studies. Expandability of the setup as well as its configurability, make it capable for testing larger complex networks, especially in the area of clustering. Moreover, an expected new version based on FPGA control section will largely extend the capability of studying distribute dynamical control issues.

Some open problems are in the area of theoretical approach to examine the stability of networks with complex links, for which we get some experimental (and numerical) results, but no theory is available to compare with.

Some future work, at the present in the form of a research proposal, is to study nearly synchronous clusters caused by approximate symmetries in the network.

Publications

Conference papers

[1] C. Petrarca, S. Yaghouti, L. Corti, M. de Magistris, Analogic realization of a non-linear network with re-configurable structure as paradigm for real time analysis of complex dynamics. Advances in Neural Networks: Computational and Theoretical Issues, pages 375-382, 2015.

[2] C. Petrarca, S. Yaghouti, L. Corti, M. de Magistris, Experimental Dynamics Observed in a Configurable Complex Network of Chaotic Oscillators, 22nd International Conference on Nonlinear Dynamics of Electronic Systems, Proceedings of, in Communications in Computer and Information Science Volume 438:203-210 July 4-6, 2014, Albena (Bulgaria)

[3] S. Yaghouti, C. Petrarca, M. de Magistris, Experiments on Clustering and Synchronous Patterns Dynamics Observed in a Configurable Network of Chaotic Oscillators. Emergent Complexity from Nonlinearity, in Physics, Engineering and the life science, pages 93-104,2017.

[4] M. de Magistris, S. Yaghouti, L. Corti, D. Assante, A Didactic Electronic Set-up for Introducing to Complex Networks of Chaotic Oscillators, IEEE Global Engineering Education Conference (EDUCON), pages 818-825, April 10-13, 2016, Abu Dhabi, (United Arab Emirates)

Journal papers

[1] M. de Magistris, M. di Bernardo, S. Manfredi, C. Petrarca, S. Yaghouti, Modular Experimental Set-up for Real Time Analysis of Emergent Behavior in Networks of Chua's Circuits, International Journal on Circuit Theory and Applications, vol. 44 (8): 1551-1571, 2015.

Book chapter

[1] M. de Magistris, C. Petrarca, S. Yaghouti, Experimental studies on reconfigurable networks of chaotic oscillators IET Book on Oscillator Cir

cuits: Frontiers in Design, Analysis and Applications,(36):209-244, 2016, DOI: 10.1049/PBCS032E

Bibliography

[1] L. Aguirre et al. Inductorless chua's circuit. *Electronics Letters*, 36(23):1915–1916, 2000.

[2] K. T. Alligood, T. D. Sauer, and J. A. Yorke. *Chaos.* Springer, 1996.

[3] A. Alvarez-Socorro, G. Herrera-Almarza, and L. González-Díaz. Eigencentrality based on dissimilarity measures reveals central nodes in complex networks. *Scientific reports*, 5, 2015.

[4] A.-L. Barabási. Linked: The new science of networks, 2003.

[5] M. Barahona and L. M. Pecora. Synchronization in small-world systems. *Physical review letters*, 89(5):054101, 2002.

[6] V. Belykh, N. Verichev, L. Kocarev, and L. O. Chua. On chaotic synchronization in a linear array of chua's circuits. *Journal of circuits, systems, and computers*, 3(02):579–589, 1993.

[7] S. Boccaletti, V. Latora, Y. Moreno, M. Chavez, and D.-U. Hwang. Complex networks: Structure and dynamics. *Physics reports*, 424(4):175–308, 2006.

[8] D. A. Burbano Lombana and M. di Bernardo. Synchronization and local convergence analysis of networks with dynamic diffusive coupling. *Chaos: An Interdisciplinary Journal of Nonlinear Science*, 26(11):116308, 2016.

[9] L. O. Chua. Chua's circuit: An overview ten years later. *Journal of Circuits, Systems, and Computers*, 4(02):117–159, 1994.

[10] L. O. Chua, M. Itoh, L. Kocarev, and K. Eckert. Chaos synchronization in chua's circuit. *Journal of Circuits, Systems, and Computers*, 3(01):93–108, 1993.

[11] L. O. Chua, L. Kocarev, K. Eckert, and M. Itoh. Experimental chaos synchronization in chua's circuit. *International Journal of Bifurcation and Chaos*, 2(03):705–708, 1992.

[12] M. Colandrea, M. de Magistris, M. di Bernardo, and S. Manfredi. A fully reconfigurable experimental setup to study complex networks of chua?? s

circuits. In *Nonlinear Dynamics of Electronic Systems, Proceedings of NDES 2012*, pages 1–4. VDE, 2012.

[13] A. M. Dabrowski, W. R. Dabrowski, and M. J. Ogorzalek. Dynamic phenomena in chain interconnections of chua's circuits. *IEEE Transactions on Circuits and Systems I Fundamental Theory and Applications*, 40(11):868–871, 1993.

[14] M. de Magistris, M. Di Bernardo, E. Di Tucci, and S. Manfredi. Synchronization of networks of non-identical chua's circuits: Analysis and experiments. *Circuits and Systems I: Regular Papers, IEEE Transactions on*, 59(5):1029–1041, 2012.

[15] M. de Magistris, M. di Bernardo, and C. Petrarca. Experiments on synchronization in networks of nonlinear oscillators with dynamic links. *Nonlinear Theory and Its Applications, IEICE*, 4(4):462–472, 2013.

[16] M. de Magistris, C. Petrarca, and S. Yaghouti. Experimental studies on reconfigurable networks of chaotic oscillators. *Oscillator Circuits: Frontiers in Design, Analysis and Applications*, (36):209–244, 2016.

[17] M. de Magistris, S. Yaghouti, L. Corti, and D. Assante. A didactic electronic set-up for introducing to complex networks of chaotic oscillators. *Global Engineering Education Conference (EDUCON)*, pages 818–825, 2016.

[18] L. Fabiny and K. Wiesenfeld. Clustering behavior of oscillator arrays. *Physical Review A*, 43(6):2640, 1991.

[19] L. Fortuna. *Chua's circuit implementations: yesterday, today and tomorrow*, volume 65. World Scientific, 2009.

[20] C. Fu, Z. Deng, L. Huang, and X. Wang. Topological control of synchronous patterns in systems of networked chaotic oscillators. *Phys. Rev. E*, 87:032909, Mar 2013.

[21] C. Fu, W. Lin, L. Huang, and X. Wang. Synchronization transition in networked chaotic oscillators: The viewpoint from partial synchronization. *Phys. Rev. E*, 89:052908, May 2014.

[22] W. Fulton and J. Harris. Representation theory, volume 129 of graduate texts in mathematics, 1991.

[23] M. Gomez-Gesteira, M. DeCastro, V. Perez-Villar, and L. Chua. Experimental chua's circuit arrays as an autowave simulator. *IEEE transactions on circuits and systems. 1, Fundamental theory and applications*, 46(4):495–499, 1999.

[24] L. Huang, Q. Chen, Y.-C. Lai, and L. M. Pecora. Generic behavior of master-stability functions in coupled nonlinear dynamical systems. *Physical Review E*, 80(3):036204, 2009.

[25] M. Jalili, A. A. Rad, and M. Hasler. Enhancing synchronizability of dynamical networks using the connection graph stability method. *International Journal of Circuit Theory and Applications*, 35(5-6):611–622, 2007.

[26] T. Kapitaniak, L. O. Chua, and G.-Q. Zhong. Experimental hyperchaos in coupled chua's circuits. *Circuits and Systems I: Fundamental Theory and Applications, IEEE Transactions on*, 41(7):499–503, 1994.

[27] M. P. Kennedy. Robust op amp realization of chua's circuit. *Frequenz*, 46(3-4):66–80, 1992.

[28] M. P. Kennedy. Three steps to chaos. ii. a chua's circuit primer. *IEEE Transactions on Circuits and Systems I: Fundamental Theory and Applications*, 40(10):657–674, 1993.

[29] H. K. Khalil. *Noninear Systems*. Prentice-Hall, New Jersey, 1996.

[30] B. D. MacArthur and R. J. Sánchez-García. Spectral characteristics of network redundancy. *Physical Review E*, 80(2):026117, 2009.

[31] M. Magistris, M. Bernardo, S. Manfredi, C. Petrarca, and S. Yaghouti. Modular experimental setup for real-time analysis of emergent behavior in networks of chua's circuits. *International journal of circuit theory and applications*, 44(8):1551–1571, 2015.

[32] A. P. Munuzuri, V. Perez-Munuzuri, M. Gomez-Gesteira, L. Chua, and V. Perez-Villar. Spatiotemporal structures in discretely-coupled arrays of nonlinear circuits: a review. *International Journal of Bifurcation and Chaos*, 5(01):17–50, 1995.

[33] M. Newman. *Networks: an introduction*. Oxford University Press, 2010.

[34] M. E. Newman. The structure and function of complex networks. *SIAM review*, 45(2):167–256, 2003.

[35] M. E. Newman and M. Girvan. Finding and evaluating community structure in networks. *Physical review E*, 69(2):026113, 2004.

[36] Y. Nishio and A. Ushida. Spatio-temporal chaos in simple coupled chaotic circuits. *Circuits and Systems I: Fundamental Theory and Applications, IEEE Transactions on*, 42(10):678–686, 1995.

[37] Y. Nishio and A. Ushida. Quasi-synchronization phenomena in chaotic circuits coupled by one resistor. *Circuits and Systems I: Fundamental Theory and Applications, IEEE Transactions on*, 43(6):491–496, 1996.

[38] Y. Nishio and A. Ushida. Phase synchronization in a ring of chaotic circuits. *Proc. of NOLTA'01*, pages 163–166, 2001.

[39] M. J. Ogorzalek, Z. Galias, A. M. Dąbrowski, and W. R. Dąbrowski. Chaotic waves and spatio-temporal patterns in large arrays of doubly-coupled chua's circuits. *Circuits and Systems I: Fundamental Theory and Applications, IEEE Transactions on*, 42(10):706–714, 1995.

[40] G. V. Osipov and V. D. Shalfeev. Chaos and structures in a chain of mutually-coupled chua's circuits. *IEEE Transactions on Circuits and Systems-Part I-Fundamental Theory and Applications*, 42(10):693–699, 1995.

[41] L. M. Pecora and T. L. Carroll. Master stability functions for synchronized coupled systems. *Physical Review Letters*, 80(10):2109, 1998.

[42] L. M. Pecora, F. Sorrentino, A. M. Hagerstrom, T. E. Murphy, and R. Roy. Cluster synchronization and isolated desynchronization in complex networks with symmetries. *Nature communications*, 5, 2014.

[43] C. Petrarca, S. Yaghouti, L. Corti, and M. de Magistris. Analogic realization of a non-linear network with re-configurable structure as paradigm for real time analysis of complex dynamics. *Advances in Neural Networks: Computational and Theoretical Issues*, pages 375–382, 2015.

[44] C. Petrarca, S. Yaghouti, and M. de Magistris. Experimental dynamics observed in a configurable complex network of chaotic oscillators. *Nonlinear Dynamics of Electronic Systems: 22nd International Conference, NDES 2014, Albena, Bulgaria, July 4-6, 2014. Proceedings*, 438:203–210, 2014.

[45] C. Posadas-Castillo, C. Cruz-Hernández, and R. López-Gutiérrez. Experimental realization of synchronization in complex networks with chua's circuits like nodes. *Chaos, Solitons & Fractals*, 40(4):1963–1975, 2009.

[46] R. Rocha, G. L. Andrucioli, and R. O. Medrano-T. Experimental characterization of nonlinear systems: a real-time evaluation of the analogous chua's circuit behavior. *Nonlinear Dynamics*, 62(1-2):237–251, 2010.

[47] M. Rosenblum, A. Pikovsky, and J. Kurths. Synchronization—a universal concept in nonlinear sciences, 2001.

[48] J.-J. E. Slotine, W. Li, et al. *Applied nonlinear control*, volume 199. prentice-Hall Englewood Cliffs, NJ, 1991.

[49] F. Sorrentino, L. M. Pecora, A. M. Hagerstrom, T. E. Murphy, and R. Roy. Complete characterization of cluster synchronization in laplacian-coupled systems. *arXiv preprint arXiv:1507.04381*, 2015.

[50] F. Sorrentino, L. M. Pecora, A. M. Hagerstrom, T. E. Murphy, and R. Roy. Complete characterization of the stability of cluster synchronization in complex dynamical networks. *Science advances*, 2(4):e1501737, 2016.

[51] S. H. Strogatz. Exploring complex networks. *Nature*, 410(6825):268–276, 2001.

[52] S. H. Strogatz. *Nonlinear dynamics and chaos: with applications to physics, biology, chemistry, and engineering*. Westview press, 2014.

[53] J. Sun, E. M. Bollt, and T. Nishikawa. Master stability functions for coupled nearly identical dynamical systems. *EPL (Europhysics Letters)*, 85(6):60011, 2009.

[54] Y. Tang, F. Qian, H. Gao, and J. Kurths. Synchronization in complex networks and its application–a survey of recent advances and challenges. *Annual Reviews in Control*, 38(2):184–198, 2014.

[55] Á. Tar, G. Gandhi, and G. Cserey. Hardware implementation of cnn architecture-based test bed for studying synchronization phenomenon in oscillatory and chaotic networks. *International Journal of Circuit Theory and Applications*, 37(4):529–542, 2009.

[56] Y. Uwate and Y. Nishio. Synchronization in several types of coupled polygonal oscillatory networks. *IEEE Transactions on Circuits and Systems I: Regular Papers*, 5(59):1042–1050, 2012.

[57] S. Wiggins. *Introduction to applied nonlinear dynamical systems and chaos*, volume 2. Springer Science & Business Media, 2003.

[58] C. W. Wu and L. O. Chua. Application of graph theory to the synchronization in an array of coupled nonlinear oscillators. *Circuits and Systems I: Fundamental Theory and Applications, IEEE Transactions on*, 42(8):494–497, 1995.

[59] C. W. Wu and L. O. Chua. Synchronization in an array of linearly coupled dynamical systems. *Circuits and Systems I: Fundamental Theory and Applications, IEEE Transactions on*, 42(8):430–447, 1995.

[60] C. W. Wu and L. O. Chua. On a conjecture regarding the synchronization in an array of linearly coupled dynamical systems. *Circuits and Systems I: Fundamental Theory and Applications, IEEE Transactions on*, 43(2):161–165, 1996.

[61] X. Wu, J. Cai, and Y. Zhao. Some new algebraic criteria for chaos synchronization of chua's circuits by linear state error feedback control. *International journal of circuit theory and applications*, 34(3):265–280, 2006.

[62] S. Yaghouti, C. Petrarca, and M. de Magistris. Experiments on clustering and synchronous patterns in a configurable network of chaotic oscillators. *Emergent Complexity from Nonlinearity, in Physics, Engineering and the Life Sciences*, pages 93–104, 2017.